Process development of electrode-based dielectrophoretic separators

Vom Fachbereich Produktionstechnik der Universität Bremen zur

Erlangung des Grades Doktor der Ingenieurwissenschaften (Dr.-Ing.)

genehmigte Dissertation

von

Jasper Matthias **Giesler**, M.Sc.

Gutachter:

Prof. Dr.-Ing. Jorg Thöming - Universität Bremen
Prof. Dr. Andreas Dietzel - Technische Universität Braunschweig

Tag der mündlichen Prüfung: 12.01.2024

Zusammenfassung

Die Trennung von Partikeln hinsichtlich ihrer Eigenschaften ist ein Feld mit etablierten und robusten Verfahren. Trenntechniken sind in der heutigen Welt allgegenwärtig aber oft unbemerkt. Kinder spielen zum Beispiel häufig mit Sieben, um größere Steine von Sand zu trennen. Verunreinigungen im Wasser können durch Filtration entfernt werden, um es trinkbar zu machen. Filtrierende Masken (z.B. FFP2) werden genutzt um uns vor infektiösen Viren zu schützen. Die Liste ließe sich mit der Aufbereitung von Mineralien in der Bergbauindustrie oder der Entfernung von Mikroplastik aus dem Meer fortsetzen, es ist jedoch offensichtlich, dass Partikeltechnologie Auswirkungen auf unser aller Leben hat. Trotz ihrer langen Geschichte werden derzeit große Anstrengungen unternommen, um bestehende Trennverfahren zu verbessern oder neue zu entwickeln.

Eine Kraft, von der bekannt ist, dass sie selektiv und stark genug ist, um DNA oder Nanopartikel einzufangen, ist die Dielektrophorese (DEP). DEP ist ein Transportprozess aufgrund einer elektrokinetischen Kraft, die auftritt, wenn ein polarisierbares Partikel einem inhomogenen elektrischen Feld ausgesetzt ist. DEP erlaubt Trennungen sowohl in der Mikrofluidik, als auch in industriellen Separatoren. Während die Mikrofluidik eine hohe Selektivität, aber einen geringen Durchsatz bietet, fehlt es größeren Separatoren häufig an Selektivität, während sie gleichzeitig einen hohen Durchsatz aufweisen. Heutzutage konzentriert sich die Forschung im Bereich DEP hauptsächlich auf hochselektive Mikroseparatoren und biologische Trennprobleme mit Proben wie Krebszellen, DNA, Proteinen und sogar Viren. Zu den gängigen Ansätzen gehören die Feldflussfraktionierung, das Einfangen von Partikeln an isolierenden Strukturen bzw. Elektrodenarrays oder die räumliche Trennung durch Manipulation der Partikeltrajektorien.

Ziel dieser Arbeit ist es, den Werkzeugkasten der DEP-basierten Separatoren um zwei neue Instrumente zu erweitern. Der erste Ansatz, der in dieser Arbeit vorgestellt wird, nennt sich frequenzmodulierte dielektrophoretische Partikelchromatographie (DPC). Der Ansatz wurde in experimentellen und numerischen Untersuchungen getestet. Dabei konnten die verschiedenen möglichen Trajektoren in einem DPC-Aufbau beschrieben und vorhergesagt werden. Der mikrofluidische Aufbau verfügt über Elektroden am Boden des Kanals, welche eine chromatographische Trennung ermöglichen. Das Verfahren wurde mit einfach detektierbaren, fluoreszierenden Polystyrol-Mikropartikeln getestet, und es konnten eine größenselektive Trennung von u.A. 2 µm und 3 µm Partikeln und eine Trennung anhand

der Oberflächenfunktionalisierung von 2 µm Partikeln gezeigt werden.

Der zweite Teil der Arbeit befasst sich mit der Erhöhung des Durchsatzes von DEP-Separatoren, welche Elektrodenarrays zur Manipulation von Partikeln verwenden. Hierbei wurde der Fokus auf die Beibehaltung der Selektivität gelegt. Es wurde ein Design auf Basis von speziell gefertigten jedoch günstigen Leiterplatten (PCBs) entwickelt und zunächst mit Polystyrolpartikeln getestet. Die selektive Trennung einer Mischung aus 3 µm und 6 µm wurde bei einer Frequenz erreicht, die eine Trennung auf der Grundlage der unterschiedlichen Polarisierbarkeit der Partikel ermöglichte. Schlussendlich wurde der Aufbau mit leitfähigen Partikeln getestet. Gängige Elektrodenmaterialien von Lithium-Ionen-Batterien wurden ausgewählt (Graphit und Lithiumeisenphosphat), um die Trennbarkeit technisch relevanter Partikel zu zeigen. Die Experimente lassen schlussfolgern, dass Graphit bei geeigneten Parametern nahezu vollständig gefangen wird, wohingegen Lithiumeisenphosphat zum Großteil den Kanal wieder verlässt.

Abstract

Separating particles with respect to their intrinsic properties is a field of established and robust methods. It is present in our world and many times without recognition. Children, for example, often play with sieves to separate rocks from sand. Impurities in water can be removed by filtration in order to make it drinkable and filtrating masks (e.g., FFP2) can even retain viruses that would otherwise infect us. The list can be continued with the processing of minerals in the mining industry or the removal of microplastics from marine environment, but it is rather obvious that particle technology has an impact on everyone's life. Despite its long history, currently, high efforts are undertaken to improve existing or develop novel separation techniques.

One force known to be highly selective and strong enough even to trap DNA or nanoparticles is dielectrophoresis (DEP). DEP is the movement of a polarizable particle due to an inhomogeneous electric field. DEP is can enable or enhance separation not only in microfluidics but also in industrial-scale separators. Whereas microfluidics offer high selectivity but lack throughput, larger separators are missing the selectivity while having significant volumetric flow rates. Nowadays, the DEP research community mainly focuses on highly selective microscale separators and the manipulation of biological samples such as cancer cells, DNA, proteins, and viruses. Common approaches include field-flow fractionation, trapping of particles at insulating posts or electrode arrays, and spatial separation via focusing and deflection.

This thesis aims to expand the toolbox of DEP based separators with two new tools. The first approach provided in this thesis is the frequency modulated dielectric particle chromatography (DPC). The microfluidic device used features an electrode array at the bottom of the channel and performs a chromatographic separation of microparticles. The procedure was tested with fluorescently labeled polystyrene microparticles and was able to achieve separation of, for example, 2 µm and 3 µm particles and of particles depending on their surface functionalization. By using experimental and numerical investigations, we could describe the different patterns of movement in a DPC setup.

The second part of the thesis focuses on increasing the throughput of DEP separators that use electrode arrays to manipulate particles while maintaining selectivity. A design based on custom-designed low-cost printed circuit boards (PCBs) was developed and first tested with polystyrene particles. The selective

separation of a mixture of 3 µm and 6 µm was demonstrated by using a frequency that allowed separation based on their different polarizabilities. Finally, we tested the device with conductive particles. We selected common electrode materials from lithium-ion batteries, here graphite and lithium iron phosphate (LFP), as particles to be separated. We could successfully show that graphite is retained almost entirely while most of LFP is eluted from the channel.

Danksagung

Mit der Abgabe der Dissertation endet ein interessanter und intensiver Abschnitt in meinem Leben. In Zeiten des Klimawandels, Pandemie und Krieg in Europa bin ich dankbar, dass ich das Privileg hatte mir Zeit für diese Arbeit nehmen zu können. Ich bin dankbar dafür, dass meine Eltern mir geholfen haben meinen Weg zu finden und mich dabei unterstützt haben diesen auch zu gehen. Meinem Sohn Henri, meinen Schwestern und Vanni bin ich dankbar dafür, dass sie mich von diesem Weg auch mal abgelenkt und andere Blickwinkel gelehrt haben. Ich bin dankbar, dass mich viele Menschen im privaten und beruflichen Umfeld in den letzten Jahren unterstützt haben. Der Mensch ist das Produkt seiner Umwelt und ich habe wahnsinniges Glück mit meiner.

Bezogen auf diese Arbeit möchte ich mich herzlich bei meinen fachlichen Betreuern Jorg Thöming, Georg Pesch und Michael Baune bedanken. Freiräume in diesem Maße zu haben ist keine Selbstverständlichkeit und für mich ein großer Vorteil in dieser Arbeitsumgebung. Die Diskussionen waren stets fruchtbar und ich habe viel lernen können. Herrn Dietzel danke ich als Zweitgutachter herzlich für die Zeit und Mühen, die er in diese Arbeit investiert hat. All meinen Kooperationspartnern möchte ich für deren Unterstützung und Zeit danken. Zuletzt möchte ich Laura Weirauch dafür danken, dass sie nach bald sechs Jahren im Büro mit mir stets gewillt war über allerhand Fachliches und nicht Fachliches zu diskutieren.

Ich bin gespannt auf das, was die Zukunft für uns bereithält.

List of publications

As first author

- Giesler, J.; Pesch, G. R.; Weirauch, L.; Schmidt, M.-P.; Thöming, J.; Baune, M. Polarizability-Dependent Sorting of Microparticles Using Continuous-Flow Dielectrophoretic Chromatography with a Frequency Modulation Method. *Micromachines* **2019**, *11*, 38, DOI: 10.3390/mi11010038
- Giesler, J.; Weirauch, L.; Thöming, J.; Baune, M.; Pesch, G. R. Separating Microparticles by Material and Size Using Dielectrophoretic Chromatography with Frequency Modulation. *Scientific Reports* **2021**, *11*, 16861, DOI: 10.1038/s41598-021-95404-w
- Giesler, J.; Weirauch, L.; Thöming, J.; Baune, M.; Pesch, G. R. High-Throughput Dielectrophoretic Separator Based on Printed Circuit Boards. *ELECTROPHORESIS* **2023**, *44*, 72–81, DOI: 10.1002/elps.202200131
- Giesler, J.; Weirauch, L.; Rother, A.; Thöming, J.; Pesch, G. R.; Baune, M. Sorting Lithium-Ion Battery Electrode Materials Using Dielectrophoresis. *ACS Omega* **2023**, DOI: 10.1021/acsomega.3c04057

Other publications (not included in this thesis)

- Weirauch, L.; Giesler, J.; Baune, M.; Pesch, G. R.; Thöming, J. Shape-Selective Remobilization of Microparticles in a Mesh-Based DEP Filter at High Throughput. *Separation and Purification Technology* **2022**, *300*, 121792, DOI: 10.1016/j.seppur.2022.121792

Contents

1 Introduction

Separating particles according to their intrinsic properties is an important task in a variety of fields, such as the processing of minerals [6, 7], biotechnology [8–10], and recycling of electronic waste [11–13]. Prominent examples for methods in particle separation are flotation [6, 14], field-flow-fractionation [15], centrifugation [16] or sieving [17]. More recently, the so-called FFP2 masks became popular because they separated an infectious virus from the air. Different separation processes can be reasonable depending on the product's value, the required purity, or the available sample size. Consequently, different techniques were developed that can handle single drops of suspension [18], volume flows in the microliter per minute range [19] or even several cubic meters per minute [20].

The processing of (bio-)particles in the lower micrometer down to the nanometer range is substance of current research efforts, as many existing approaches lack either throughput or selectivity for particles in this size range. In biotechnology, for example, detecting circulating tumor cells [8–10], sorting of proteins or DNA [21–23], or the collection of microalgae with high lipid content [24–26] are operations to be performed in this size range. Currently, the recycling of lithium-ion batteries gets significant attention by public and industry [27]. Since the active electrode materials in batteries are basically microparticles [28–30], particle separation techniques could play a vital role within the recycling process. Apart from these examples, numerous others can be found as the separation of metallic and semiconducting carbon-nanotubes [31, 32] or recovery of metals from the recycling of printed circuit boards [11].

Plenty of forces to manipulate microparticles have significantly different magnitudes depending on the particle size and properties. Gravity is, for instance, a prominent force to be used for separation techniques. However, particles with small volume or similar density compared to the surrounding medium are less affected by it. Further, its effect can vanish when the diffusion becomes dominant, which can be the case for nanoparticles [33]. Other techniques, such as density gradient centrifugation, accelerate particles and sort them according to their density. However, this technique is considered costly and slow [31]. Electrophoresis, in contrast, is inexpensive and fast. Unfortunately, it is considered hard to scale [31] and often processes batches of particles. Additionally, it requires particles with a net-charge present [34]. Many more approaches exist as the classification via aerodynamic lenses [35] and dynamic lateral displacement arrays [36–38] that

both focus on inertia effects of particles. The list can be extended with acoustic waves [39, 40], flotation [14, 41] or electric curtains [42, 43] and so on. Despite all these ideas and efforts, the combination of selectivity and throughput remains challenging. The plurality of approaches inherits high value to face the diversity of separation problems.

Substance of this thesis is the development of separation processes that use dielectrophoresis (DEP). DEP is the movement of a polarizable particle due to an inhomogeneous electric field and, in contrast to electrophoresis, does not need a net-charge present on particles. In the last decades, dielectrophoresis was mainly used in the biomedical field and in microfluidic setups [44]. The first two publications of this cumulative thesis focus on such a microfluidic setup and the development of a procedure that allows a fast chromatographic separation of particles. We could not only develop such a process but also simulate it, which helped to select process parameters to design the experiments. The size-selectivity of this process was shown by using polystyrene (PS) particles below 10 µm, and PS particles of the same size were separated only depending on their surface conductance.

The second part of this thesis aims at overcoming one limitation of DEP systems. While having significant volumetric flow rates and high removal rates of particles with using dielectrophoresis was shown at least 40 years ago [20], the combination of throughput, selectivity, and high frequency bandwidth of the electric field when using an aqueous medium still is unresolved. High bandwidth can be crucial to achieve selectivity, as changing the frequency can alter the DEP force in magnitude and direction. In our group, approaches were developed that showed selectivity and throughput [5, 45, 46] but were limited in the frequency range. Here the usage of custom-designed, low-cost printed circuit boards as electrode arrays is presented. Using these, the throughput was significantly increased, and the selective removal of particles by applying high frequencies was shown. Additionally, we showed the potential of this approach in the recycling of spent lithium-ion batteries.

In the following, important physical background information will be provided. Subsequently, a literature survey provides an overview of important literature related to this work. Then, four peer-reviewed, open-access publications with a brief introduction are included. Finally, the conclusion and outlook close this thesis.

2 Theory

In a DEP separator, commonly multiple physical forces compete. Obliviously, one of them is the dielectrophoretic force, but particles do not experience DEP solely. In this chapter, the relevant physical phenomena to understand the behavior of particles inside electrode-based dielectrophoretic separators will be described. The relevant forces and governing equations to describe viscous and electrical fields will be introduced. Connections between these equations and the application afterward will also be substance of this work. This overview does not aim to list and discuss all phenomena that could be relevant for other DEP setups. For this purpose, excellent textbooks were published and should be considered for more details than presented here. First, I would like to recommend *AC Electrokinetics* by Hywel Morgan and Nicolas G. Green [47]. Both authors made important contributions in the field of DEP and wrote a compact book while providing a widespread overview at the same time. Second, Ronald Pethig wrote a book simply named *Dielectrophoresis* [48], which provides an extensive overview of not only the theory behind DEP but also its history. Another excellent source for the history of dielectrophoresis is the review „Fifty Years of Dielectrophoretic Cell Separation Technology“ by Hughes from 2016 [49].

2.1 Fluid flow and drag

In many DEP separators a fluid flow can be observed. In the setups presented in this thesis, a pressure driven flow is generated through pumping. The fluid flow with external forces $\mathbf{f}$, can be described using the following representation of the Navier-Stokes equation [50]

$$\rho\frac{\partial \mathbf{u}}{\partial t} + \rho\mathbf{u} + \nabla\mathbf{u} = -\nabla p + \eta\nabla^2\mathbf{u} + \mathbf{f}. \tag{2.1}$$

Here, $\mathbf{u}$ represents the fluid velocity field, p the pressure, ρ the fluid density, which here is assumed to be constant (incompressible flow),t represents the time, and η the dynamic viscosity. From this equation the Reynolds number Re can be

derived as [50, 51]

$$Re = \frac{\rho U L}{\eta}. \tag{2.2}$$

U is a characteristic velocity of the fluid and represents the inertial forces, whereas the dynamic viscosity brings the viscous forces into this dimensionless number. Consequently, Re provides information about the ratio of these two influences and can be used to describe the dominating force and to describe the flow regime. Using the Reynolds number, the Navier-Stokes equation can be rewritten in a dimensionless form [50, 51]

$$Re\left(\frac{\partial \mathbf{u}^*}{\partial t^*} + \mathbf{u}^* \cdot \nabla^* \mathbf{u}^*\right) = \nabla^{*2}\mathbf{u}^* - \nabla^* p^* + \mathbf{F}*, \text{ with} \tag{2.3}$$

$$\begin{aligned}
\mathbf{u}^* &= \frac{\mathbf{u}}{U}, \\
\nabla^* &= L\nabla \\
\frac{\partial}{\partial t^*} &= \frac{L}{U}\frac{\partial}{\partial t} \\
p^* &= \frac{L}{\eta U}p \\
\mathbf{F}* &= \frac{L^2}{\eta U}\mathbf{F}.
\end{aligned}$$

The left-hand side of Equation 2.3 represents the inertial forces. The viscous, pressure and body forces are incorporated in the right-hand side. For low Re numbers ($Re \ll 1$) the unsteady and convective terms can be neglected and the Stokes flow approximation, without external forces, is obtained as [50]

$$\nabla p = \eta \nabla^2 \mathbf{u}. \tag{2.4}$$

This equation can be used to numerically calculate a fluid flow field at low Re numbers as they are present in many microfluidic systems. For simple geometries also analytical solutions can be found [50].

When a particle is suspended in a medium, it will experience friction from the interaction with the surrounding fluid and a gravitational pull. The result of this friction is the so-called drag force. When a particle has a higher velocity than the surrounding medium, the drag force $\mathbf{F}_{\text{drag}}$ is opposed to the direction of movement and thus slowing the particle down. The acceleration $\ddot{x}$ of a spherical particle with the mass m and the diameter d_{p} can be calculated by [52]

$$m\ddot{\mathbf{x}} = \mathbf{F}_{\text{drag}}, \text{with} \tag{2.5}$$

$$\mathbf{F}_{\text{drag}} = \frac{C_{\text{D}}\pi d_{\text{p}}^2}{8}\mathbf{u}^2\rho_p. \tag{2.6}$$

The drag coefficient C_D is a function of the particles Re number and for spherical particles and $Re < 1000$ it can be approximated via [52]

$$C_\mathrm{D} = \frac{24}{Re}\left(1 + 0.158Re^{2/3}\right). \tag{2.7}$$

Again, for low values of Re the equation can be simplified and results in

$$\mathbf{F}_\mathrm{drag} = \frac{C_\mathrm{D}Re}{24}\left(3\pi\mu d_\mathrm{p}\mathbf{u}\right). \tag{2.8}$$

In most cases experiments will not take place in space and as a consequence under the influence of gravity. Additionally, the buoyancy due to differences in density of medium and particle is likely to effect the movement of a particle in direction of gravitation. As a consequence, particles will start to sediment (or rise) in direction of the gravitational force (or opposed to it). The resulting force out of these effects is [52]

$$\mathbf{F}_\mathrm{g} = \frac{\pi d_\mathrm{p}^3}{6}(\rho_\mathrm{p} - \rho_\mathrm{m})\boldsymbol{g}, \tag{2.9}$$

where $\boldsymbol{g}$ is the gravitational acceleration.

2.2 Lift force

This section is mainly based on the review „Fundamentals and Applications of Inertial Microfluidics“ by Zhang, Yan, Yuan, Alici, Nguyen, Warkiani, and Li [53], which I recommend reading for more details on lift or drag force and diffusion of particles.

In microfluidic devices, equally dispersed particles at the inlet can be focused onto an annulus [53, 54]. The reason behind this is the lift force, that is composed out of four parts [53]. The lift force can release immobilized particles and have an impact on residence time distributions which can be relevant for chromatographic separations as presented in this thesis. The first mechanism of the lift force, is caused by a (induced) rotation of a particle and thus a pressure difference at its surface according to the Bernoulli principle at top and bottom (Magnus effect) [53]. Second, a lift force can rise, if a particle experiences a shear rate. This will direct a particle towards the center of the channel, when the particle lags the flow or push it towards the stagnant walls when the particle is leading the flow. The effect is called Staffman force and can rise if non-neutrally buoyant particles are present in a vertical flow, experiencing an outer force (as dielectrophoresis) or lag or lead the fluid flow for any other reasons. This force $\mathbf{F}_\mathrm{S}$ can be calculated with

$$\mathbf{F}_{\mathrm{S}} = \frac{K}{4}\mathbf{u}_{\mathrm{r}} d_{\mathrm{p}}^2 \left(\gamma \nu^{-1}\right)^{1/2}. \tag{2.10}$$

K is a numerical constant and about 81.2, γ is the shear rate, u_{r} the relative velocity between particle and the fluid at the streamline through the center of the particle and ν the kinematic viscosity. As a shear gradient can result in a rotation of the particle, and lead to the Magnus effect discussed above, an approximation of this effect is challenging to derive. A simple superposition is not sufficient. [53]

The third contribution to the lift force originates from the interaction of fluid flow and particles in proximity of a wall. A stationary wall (e.g, channel bottom) causes a velocity gradient within the fluid flow, as the flow velocity is zero at the wall (no slip). This can result in a shear rate a particle is subjected to and thus to the Magnus and Staffmann effect. When the particle is much smaller than the height of the channel, which is the case in our studies, only one wall is influencing the motion of a particle directly. The lift force will push the particle away from the wall and can be calculated in dependency from its sedimentation velocity in a stagnant fluid, the distance from the wall and the Reynolds number at the sedimentation velocity (equations see [53] in chapter 2.5). The wall will further increase the drag experienced by the particle in its proximity and the particle will lag the fluid flow [53].

If a curvature inside the channel is present, this can result in the fourth origin of lift force. The shear gradient lift force rises if a curvature in the fluid velocity is present along the axis of the particle. This condition can already be fulfilled by a parabolic flow profile. If the relative velocity of the fluid (compared to the particle) is larger at one side of the particle it will be accelerated into that direction due to the pressure difference similar to what causes the Staffman force. [53]

The authors conclude in the above-mentioned review [53], that wall induced and shear gradient induced lift are dominant and act as two opposing lift forces that push particles away from center lines (shear gradient induced) and repulse them from walls (wall-induced) and thus leading to the aforementioned annulus. The two effects can be combined into one equation for $Re < 100$ and small rigid spheres to

$$F_{\mathrm{L}} = \kappa_{\mathrm{L}} \rho_f \gamma^2 d_{\mathrm{p}}^4. \tag{2.11}$$

κ_{L} is the lift coefficient and F_{L} the combined lift force. The lift coefficient can be positive or negative and is a function of the radial coordinate in a channel. Consequently, the force can be directed towards the wall of the channels or pointing away from them. For deformable particles as cells, other correlations apply [53].

In proximity to the wall the lift force can be an important effect to release particles trapped at a wall. A correct approximation of the lift force for DEP

experiments seems not easily obtainable as the Staffmann force might be important as well. However, Wang, Vykoukal, Becker, and Gascoyne [55] conducted experiments for dielectrophoretic field-flow fractionation and concluded that hydrodynamic lift forces typically are not dominant in DEP-FFF. Further, if lift force would be dominant, no DEP trapping would be observable in the experiments. However, trapping due to DEP was achieved in the setups which are substance of this thesis. Therefore, it can be assumed that lift force is not a limiting mechanism in dielectrophoretic separators as long as sufficient electric field is applied.

As particles get smaller, the influence of lift ($\propto d_\mathrm{p}^4$) and drag force ($\propto d_\mathrm{p}^2$) but also gravitation and dielectrophoresis (Section 2.6.1) ($\propto d_\mathrm{p}^3$) becomes smaller. Diffusion, in contrast, increases with decreasing particles size and is discussed in the following section.

2.3 Brownian motion and diffusion

In 1827 Robert Brown reported a random movement of small particles in a fluid. He observed a motion of pollen and mineral particles in a solution. Thus, a fluid with no net movement can contain particles that are moving. This movement is called Brownian motion and rises from the thermal motion of molecules of the surrounding fluid [52]. For small particles Brownian motion can be an important transport mechanism and exceed the influence of gravitation and electrokinetic effects [33]. The random movement of the particles can lead to a net flux of particles if a gradient of particle concentration n is present. This effect is termed diffusion. Such gradients can rise, when particles sediment or are manipulated by effects as dielectrophoresis. The mean diffusion length $\bar{x}$ of a particle or a molecule with a diffusion coefficient D after a time t can be calculated using [48, 52]

$$\bar{x} = \sqrt{2Dt}. \tag{2.12}$$

In cases of a spherical particle where the mean free path is much smaller than the particle (mean free path in water ≈ 0.1 nm [56]) the diffusion coefficient can be calculated using the Boltzmann constant k_B and Temperature T as [52]

$$D = \frac{k_\mathrm{B} T}{3\pi\mu d_p}. \tag{2.13}$$

The resulting flux $\tilde{\mathbf{J}}$ can be described by Fick's first law [52]

$$\tilde{\mathbf{J}}_x = -D\frac{\partial n}{\partial x}, \tag{2.14}$$

$$\tilde{\mathbf{J}}_y = -D\frac{\partial n}{\partial y}, \text{ and} \tag{2.15}$$

$$\tilde{\mathbf{J}}_z = -D\frac{\partial n}{\partial z}. \tag{2.16}$$

The time-dependency of the concentration can be obtained by solving Fick's second law [52]

$$\frac{\partial n}{\partial t} = D\left(\frac{\partial^2 n}{\partial x^2} + \frac{\partial^2 n}{\partial y^2} + \frac{\partial^2 n}{\partial z^2}\right) = D\nabla^2 n. \tag{2.17}$$

In water, depending on the density difference between particle and medium and in absence of an electric field, Brownian motion can be the dominant mechanism of movement for a particle in the 100 nm range [33].

2.4 Electric fields

In addition to the hydrodynamic field, the electric field is important in dielectrophoretic separators. The electric field $\mathbf{E}$ [V/m] in an electrostatic case is defined as

$$\mathbf{E} = -\nabla\Phi \tag{2.18}$$

where Φ is the electrical potential (often referred to as voltage) [50, 57]. The electric potential is linked to the work that is required to move a point charge Q from point 1 to 2 within an electric field [58]

$$W_{12} = -\int_1^2 Q\mathbf{E}\cdot dx, \tag{2.19}$$

in combination with equation 2.18 follows [58]

$$W_{12} = Q\left(\Phi_2 - \Phi_1\right). \tag{2.20}$$

According to one of Maxwell's equations (Gauss's law for electricity), the field can also be defined by the volumetric net free charge density ρ_f in a material [50, 58]

$$\varepsilon_0\varepsilon_\mathrm{r}\nabla\cdot\mathbf{E} = \rho_\mathrm{f}, \tag{2.21}$$

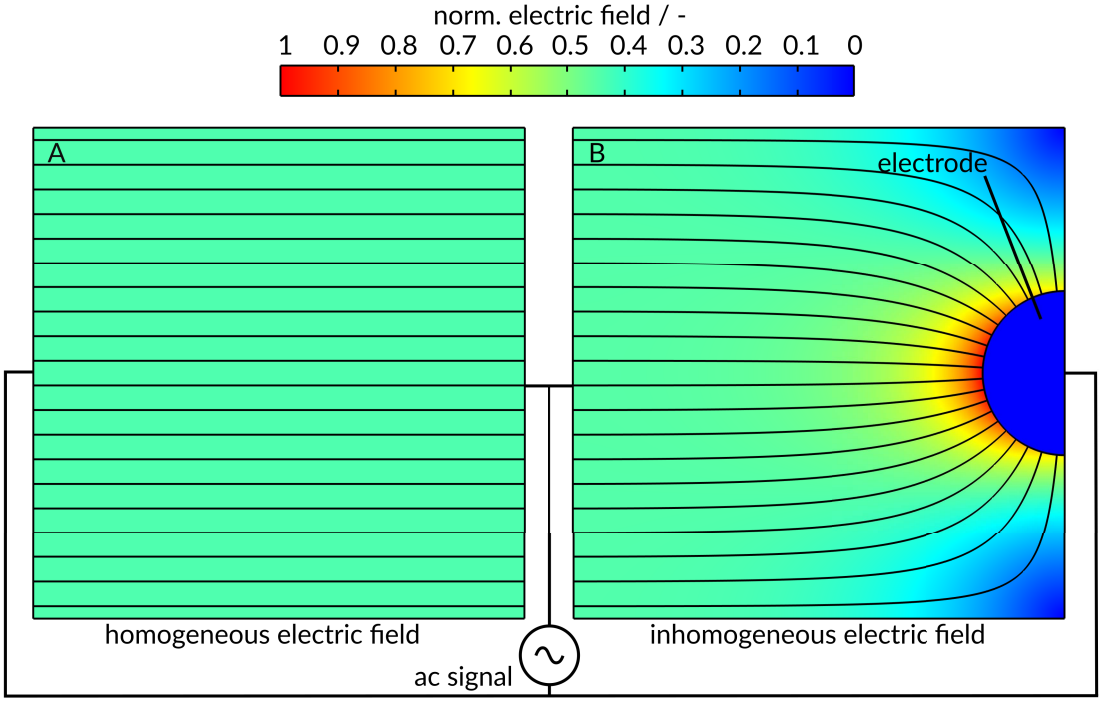

Figure 2.1: Comparison of a homogeneous electric field (A) and an inhomogeneous electric field (B). The inhomogeneous field is generated by different electrode geometries. Simulated with COMSOL Multiphysics.

where ε_0 is the permittivity of the vacuum (ε_0 =8.85 $\times$ 10^{-12} C/Vm). Please note that, although only the free charges are directly visible in equation 2.21, the bound charges are also incorporated as the relative permittivity of a material ε_r is linked to the polarizability of a material. This connection between electric field and polarizability is via the displacement field $\mathbf{D}$, which is defined as [58]

$$\mathbf{D} = \varepsilon_0 \mathbf{E} + \mathbf{P}, \tag{2.22}$$

with $\mathbf{P}$ as polarization field strength. For linear dielectrics the polarization is proportional to the electric field by using its electric susceptibility χ and the permittivity of the vacuum ε_0 [58]

$$\mathbf{P} = \chi \epsilon_0 \mathbf{E}. \tag{2.23}$$

Its divergence is the volumetric polarization charge density ρ_p [58]

$$\nabla \cdot \mathbf{P} = -\rho_\mathrm{p}. \tag{2.24}$$

The total volumetric charge density ρ consists of both parts, the free and the polarization charge density ($\rho = \rho_\mathrm{p} + \rho_\mathrm{f}$). With defining the relative permittivity as [58]

$$\varepsilon_r = 1 + \chi \tag{2.25}$$

we obtain [58]

$$\mathbf{D} = \varepsilon_0 \varepsilon_\mathrm{r} \mathbf{E}. \tag{2.26}$$

This shows that equation 2.21 already incorporates the polarization of matter as the permittivity (or dielectric constant) of the vacuum and the relative permittivity of a material act as constants of proportionality between the electric field and the electric displacement field. The electric permittivity describes how much electric field is generated by a source charge in a material [50]. The permittivity is not a constant but may decrease with increasing frequency of the electric field [57, 59] or temperature [58]. For gases, the relative permittivity is around unity, ranges from 2 to 4 for oil crudes, from 15 to 35 for alcohols and is approximately 80 for water due to its high polarizability (section 2.5) [58].

According to their electrical parameters, materials can be divided into three groups, namely conductors, semiconductors and dielectrics/insulators. Materials with a large supply of free charge, that can move unhindered within the material, are called conductors. Well known examples for this type of material are gold and copper. Here, the free charge carries are mobile electrons. In conductive solutions, ions are the carrier of free charge. When applying a potential, the carriers of free charges, depending on their charge, will migrate towards regions of different electric potential. This leads to a current which is linked to the conductivity σ of a material. In contrast, materials with negligible conductivity are called insulators [57, 58]. Materials with an electrical conductivity that is not negligible nor highly conductive are called semiconductors. When knowing the electric field, the conductivity σ_m of a medium and the electric displacement field one can calculate the total current $\mathbf{J}$ flowing in an electrical system [57]

$$\mathbf{J} = \sigma_m \mathbf{E} + \frac{\partial \mathbf{D}}{\partial t} \tag{2.27}$$

Following this equation and equation 2.26, the total current of a system also linked to the permittivity and thus to the polarization of the material.

Utilizing the equations in this chapter and suitable boundary conditions (e.g., see [58] Chapter 3.5) the electric field can be calculated. Electric fields can either be homogeneous (Figure 2.1 A) meaning that the electric field strength is equal at all points, or inhomogeneous (Figure 2.1 B) where a gradient within the electric field is present. Inhomogeneous electric fields in combination with the polarization are key prerequisites for dielectrophoresis.

2.5 Polarization

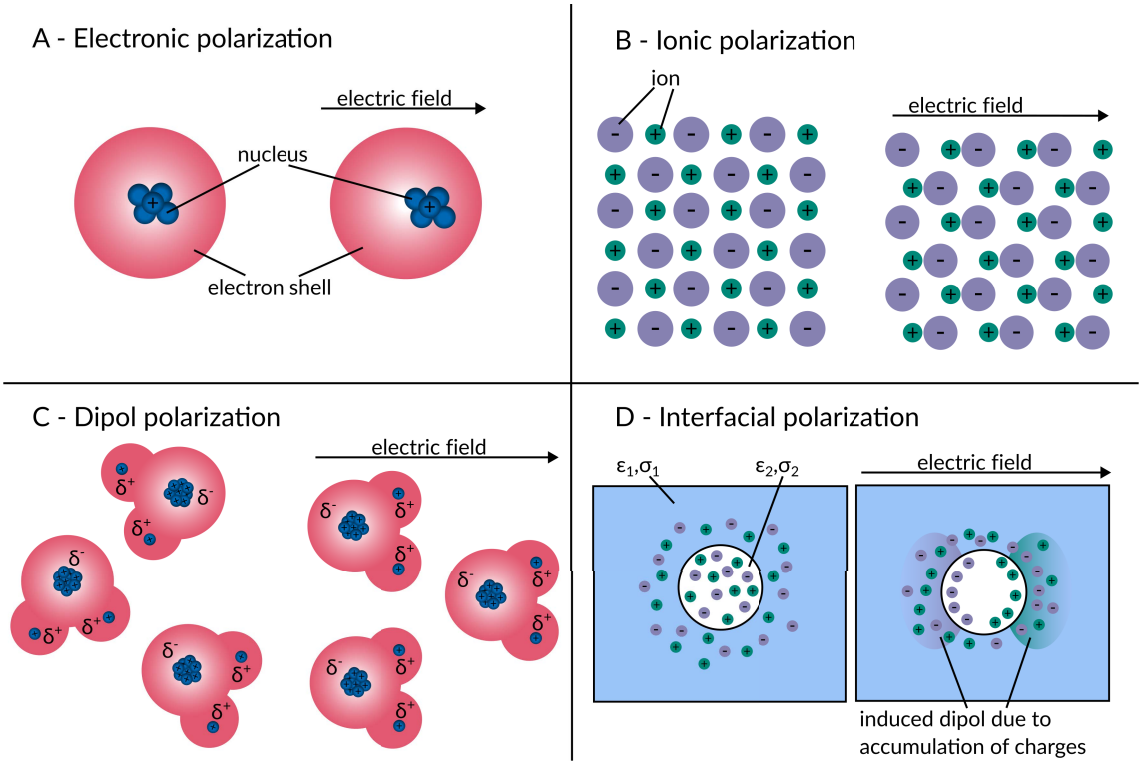

Figure 2.2: Different mechanisms of polarization. Electronic polarization (A) occurs on a atomic level. Ionic (B) and dipole (C) polarization involve multiple atoms and (partial) charges. Interfacial polarization (D) is a macroscopic effect on material interfaces. Inspired by [48, 60].

Dielectric materials will polarize when subjected to an electric field. Polarization is defined as the accumulation of charges at the ends of a dielectric material. Ideal dielectrics are insulators and have no electrical conductivity or mobile charges. Polarization is either caused by processes on the molecular or atomic level or on those that are have a more macroscopic nature as polarization at material interfaces. [48, 58] As DEP would not exist without the polarization of medium and particles, the theory of polarization is crucial to understand dielectrophoresis.

2.5.1 Electronic polarization

The negatively charged electrons and the positively charged nucleus of an atom will react to an applied electric field and cause a distortion with respect to their equilibrium position. This leads to a polarization on the atomic level (Figure

2.2 A). The mechanism is known as electronic polarization and will take place up to field frequencies of up to $\sim 2 \times 10^{14}$ Hz. Additionally, the displacement of nucleus and electrons can lead to the polarization of molecules. Here, the bonding electrons may be affected as well [48, 61] and lead to a polarization of molecules (atomic polarization).

2.5.2 Ionic and dipole polarization

For other mechanisms of polarization, the electronegativity (EN) of atoms is an important variable. It describes the ability of an element to attract electrons in chemical bonds. The EN ranges from its theoretical minimum of 0 to a maximum value of 4. As long as the difference of electronegativities in a chemical bond is in the range of 0.5 or lower, the bond is classified as nonpolar (e.g., H_2). Up to a difference of the EN of about 1.8 to 2.0 a polar bond is occurring (e.g., H_2O or NH_3). Here, on average the electronic charge spends more time at atoms with the higher EN resulting in an partial charge (δ^-). The corresponding positive partial charge δ^+ can be found at the atom with lower EN. Finally, above these differences ionic bonds occur. Ionic bonds are characterized by a complete transfer of electrons from one binding partner to the other. Prominent examples are salts as NaCl, KCl or NaOH. [48, 62].

In ionic and polar bonds two additional polarization mechanisms can be observed. In an ionic crystal, net charges are present at the ions due to the high difference in the EN. When an electric field is applied, the positive and negative ions are attracted by the opposing pole, leading to a polarization of material and a deformation of the crystal structure (Figure 2.2 b). Due to this deformation, net dipoles per unit volume are present. Their influence can significantly exceed the impact of electronic polarization [48].

Depending on their spacial structure, molecules with a polar bond can form dipoles. One prominent example of such a molecule is water. Dipoles interact with each other due to their partial charges (δ^+/δ^-, Figure 2.2 c). These interactions can have significant impact on the properties such as permittivity, melting and boiling point of a material [62]. When a dipole is subjected to an electric field, the molecule will experience a torque and orientate itself in the electric field which leads to polarization of the volume. Dipole polarization or, as it is also called, orientational polarization is present up to the GHz range [47] and is the origin of the increased relative permittivity of molecules with high electric dipole moment.

2.5.3 Interfacial polarization

Different electrical properties can also lead to polarization at material interfaces [47, 63]. The ratio of permittivity and conductivity $\tau = \varepsilon/\sigma$ is referred to as the

relaxation time of a dielectric material. At interfaces of two materials (index 1 and 2) with different relaxation times charge accumulation can occur, which is called the Maxwell-Wager effect [63]. At the interface of dielectrics the normal components (index n) of the displacement current and the potential are continuous [48, 57, 58]

$$\Phi_1 = \Phi_2 \tag{2.28}$$

$$\mathbf{D}_{\mathrm{n}1} + \mathbf{D}_{\mathrm{n}2} = -\rho_{\mathrm{f}}. \tag{2.29}$$

Here, ρ_{sf} are the free surfaces charges at the material interface. In combination with equation 2.26, we obtain for the electric potentials normal to the interface $\mathbf{E}_{\mathrm{n}1}$ and $\mathbf{E}_{\mathrm{n}2}$ [48, 58]

$$\varepsilon_1 \mathbf{E}_{\mathrm{n}1} + \varepsilon_2 \mathbf{E}_{\mathrm{n}2} = -\rho_{\mathrm{f}}. \tag{2.30}$$

For materials with $\varepsilon_1 \neq \varepsilon_2$, the electric field is discontinuous [58]. Additionally, with the continuity equation of charges [48, 64]

$$\nabla \cdot (\sigma \mathbf{E}) = -j\omega\rho_{\mathrm{f}} \tag{2.31}$$

and ω as the angular frequency of the electric field and j as imaginary unit, we find [48]

$$\sigma_1 E_{\mathrm{n}1} - \sigma_2 E_{\mathrm{n}2} = j\omega\rho_{\mathrm{f}}. \tag{2.32}$$

Equations 2.30 and 2.32 can be combined to [64]

$$(\sigma_1 + j\omega\varepsilon_1)\mathbf{E}_{\mathrm{n}1} + (\sigma_2 + j\omega\varepsilon_2)\mathbf{E}_{\mathrm{n}2} = 0, \tag{2.33}$$

which gives us the boundary condition between materials for a sinusoidal electric field. Summarizing, the interfacial polarization is an effect due to different electrical properties that give rise to a surface charge at the interface of materials that can polarizes a piece of matter. Interfacial polarization is a strong polarization mechanism up to around 10^5 Hz [45].

2.5.4 Complex permittivity

From equation 2.33 the so-called complex permittivity $\tilde{\varepsilon}$ can be derived straight forward, which does include the permittivity, conductivity and the frequency of the electric field [64]

$$\tilde{\varepsilon} = \frac{\sigma + j\omega\varepsilon}{j\omega}$$

$$\tilde{\varepsilon} = \varepsilon - j\sigma/\omega. \tag{2.34}$$

The complex permittivity is an important parameter to describe the polarizability of a material at a given frequency (section 2.6.1) and incorporates the above-mentioned mechanisms of polarizability. The dipole polarization is reduced in the GHz range. At lower frequencies ε can be considered as a constant [47, 65].

The importance of the electric properties with respect to the electric field was described within this section. In the following, dielectrophoresis (DEP) as an effect of different polarizabilities will be introduced among other important electrokinetic effects.

2.6 Electrokinetic effects

The electric field and the polarization of matter in it can lead to electrokinetic effects. One of these effects is dielectrophoresis.

2.6.1 Dielectrophoresis

Dipole approximation

The first approximation of the DEP force $\mathbf{F}_{\mathrm{DEP}}$ was derived by Pohl and Crane in 1972 [64]. The force $\mathbf{F}$ on a test point charge Q in an electric field is given by (compare Equation 2.19 [47])

$$\mathbf{F} = Q\mathbf{E}. \tag{2.35}$$

When a polarized particle with two opposed charges that are separated by the distance d is in an inhomogeneous electric field (Figure 2.3), the forces on each side of the particle will be different. The resulting force exerted by the particles will be [47]

$$\begin{aligned} \mathbf{F} &= Q\mathbf{E}_{x2,y2,z2} - Q\mathbf{E}_{x1,y1,y1}, \text{with} \\ x2 &= x1 + d_{\mathrm{x}} \\ y2 &= y1 + d_{\mathrm{y}} \\ z2 &= z1 + d_{\mathrm{z}}. \end{aligned} \tag{2.36}$$

As the electric field is not constant over the particle's diameter, the force will be nonzero. A first-order Taylor series around the first point (subscript 1) results in [47]

$$\mathbf{F} = Q\mathbf{E}_{x1,y1,z1} + Q\left(d_x\frac{\partial}{\partial x} + d_y\frac{\partial}{\partial y} + d_z\frac{\partial}{\partial z}\right)\mathbf{E} - Q\mathbf{E}_{x1,y1,z1} \tag{2.37}$$

$$\mathbf{F} = Q(\mathbf{d}\cdot\nabla)\mathbf{E}. \tag{2.38}$$

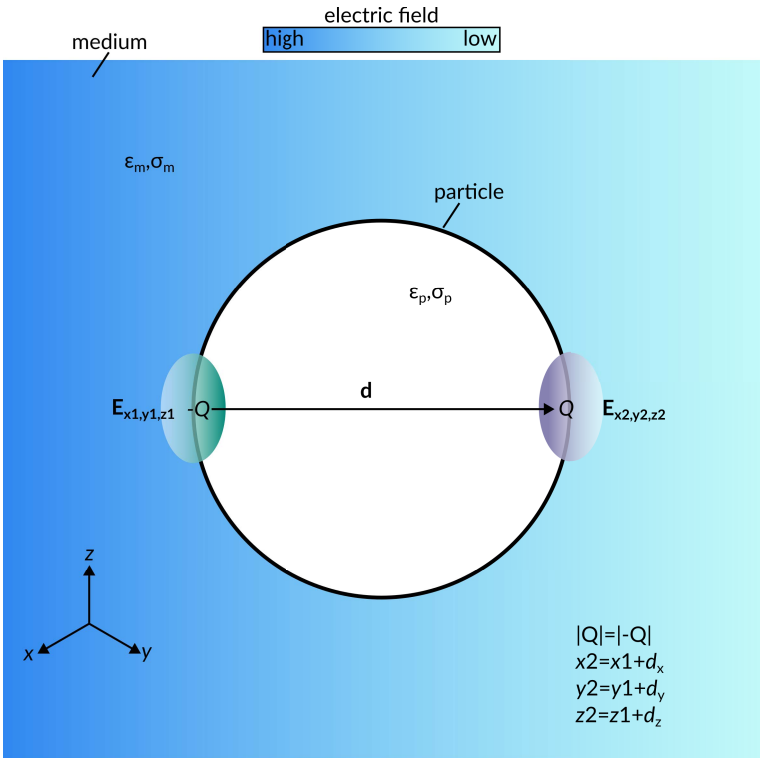

Figure 2.3: Particle (subscript p) suspended in a medium (subscript m) in an inhomogeneous electric field. The particle has charges Q and $-Q$ on both sides that are separated by the distance $\mathbf{d}$ and thus is a dipole. The charges have opposed sign but same absolute value. Inspired by [44] and [47] Figure 4.1.

The dipole momentum $\mathbf{p} = Q\mathbf{d}$ simplifies the approximation of the DEP force $\mathbf{F}_{\mathrm{DEP}}$ to [47]

$$\mathbf{F}_{\mathrm{DEP}} = (\mathbf{p} \cdot \nabla)\mathbf{E}. \tag{2.39}$$

This approximation is referred to as the dipole approximation. For multipoles, more advanced calculations are needed that can also be used for arbitrary shaped particles. Here, a solution for the electric field is required to calculate the dielectrophoretic force using the Maxwell stress tensor as proposed by Wang, Wang, and Gascoyne [66].

The DEP force on a spherical particle

The dipole moment for a homogeneous and spherical particle (subscript p) in a medium (subscript m) can be derived as [47, 48]

$$\mathbf{p} = 4\pi\varepsilon_m \left(\frac{\tilde{\varepsilon}_p - \tilde{\varepsilon}_m}{\tilde{\varepsilon}_p + 2\tilde{\varepsilon}_m} \right) r_{\mathrm{p}}^3 \mathbf{E}. \tag{2.40}$$

In the dipole moment, the so-called Clausius-Mossotti $\tilde{f}_{CM}$ factor is incorporated via

$$\mathbf{p} = 4\pi\varepsilon_m \tilde{f}_{CM} r_{\mathrm{p}}^3 \mathbf{E}, \text{with} \tag{2.41}$$

$$\tilde{f}_{CM} = \frac{\tilde{\varepsilon}_p - \tilde{\varepsilon}_m}{\tilde{\varepsilon}_p + 2\tilde{\varepsilon}_m}. \tag{2.42}$$

We now can rewrite equation 2.39 for spherical particle in a sinusoidal AC field [48]

$$\mathbf{F}_{\mathrm{DEP}} = 4\pi\varepsilon_m \mathrm{Re}(\tilde{f}_{CM}) r_{\mathrm{p}}^3 \mathbf{E} \nabla \cdot \mathbf{E} \tag{2.43}$$

$$\mathbf{F}_{\mathrm{DEP}} = 2\pi\varepsilon_m \mathrm{Re}(\tilde{f}_{CM}) r_{\mathrm{p}}^3 \nabla \mathbf{E}^2, \text{with} \tag{2.44}$$

$$2(\mathbf{E} \cdot \nabla \mathbf{E}) = \nabla \mathbf{E}^2. \tag{2.45}$$

Equation 2.44 gives the time averaged DEP force on the particle. Please note, $\mathbf{E}$ is the root-mean-square (rms) of the magnitude of the electric field and not its amplitude.

The Clausius-Mossotti factor

The dielectrophoretic force is a vector pointing, depending on its sign, in the direction of local field maxima or away from them. The sign is determined by the real part Clausius-Mossotti factor (equation 2.42) which can either be positive, negative or zero. Analog, the corresponding dielectrophoretic movement is also referred to as positive ($\mathrm{Re}(\tilde{f}_{CM}) > 0$, pDEP) and negative ($\mathrm{Re}(\tilde{f}_{CM}) < 0$, nDEP) dielectrophoresis. The frequency at which $\mathrm{Re}(\tilde{f}_{CM}) = 0$ holds, is called crossover frequency. Particles that show pDEP migrate towards local field maxima, whereas nDEP pushes them away from these locations. As the complex permittivity is a frequency-dependent property of a material, the sign of $\mathrm{Re}(\tilde{f}_{CM})$ can change with frequency. This change of direction can be used to manipulate the trajectories of microparticles by changing the frequency in a periodic scheme. This is in more detail presented in the first two publications that are part of this thesis [1, 2] in chapter 4 and 5.

At low frequencies the behavior of a particle is dominated by the electrical conductivity of the material, or in some cases by the conductivity given due to

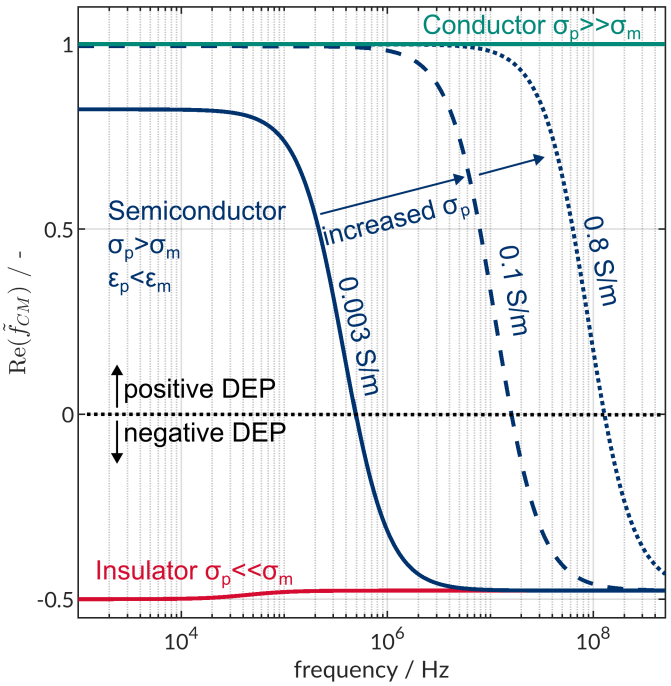

Figure 2.4: Exemplary real parts of the Clausius-Mossotti factor $\mathrm{Re}(\tilde{f}_{CM})$ as a function of the electric field frequency for conducting, semiconducting, and insulating particles (subscript p) in a medium (subscript m). Conductivity of medium is set to 2 µS/cm and a dielectric constant of 80 is assumed.

the diffusive layer around the particle [67]. For higher frequencies, the permittivity becomes the dominating factor to describe the particle polarizability (equations 2.42 and 2.34). Figure 2.4 shows the dependency of $\mathrm{Re}(\tilde{f}_{CM})$ on the frequency of the electric field and the electrical properties. Conductors will normally show pDEP over the complete relevant frequency range (green line) [68]. Scenarios exist, where conductive particles show nDEP due to shielding effects of the double layer but these are limited to frequencies substantially below 1 kHz [69]. In contrast, insulators will show nDEP in a medium like water (red line). In between of those two cases, semiconductors show a different behavior as their conductivity can be higher than that of the surrounding medium, whereas the permittivity will most likely be smaller compared to that of water, which is used as medium within this thesis. As a consequence, a crossover can be observed (blue lines). The position of the crossover changes with the electrical properties of a particle. Depending on the frequency these particles can show both, pDEP and nDEP.

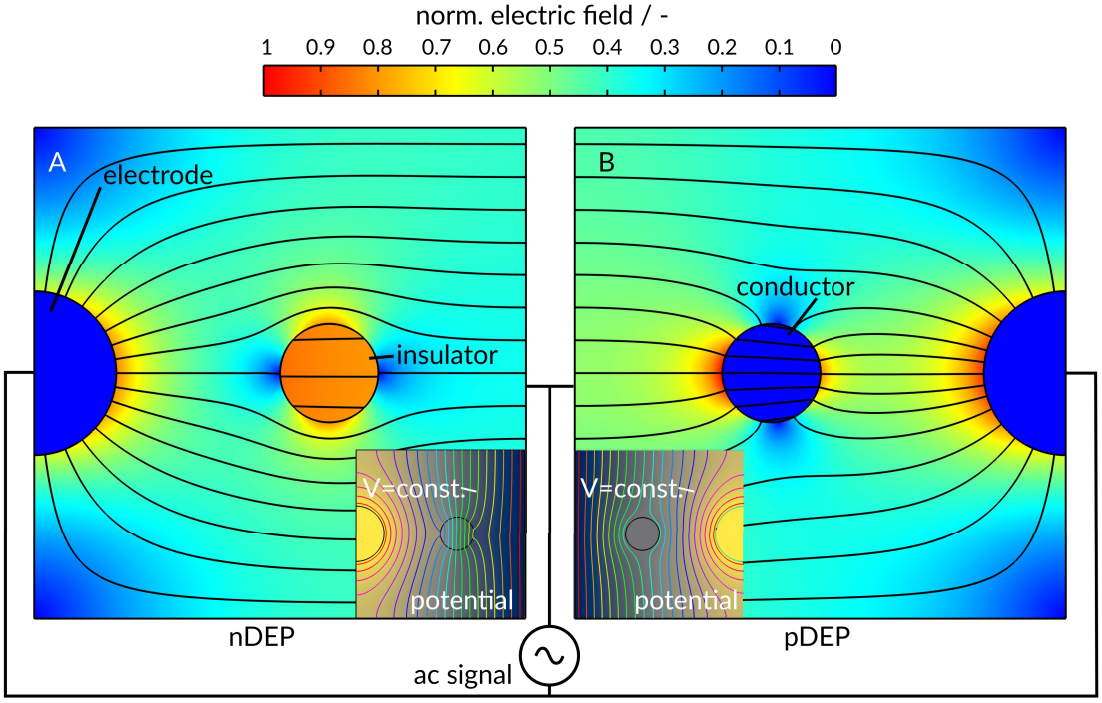

Figure 2.5: Polarization of an insulating (A) and a conducting sphere (B) in an inhomogeneous electric field. The insulator (silica) shows lower polarizability due to lower conductivity and permittivity compared to the medium (water). Consequently, this sphere would show negative dielectrophoresis (nDEP). The conducting sphere (copper) is highly polarizable and would show positive dielectrophoresis (pDEP). The inlets show a representation of the electric potential for both cases with isopotential lines. Simulated with COMSOL Multiphysics. The field is normalized to its maximum value.

Figure 2.5 shows the example of an insulating (A) and conductive particle (B) in an inhomogeneous electric field. Both, the insulating and the conductive structure, scatter the electric field. Yet the electric and potential field are different in these two cases. The conducting particle has a nearly constant potential in its inside due to the high conductivity and thus a negligible electric field in it. The very opposite can be observed in the insulating particle. As a consequence, the field distributions around them are different and their dielectrophoretic movement would be opposed to each other.

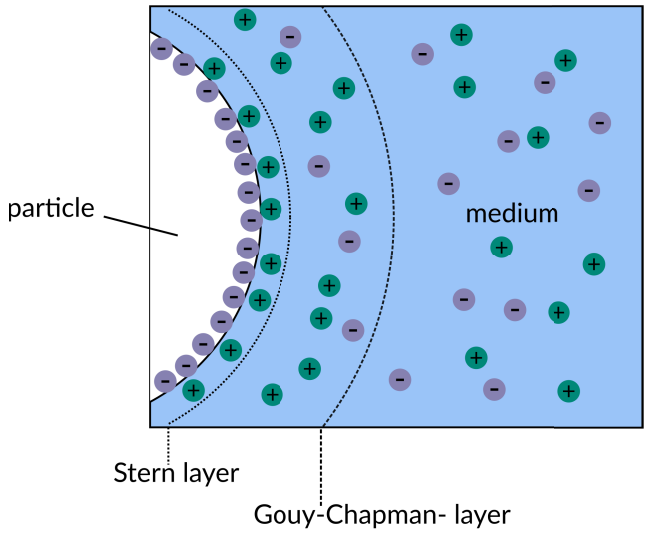

Figure 2.6: Representation of the electrical double layer according to the Gouy-Chapman-Stern model. The particle carries a negative net surface charge at its surface that gives rise to the alignment of anions and cations present in the solution. Inspired by [56] Figure 2.8.

Particle-particle interactions due to DEP

From Figure 2.5 a phenomenon often observed in DEP experiments can be explained. Particles in experiments tend to form so-called pearl chains in the electric field [70, 71]. A particle will scatter the electric field around it when its electrical properties differ from the surrounding. This leads to the formation of novel maxima and minima in the electric field. A conducting particle will align parallel to the applied electric field when in proximity to a conductive particle (Figure 2.5) and perpendicular to it when the sign of $\mathrm{Re}(\tilde{f}_{CM})$ is different. [47]

Polarization due to the electrical double layer

It is worth noting, that microparticles with negligible material conductivity can show pDEP when suspended in an aqueous solution. The origin of this behavior lays in the electrical double layer (EDL) around particles. A surface charge present at the surface of a particle will result in an EDL. In the Gouy-Chapman-Stern model, a double layer consists of two parts, the Stern and the diffuse layer (Figure 2.6). The Stern layer is characterized by strongly attracted and fixed charges on the particle surface, whereas the charges in the diffuse layer are attached more loosely and are affected by, for example, fluid flow which creates a shear plane in the EDL [47, 48]. The potential at this shear plane is measurable in experiments

and referred to as zeta potential. An external electric field can induce a mobility within the EDL which leads to a polarization of the particle and thus to altered DEP response. This effect was not only reported for PS particles but is also considered important for the DEP behavior of DNA, cells and proteins. [48]

A prominent, at least in the DEP community, example of particles that show this behavior are polystyrene (PS) particles. These can have functional groups as carboxylic groups (-COOH) at their surface, that result in a net surface charge. Ermolina and Morgan [67] measured the so-called surface conductance K_s of PS particles in aqueous suspensions and found it to be in the range of 1 nS. A result we were able to reproduce in reference [2]. Our experiments, however, also showed, that 1 nS is more a rule of thumb rather than a fixed value as PS particles can have quite different surface conductance. The conductivity of a particle with negligible bulk conductivity and a size larger than 1 µm can be calculated with [48, 67]

$$\sigma_\mathrm{p} = \frac{2(K_\mathrm{s} + K_\mathrm{dl})}{r_\mathrm{p}}. \tag{2.46}$$

For particles with smaller diameters, the conductivity of the diffuse layer K_dl becomes important and additionally increases the particle's polarizability [67]. Consequently, microparticles out of a non-conducting material can show the same DEP behavior as a semiconducting particle.

2.6.2 Effect of temperature on fluid flow

In dielectrophoretic setups, heating and even boiling of fluid can be observed [33]. The temperature T in a device can be obtained by solving the energy balance equation while neglecting the viscous dissipation term [72]

$$\rho_\mathrm{m} c_\mathrm{p} \frac{\partial T}{\partial t} + \rho_\mathrm{m} c_\mathrm{p} \mathbf{u} \cdot \nabla T = k \nabla T^2 + \sigma \mathbf{E}^2. \tag{2.47}$$

Here, ρ_m is the density of the medium, c_p the specific heat at a constant pressure, k the thermal conductivity of the material [72]. Joule heating corresponds to $\sigma\mathbf{E}^2$ and is a source of heat in DEP devices. The energy equation can be further simplified under the assumption of steady-state and neglecting the convective heat transport as described by Green, Ramos, González, Castellanos, and Morgan to [33, 72]

$$k \nabla^2 T = -\sigma \mathbf{E}^2. \tag{2.48}$$

Another source of heat can be the dielectric loss which will not be discussed here. For details on this topic please consult chapter 7.3 in [48] or reference [73]. For systems that are observed with a microscope, a significant influence of the illumination source on the temperature field was described [74]. Independent of

the source of heat, the resulting temperature differences in a device can have impact on suspended particles. As the density for many fluids is not constant over temperature, a flow can rise driven by buoyancy that also affects particles via viscous drag. The corresponding buoyancy body force $\mathbf{f}_\mathrm{g}$ is

$$\mathbf{f}_\mathrm{g} = \frac{\partial \rho_\mathrm{m}}{\partial T} \Delta T \mathbf{g}, \tag{2.49}$$

with $\mathbf{g}$ as the acceleration due to gravity [47]. Further, the temperature effects permittivity and conductivity of the medium. Gradients in this properties generate the so-called electrothermal fluid flow which can be dominant in DEP separators [33, 47, 75]. For more details and equations please see references [47] chapter 5.3.2 f. and [75]. The heat generation can be reduced by the usage of low solutions with low conductivity.

2.6.3 AC electroosmosis

AC electroosmosis (ACEO) is a phenomenon in the field of induced charge electroosmosis (ICEO). ICEO is characterized by a fluid flow due to a polarization of the electrical double layer. The electric potential at the surface of electrodes give rise to electro-migration of counter-ions that form an EDL. Along with the migration of the ions, the EDL builds up a charge. This results in a distortion of the electric field which, as a consequence, develops a tangential component with respect to the electrode surface. This tangential electric field produces a flow pointing inward from the electrode edges. As both, potential and double layer charge polarity change sign in an AC field in each half cycle, the direction of the flow does not alter over time. [76–78]

When using asymmetric interdigitated electrodes, ACEO can result in a net fluid flow into one direction which can be used for pumping. Further ACEO is used for mixing of suspensions in microchannels, which is an often unwanted effect for DEP experiments. [33, 78, 79] Green, Ramos, González, Morgan, and Castellanos [80] conducted a series of experiments which revealed that the fluid flow due to ACEO is drastically reduced for frequencies above around 10 kHz and thus can be avoided. When the frequency increases, ions have not enough time to migrate and form a complete electric double layer which results in a weakened fluid flow [78].

3 Status quo and challenges of applied dielectrophoresis

When neglecting the enormous variety in purpose, volume, throughput, or fabrication method, dielectrophoretic apparatuses can be divided in two categories. On the one hand, there are insulator-based setups (iDEP, Figure 3.1) and on the other hand we have electrode based techniques (eDEP, Figure 3.3). In iDEP devices an otherwise homogeneous electric field is scattered by insulating structures. Here, the electrodes are not in proximity to the regions with high DEP force. In eDEP devices, on the other hand, the configuration of electrodes is resulting in an inhomogeneous field which than can be used for dielectrophoresis.

In the following, a selection of published techniques in these two fields will be discussed. Further literature can be found in more extensive reviews as „On the Recent Developments of Insulator-Based Dielectrophoresis“ by Lapizco-Encinas [81] or the review on DEP of non-biological particles by Pesch and Du [82]. Sarno, Heineck, Heller, and Ibsen also provide an overview of developments in the field of DEP in the past decade [83].

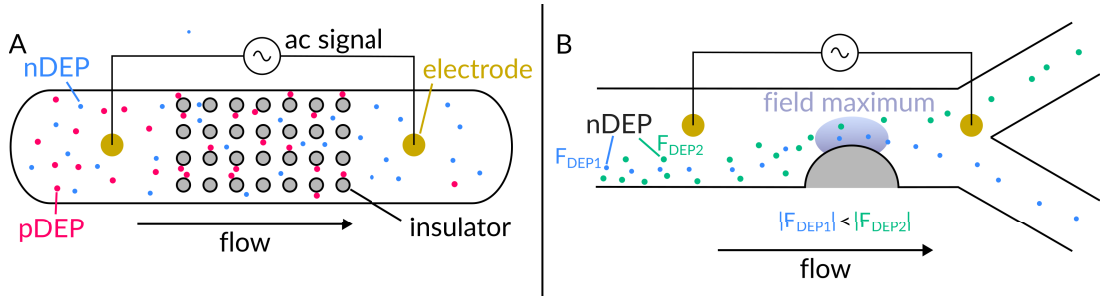

Figure 3.1: Examples of insulator-based DEP devices. A: Insulating posts scatter an otherwise homogeneous electric field and create many local field maxima and minima. Particles that show pDEP can be trapped, whereas particles with nDEP behavior are eluted. C: A single constriction scatters the electric field and deflects focused particles according to the magnitude of $\mathbf{F}_{\mathrm{DEP}}$ in different outlets.

3.1 Insulator-based dielectrophoresis

Patents that use packed beds out of insulating materials in an electric field to remove particles from a suspension date back to 1924 by Stafford [84] and are also granted in the following decades as well [85, 86]. Literature in academic journals is rare until the 1980s. Guillory, Placer, and Grace present in 1981 an enhancement of granular bed filter used by a combustion power company [20]. By applying an electric field to a packed bed with voltages up to 20 kV DC (currents up to 56 mA), they increased the collection efficiency of particles with an aerodynamic diameter as low as 500 nm to over 90 % which is quite an increase compared to 60 % up to around 80 % depending on the particle size without applied electric field. The authors account the increase in trapping to local gradients of the electric field and the resulting DEP. Here, 3×6 mm gravel was used to scatter the electric field. Corona discharge was not observed. Finally, the authors discussed a scaled version of their apparatus, that was designed to handle volume flows of up to 1200 m^3/min. This early report shows the potential of these so-called electrostatic filters and the potential of DEP even in industrial-scale devices. Interestingly, nowadays dielectrophoresis is often utilized in microfluidic devices in the biotechnological field of research [44] which obviously require different setups. It was a report from 1989 by Masuda, Washizu, and Nanba that started this development. According to Lapizco-Encinas [81] this was the first study with the application of iDEP in a microfluidic setup. The authors used an AC voltage and a single constriction to create a local field maximum and trap two cells in proximity to each other. As soon as two cells were trapped, an electric pulse was automatically applied to fuse them. The authors claim that it is beneficial for the cells to not have direct contact to the electrodes [87]. The channel in this study was created by using photolithography and featured elements significantly below 100 µm. The possibility to create such small elements and to manipulate cells with iDEP setups gave rise to research in this field.

About 10 years later Cummings and Singh presented arrays of circular or square insulating posts to scatter the electric field in a series of publications [88–90]. By applying a DC potential to electrodes outside the array, a fluid flow is generated due to electroosmosis. Particles or cells in the medium will experience effects as drag, electrophoresis but also dielectrophoresis. The setup is similar to what is shown in Figure 3.1 A. The idea was and still is adapted quite frequently. It was not until a few years ago, that it was shown that DEP is often not the dominating force as it was assumed for DC driven *DEP*-setups but that nonlinear electrokinetics, especially higher-order electrophoresis, are needed to be considered to describe the behavior in the setups correctly [91]. As DC (offset) is not used within this thesis and consequently electrophoresis is negligible, the reader is recommended to investigate this topic in detail starting with the study „Di-

rect Current Electrokinetic Particle Trapping in Insulator-Based Microfluidics“ by Cardenas-Benitez, Jind, Gallo-Villanueva, Martinez-Chapa, Lapizco-Encinas, and Perez-Gonzalez [91]. Although DEP might not be the driving force in these channels, interesting results could be achieved. Blanca Lapizco-Encinas and her group could, for example, separate live from dead bacteria [92], selectively concentrate bacteria [93], spores, viruses [94], and also manipulate proteins [95].

Arrays of posts are also used in the field of deterministic lateral displacement (DLD) which can fractionate microparticles depending on whether particles are capable of following the fluid flow around a post on the same streamline [36, 37, 96]. In DLD setups, the post arrays have a lateral shift with respect to the direction of the fluid flow, which, in combination with a laminar fluid flow, can lead to separation of particles [36]. When manufacturing the posts out of an insulating material, a superimposed electric field will be scattered the same way as in other iDEP setups. A superimposed electric field on a DLD array was successfully shown to enable continuous particle separation for micrometer and sub-micrometer sized particles [38, 96, 97].

Another concept in iDEP devices uses the deflection of particles into different outlets without trapping first which allows a continuous separation. A simplified example of a such a device is provided in Figure 3.1 B. Particles enter the microchannel and sometimes, focused by using a sheath flow, on specific flow lines. The particles do then reach a constriction which is made out of an insulating material and thus scatters the electric field. Depending on the direction and magnitude of the DEP force that the particles are experiencing, they are sorted in different outlets. The Ros-group made numerous contributions in this field, with both, DC and AC signals applied. Their devices were used to sort DNA molecules [22], single-walled carbon nanotubes [98], and mitochondria [99].

Many of the listed studies in this chapter focus on the manipulation of bio-particles. Yet, in many published studies PS particles are used for developing and testing processes [45, 100–105]. The reason behind this choice is the good availability of monodisperse, fluorescent labeled PS particles. The fluorescent labeling makes them easy to detect by using fluorescent microscopy or spectrometers. In addition, the cultivation of cells or other bio-particles is often more time-consuming compared to just dispersing latex spheres. Polystyrene particles can therefore accelerate the research and are also used for process development in this thesis.

The microchannels based on iDEP that were developed within the last decades may lack volumetric throughput, but showed high selectivity which can be important for detecting, for example, tumor cells [9, 106]. Also, iDEP devices are often capable of working with aqueous suspension which increases cell viability and additionally allows separations due to frequency shifts because of its high

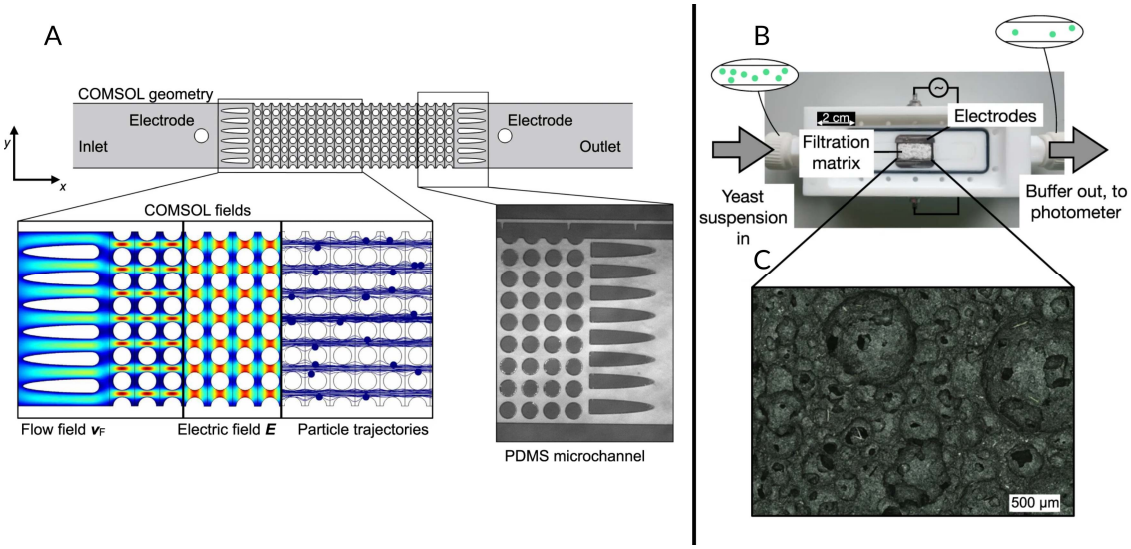

Figure 3.2: A: Microchannel with arrays of insulating posts. Electric field, fluid field and particle trajectories are simulated with COMSOL. A bright-field microscopic image shows the microchannel in detail. B: Macroscopic high throughput iDEP separator that features a ceramic foam (C) to scatter the electric field. This figure is remixed from figures from [45] (published under CC BY 4.0 license).

dielectric constant (see Chapter 3.3). Nonetheless, higher throughput in combination with selectivity remains desirable. Over the last years, the Thömings research group, out of which this thesis also originates, focused on developing scaleable iDEP setups that combine throughput and selectivity. Starting from microchannels (Figure 3.2 A) that operate below 1 mL/h, the flow rate could be increased by several orders of magnitude.

Malte Lorenz and Georg Pesch from this group developed a switchable DEP filter (Figure 3.2 B). They used a ceramic foam as insulating structure placed between two stainless steel plates acting as electrodes. The device operates at up to 9 mL/min and is capable of trapping yeast, polystyrene (PS) particles or separating PS from graphite. Voltages up to 600 V_{rms} ($\approx$ 1700 V_{pp}) and frequencies up to 15 kHz were applied in aqueous suspensions. [45, 46, 107] The frequency range for high throughput iDEP devices was enlarged in a simple and inexpensive mesh-based setup as Weirauch, Giesler, Baune, Pesch, and Thöming could demonstrate in a recent publication [5] to 75 kHz. This newer setup features a highly regular polypropylene mesh as insulating material, which makes it an easy to scale version of the post arrays known from the microchannels. However, many separations benefit from even higher frequencies in the range of a few hundred

kHz to even MHz. For example, the separation of microalgae depending on their lipid content [25, 108] or the separation of different types of carbon nanotubes [98] can not be addressed with iDEP setups at the current state. In a recent review, Rabbani, Sonker, and Ros conclude that iDEP does offer many advantages, however, the challenge to access higher frequencies and the requirement of high electric potentials to achieve equivalent DEP force compared to eDEP setups, limits the application of iDEP [98]. The reason behind this limitation, in our experience, is the challenge to find a suitable amplifier which can deliver high voltages at frequencies in the upper kHz or even MHz range. Substantially higher frequencies can be achieved by using electrode-based DEP systems, which are discussed in the following section.

3.2 Electrode-based dielectrophoresis

Figure 3.3 A depicts a section of an electrode array. Interdigitated electrodes (IDE) are also used in this thesis and are able to generate high gradients in the electric field and showed applicability at frequencies of 100 MHz and higher [109, 110]. The electrodes can lay flat at one side of the channel and be therefore two-dimensional or implemented as three-dimensional structures [111]. Different electrode geometries exist. For example, interdigitated electrodes (Figure 3.3 A) have arrays of rectangular electrodes [1], castellated electrodes have distinct regions for nDEP trapping [75] and three-dimensional electrodes offer additional degrees of freedom when designing the device [112].

In contrast to iDEP, smaller voltages are required [98] but often clean room techniques are necessary to fabricate eDEP devices which limits the access to this technique. However, as many iDEP setups also are fabricated by photolithography, this is a common drawback of both approaches. For both, iDEP and eDEP, ideas exist how to overcome this limitation [5, 46, 113–115]. One of these approaches is subject of this thesis and shown in Chapter 6 and 7. A closer look into the plurality of eDEP setups is provided in the following to highlight the differences of the techniques presented in the literature and those of that are subject this thesis.

Arrays of electrodes are very common in DEP setups as they can develop high field gradients at low voltage. The electric field distribution has been studied extensively in the last decades and can not only be solved numerically [116] but also analytical solutions exist [117, 118]. Competing forces in these setups as buoyancy, thermal movement, DEP or AC electroosmosis are well described in the literature and scaling laws could be developed [33, 72, 79]. This combination makes them a reasonable selection for many DEP devices and it was also used in all studies of this thesis.

Electrodes can be used to determine the polarizability of single particles. This can be done by detecting the direction of the dielectrophoretic movement, as it is done by the commercially available 3DEP device [18] or by electrorotation [119, 120]. Typically, an electrorotation cell has four electrodes with a 90 ° phase-shifted signal between two neighboring electrodes (Figure 3.3 B) [120]. The rotating electric fields results in a rotation of a particle placed in the setup. By monitoring the rotation speed and direction of the movement, the polarizability can be calculated and used to design experiments. Another approach to obtain values of the effective polarizability of a particle, is to detect the residence time in a dielectrophoretic field-flow-fractionation (DEP-FFF) device and derive it from this data.

In DEP-FFF (bio-)particles are focused on specific streamlines in a parabolic flow profile depending on the interplay of lift force, gravitation, and dielec-

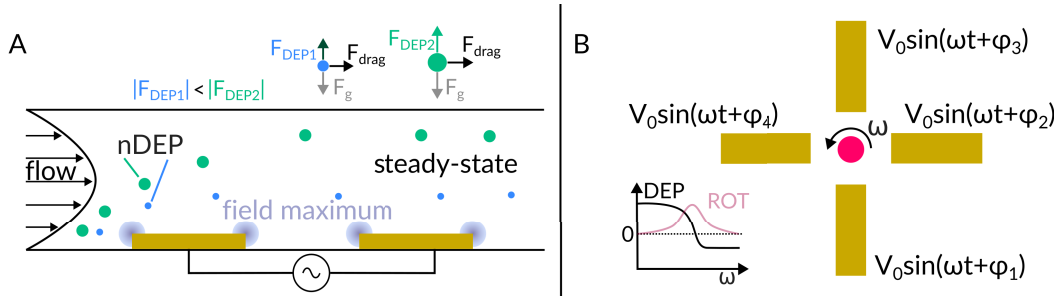

Figure 3.3: Examples of electrode-based DEP devices. A: In a DEP field-flow-fractionation device, particles that show nDEP are levitated to a steady state height until the magnitude of gravity are equal. The levitation height depends on the particle properties. B: In electrorotation a phase shift between electrodes can be used to rotate a polarizable particle. From the rotation spectrum (ROT), the polarizability of a particle can be derived. A is inspired by [121] Figure 1.

trophoresis [55]. If a particle suspension is injected into a carrier flow with a defined flow profile, the crossover frequency can be determined by DEP-FFF straight forward. When testing various frequencies, the frequency where residence time distribution (with sufficiently high voltage applied) of experiments without electric field and those with electric field match, the crossover frequency is found as no retardation due to DEP is observable. The procedure was proposed by Sano, Kabata, Kurosawa, and Washizu [23] and further refined by Gascoyne et.al. [8, 122]. The group around Peter R. C. Gascoyne made important contributions in the field of DEP in general and especially in the area of DEP-FFF and showed interesting applications of this technique. They further demonstrated the usage of flexible electrodes manufactured by a "commercial flex-circuit process"[121]. Their electrodes have 50 µm width and a pitch of 100 µm [121]. Unfortunately, they did not provide the costs of manufacturing for these electrodes. As the minimum feature size of standard commercial PCB manufacturers is about 100 µm [123], the availability of these electrodes used might be limited. The results of this research group are, however, impressive. Starting from the separation of PS microbeads by DEP-FFF [55], they developed processes to remove cancer cells from mixtures [124, 125], differentiate between types of human leukocytes [126] and even the removal and subsequent detection of circulating tumor cells from blood was investigated using the ApoStream apparatus [9, 127]. The ApoStream device is able to process 2.4 mL/min of sample [127], which is in the range of other DEP-FFF systems [15]. In the review „Dielectrophoresis-Field Flow Fractionation for Separation of Particles“ [15] the authors conclude that the throughput of DEP-FFF remains the limiting factor. This is because the DEP force expo-

nentially decreases with increasing distance to the surface of the electrode arrays and thus limits the channel height [15]. The implementation of three-dimensional electrodes is one possibility to further scale the throughput [15, 111].

As the upscaling of eDEP devices by using PCBs is one part of this thesis, some existing approaches that focus on upscaling or PCBs will be presented. Williams, Romero, Parkes, Jackson, and Naber [114] developed a device with PCB structured by milling. According to the authors, this enables low cost patterning of copper-clad boards down to structures of 25 µm. In their study, the feature size was around 100 µm which was sufficient to manipulate 8 µm PS particles in two different electrode configurations. PS particles could be concentrated and their frequency response evaluated by observing their direction of movement. One interesting point about this fabrication method is that the produced electrodes are three-dimensional as the milling produces electrode heights in the range of 36 µm to 80 µm, which is significantly larger than the size of the particles and in the range of the height of many microfluidic devices. These three-dimensional electrodes offer a larger region of high DEP force which can be beneficial for further scaling.

An even earlier approach of using copper clad boards to produce electrode arrays was described by Burt, Al-Ameen, and Pethig in 1989 [128] with standard photolithographic techniques and was based on a design developed a year before [129]. Their board featured two electrode arrays with a size of 5×5 mm. The electrodes were placed 1 mm apart and the optical absorbance was measured in between of the electrodes to determine the dielectrophoretic collection rate. The collection rate for different (bio-)particles as yeast, silicon powder and bacteria was recorded in the frequency range from 1 Hz to 4 MHz allowing to derive data of the polarizability of these particles. The focus of this study was to analyze the frequency response of particles and not their separation.

In a recent publication Faraghat, Fatoyinbo, Hoettges, and Hughes [113] demonstrated approach to increase throughput of eDEP devices while keeping manufacturing costs low. A cutter-plotter is used to cut sheets of conducting and insulating materials which are stacked upon afterward (Figure 3.4). A cutter-plotter is a device that features a blade which position and movement is computer-controlled and thus can be used to cut thin sheets of a material with a high resolution. Due to the stacking, the setup features electrode arrays at the walls and was successfully tested by continuously separating live from dead yest cells via guiding them into different outlets via nDEP and pDEP. In the study a maximum flow rate of 0.5 mL/min was tested.

Electrode arrays on membranes were also used to prevent clogging in filtration processes with flow rates of up to 12 mL/min [130] or even 258 L/(hm^2) [131]. The latter one featured an effective surface area of the membrane of 162 cm^2,

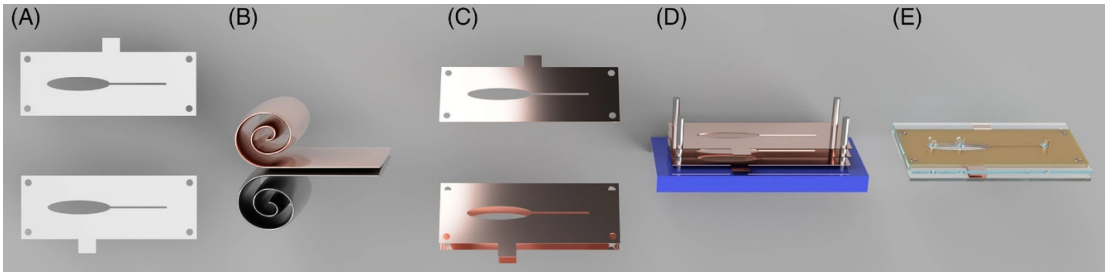

Figure 3.4: Overview of the fabrication process of the device described in [113]. Templates of the layers (A) with connection pads at the side and holes for alignment. The layers were made of adhesive layers that were bonded to a conductive material (B). The final layers (C) than were assembled by using alignment posts (D). The stack of layers then was sealed by using glass slides (E). Figure originally from [113] (published under CC BY-NC-ND 4.0 license).

resulting in a flow rate of the permeate of 70 mL/min. It could be shown that DEP can be used to enhance the performance of submerged membranes as DEP can repel particles from the surface of the membranes that would otherwise clog its pores. In these two publications, the focus is not on selective trapping of particles, but on repulsion of particles to reduce clogging. The authors did not test the impact of particles that would show pDEP at the process parameters. In Reference [130] the authors conclude, however, that this method is not applicable for conductive particles.

In 2017 Moschou and Tserepi summarized in „The Lab-on-PCB Approach“ [123] the current approaches of using commercially available custom designed PCB boards to reduce costs in the field of micro total analysis systems (µTAS). In their review, sensor arrays and microfluidic devices are listed, that are similar to approaches of eDEP used in the literature. The commercial manufactures of custom designed PCB boards allow manufacturing large scale (e.g., 46×61 cm [123]) PCB boards with feature sizes down to 100 µm, making them promising candidates for DEP setups. In two of the presented studies within this thesis (Chapter 6 and 7), large scale electrode arrays reach throughput as high as 10 mL/min while still being able to reach high frequencies up to 500 kHz.

3.3 Frequency shifts in dielectrophoresis

The studies in Chapter 4 and 5 focus on the development of a fast and chromatographic separation technique by using a frequency modulation method. As the polarization of a particle is frequency-dependent according to Equation 2.42 and

2.34, frequency shifts are an established tool to manipulate the DEP response of particles. In the following differences between approaches in the literature and those presented in our studies will be highlighted.

The modulation of a frequency in the context of DEP can be used to account for distributed cell properties in DEP-FFF. In 2000 Yang, Huang, Wang, Becker, and Gascoyne [126] maximized the differences in levitation heights of leukocyte subtypes through sweeping the frequency and additionally avoided that cells are being irreversibly trapped during the experiments. In separation experiments two types of leukocyte were present. A frequency sweep was applied for 8 to 10 minutes. The frequencies between which was swept were selected in such a way that only one species can elute whereas the other remains in the channel. Subsequently, a fixed frequency was applied to levitate the remaining cells in the DEP-FFF chamber and elute them. A similar procedure was applied by this research group to separate T-lymphocytes from $CD34^+$ hematopoietic stem cells [125]. Years later, Shim, Stemke-Hale, Noshari, Becker, and Gascoyne [122] modified the approach by decreasing the frequency continuously. They started at a frequency at which all cells showed pDEP (100 kHz or 300 kHz) and then, due constantly decreasing it to 15 kHz over a duration of 600 s, release the cells depending on their crossover frequency. In contrast to these studies, we aimed to develop a more rapid separation of the particles. In the protocol in Chapter 4 and 5, we swept the frequency in such a way that all suspended particles are eluted fast and without the requirement to set a fixed frequency. The separations were achieved in below 100 s. However, significantly higher voltages were applied compared to those in References [126], [122] and [125], which might limit the applicability or call for adjustments for some type of cells as otherwise electroporation could harm the cells. For more details to this technique please consider reading Chapter 4.

Hakoda and Otaki [132] published a similar approach as the one we used in our study. Here, frequency decreased from 300 kHz to 1 kHz over at least 30 s to 240 s and then starting at 300 kHz again. They tested their device with mouse cancer cells and yeast. Yeast could not be retarded using this device, whereas the cancer cells showed retardation. Although it is quite essential data, no absolute retention times or chromatograms are shown in their study. Thus, it is hard to evaluate and to compare the results. Their sweeping times are substantially higher compared to our studies (3.33 s vs. min. 30 s) and the flow rate was much lower with 0.25 mL/h compared to 5 mL/h in our studies.

Another publication by Modarres and Tabrizian in the year of 2019 [76] introduced the so-named frequency hopping DEP in a microfluidic channel based on interdigitated electrodes. In contrast to the approaches by the group of Gascoyne, the changes of frequency here were conducted more abrupt. The authors demonstrated trap and release cycles of 10 µm, 5 µm and 3 µm PS-particles as

well as the enrichment of MCF7 cancer cells from a mixture with red blood cells. The results were quantified via flow cytometry. However, the flow rates were low ($40 - 80$ µL/h) and the required time to separate the samples were not specified in their report. Nonetheless, their report showed once more the benefits that frequency changes can have.

A study that resulted in a chromatographic separation of spherical and ellipsoidal PS particles by using a frequency shift was published by my colleague Laura Weirauch as first author in 2022. The device features two transparent ITO electrodes in the size of a microscopy slide which makes it possible to observe the motion of suspended particles via microscopy (Figure 3.5 A & B). Between the electrodes, a PP-mesh is sandwiched with pores significantly larger than the particles. Upon application of an electric potential, the mesh scatters the otherwise homogeneous field which leads to DEP of the suspended particles. This device shows a relatively high range of frequencies that can be applied (up to 75 kHz). In combination with the flow rate of 2 mL/min and the high achievable recovery rates (Figure 3.5 C & D), it has an interesting combination of parameters.

3.4 Conclusion

Within this chapter different eDEP and iDEP approaches were presented and challenges highlighted. Especially, the combination of throughput, selectivity and frequency bandwidth is an unresolved challenge in the field of separations with DEP. As eDEP approaches require lower voltage and thus allow higher bandwidth, eDEP devices are used within this thesis. High bandwidth does not only allow choosing a frequency where effects as ACEO are negligible, but, it can also be crucial to allow separation at all, as magnitude and direction on DEP can be frequency dependent.

The frequency dependency of the DEP force is exploited in the following two chapters that describe the frequency modulated dielectrophoretic particle chromatography. While this approach offers rapid chromatographic separation, it is realized in a microfluidic channel with a rather low throughput in the mLmin^{-1} range. This drawback is addressed by the two studies that are presented afterward and focus on the upscaling of eDEP separators.

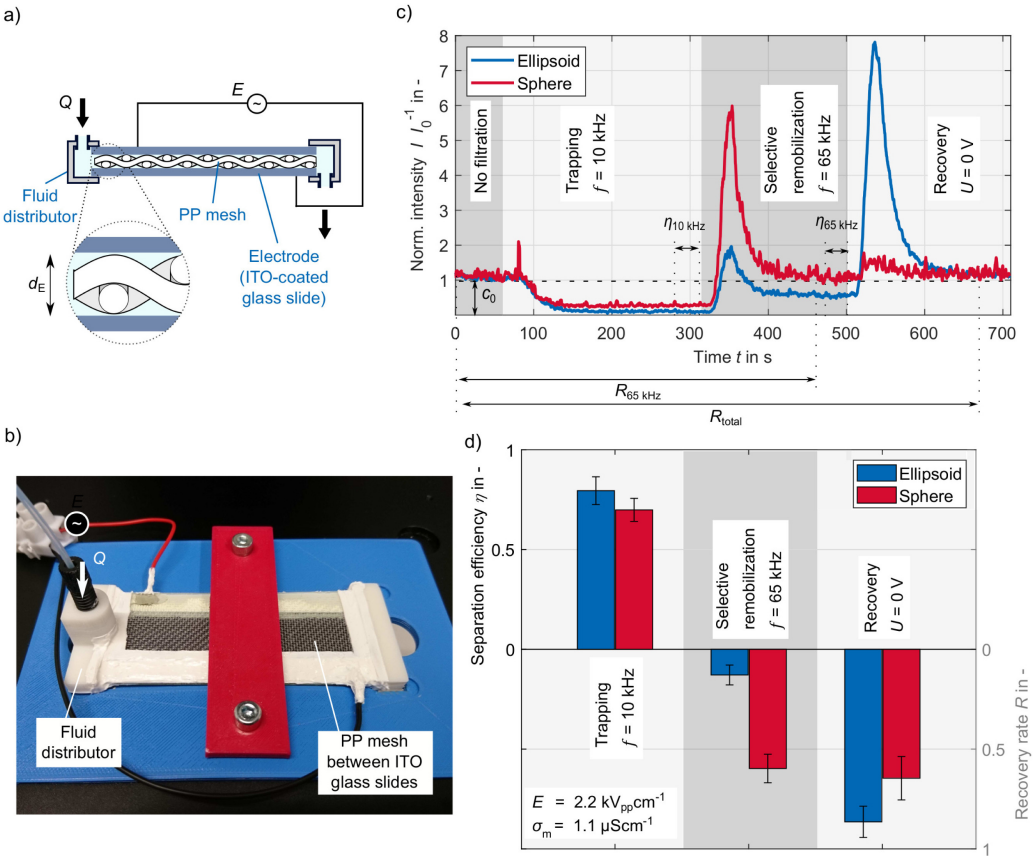

Figure 3.5: a) and c) Mesh-based setup in which frequency shifts can be used to selectively trap and release PS particles via shift from pDEP to nDEP by varying the frequency. b) Both, spherical and ellipsoidal particles are trapped at 10 kHz. Afterward, frequency is shifted to 65 kHz to release spherical particles primarily. When the voltage is turned off, trapped ellipsoids are released. d) The device shows substantial trapping and recovery depending on frequency and voltage for both particles. Figure originally from [5] (published under CC BY 4.0 license).

4 Dielectrophoretic particle chromatography I

This study was previously published as

Giesler, J.; Pesch, G. R.; Weirauch, L.; Schmidt, M.-P.; Thöming, J.; Baune, M. Polarizability-Dependent Sorting of Microparticles Using Continuous-Flow Dielectrophoretic Chromatography with a Frequency Modulation Method. *Micromachines* **2019**, *11*, 38, DOI: 10.3390/mi11010038.

This manuscript aims to introduce the frequency modulated dielectrophoretic particle chromatography (DPC) and provides a proof-of-principle experiments. The supporting information can be found in the online version of the published article at https://doi.org/10.3390/mi11010038. The supporting information contain videos that illustrate the chromatogrpahic separation in the experiment.

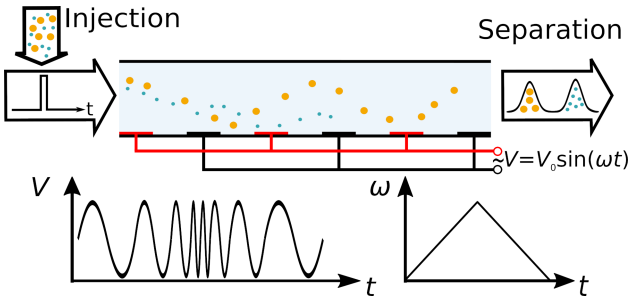

Figure 4.1: Graphical abstract of the publication. A particle suspension is injected in a carrier flow. An electrode array is creating an inhomogeneous electric field that give rise to DEP. The frequency of the electric field (ω) changes periodically. The particles experience a retardation depending on their dielectrophoretic mobility and thus a fractionation is achieved. Figure was previously published as graphical abstract of [1] (published under CC BY 4.0 license).

micromachines

MDPI

Article

Polarizability-Dependent Sorting of Microparticles Using Continuous-Flow Dielectrophoretic Chromatography with a Frequency Modulation Method

Jasper Giesler [1], Georg R. Pesch [1,2,*], Laura Weirauch [1], Marc-Peter Schmidt [3], Jorg Thöming [1,2] and Michael Baune [1]

1 Chemical Process Engineering, Faculty of Production Engineering, University of Bremen, Leobener Straße 6, 28359 Bremen, Germany; j.giesler@uni-bremen.de (J.G.); lweirauch@uni-bremen.de (L.W.); thoeming@uni-bremen.de (J.T.); mbaune@uni-bremen.de (M.B.)

2 MAPEX Center for Materials and Processes, University of Bremen, 28359 Bremen, Germany

3 Department of Engineering, Brandenburg University of Applied Sciences, Magdeburger Straße 50, 14770 Brandenburg an der Havel, Germany; schmmarc@th-brandenburg.de

* Correspondence: gpesch@uni-bremen.de

Received: 7 November 2019; Accepted: 23 December 2019; Published: 28 December 2019

Abstract: The separation of microparticles with respect to different properties such as size and material is a research field of great interest. Dielectrophoresis, a phenomenon that is capable of addressing multiple particle properties at once, can be used to perform a chromatographic separation. However, the selectivity of current dielectrophoretic particle chromatography (DPC) techniques is limited. Here, we show a new approach for DPC based on differences in the dielectrophoretic mobilities and the crossover frequencies of polystyrene particles. Both differences are addressed by modulating the frequency of the electric field to generate positive and negative dielectrophoretic movement to achieve multiple trap-and-release cycles of the particles. A chromatographic separation of different particle sizes revealed the voltage dependency of this method. Additionally, we showed the frequency bandwidth influence on separation using one example. The DPC method developed was tested with model particles, but offers possibilities to separate a broad range of plastic and metal microparticles or cells and to overcome currently existing limitations in selectivity.

Keywords: dielectrophoresis (DEP); microparticles; polystyrene; chromatography; interdigitated electrodes; microfluidic; separation

1. Introduction

Separating microparticles according to specific properties such as size, material, and shape is a research area of great interest for instance in cell or biomolecule manipulation [1–5] and waste recovery [6,7]. To separate microparticles, field-flow fractionation [8], gel electrophoresis [9], and size-exclusion chromatography [10] are state-of-the-art approaches. A major drawback of these approaches is their low throughput or low selectivity for particle mixtures with similar separation properties (e.g., shape, density) below a particle size of 10 µm [11–13]. Dielectrophoresis (DEP), which is referred to as the movement of polarizable particles in an inhomogeneous electric field, offers an alternative tool to address a wide range of particles and at the same time is able to achieve relevant throughputs [14,15]. The dielectrophoretic force not only depends on one specific property of a particle, but on a variety of particle properties, such as size [16,17], permittivity, and electrical conductivity [1], allowing for multi-dimensional particle fractionation. Apart from

established DEP concepts such as field-flow fractionation [17,18], filtration [19], selective trapping (e.g., insulator-based dielectrophoresis) [20], dielectrophoretic particle chromatography (DPC) is a promising concept to achieve high throughput separation of particles. Since DPC was introduced by Washizu et al. [5], different approaches were done using selective trapping of particles [21,22], packed bed columns [23], or stepwise change of the frequency [24]. DEP chromatography proved to be very successful in isolating circulating breast tumor cells (CTCs) from blood [25] at a very low concentration. Such studies later led to the development of a clinical high throughput device to separate CTCs from blood samples [26,27]. Aldaeus et al. [28] developed an analytical model for a DPC device that was based on multiple trap and release cycles for fractionation. A related technique to manipulate micrometer sized particles is using traveling wave dielectrophoretic separators [29,30]. In these microfluidic devices, a 90° phase angle is present between adjacent electrodes, which changes the dielectrophoretic movement a particle experiences [31,32]. Such traveling wave systems offer versatile particle separation techniques, but are usually complex to fabricate and operate [30,33]. The other presented dielectrophoretic chromatography techniques have in common that they depend on strongly diverging polarizabilities (e.g., one type of particle showing positive dielectrophoresis, whereas the other particles show negative dielectrophoresis or exhibit no dielectrophoretic movement). This requirement limits the applicability when addressing particle mixtures with less pronounced differences in polarizability. Addressing binary (or more) mixtures in which there is heterogeneity in the two (or more) classes is even more complex, especially when the cross-over frequencies of the classes are so close that the heterogeneity causes an overlap (an example is the separation of cells according to only small differences in their expression).

Here, we introduce the novel concept of frequency modulated dielectrophoretic particle chromatography. The frequency of the applied field changes constantly to exploit small differences in the dielectrophoretic mobilities of target particles. In this technique, by switching the frequency, we switch between positive and negative dielectrophoretic movement of target particles to generate multiple trap-and-release cycles, which leads to a polarizability dependent chromatographic separation. In principle, this allows separating particles that even show only minute differences in their polarizability and to separate mixtures with heterogeneity in the classes. The simplicity of our approach allows for a simple fabrication and operation and could be easily scaled up by using different ways to introduce the electric field gradient (for example using a porous medium as demonstrated in our recent work [14]).

2. Method

2.1. Theory

In classic chromatographic processes (e.g., gas chromatography), mixtures are separated due to different interactions of the sample and stationary phase, leading to characteristic retention times for each class in the sample. In dielectrophoretic particle chromatography, the stationary phase is represented by the inhomogeneous electric field rising over interdigitated electrodes. The electrode chip forms the bottom of a microfluidic device, where a polydimethylsiloxane (PDMS) channel is used as the separation column. The microparticle suspension is injected into the flow chamber and further transported by a carrier flow. The electrodes are connected to an AC voltage source to generate a highly inhomogeneous electric field. This gives rise to a dielectrophoretic force on the particle caused by the action of the inhomogeneous field on the induced dipole (or multipole) of the particle. In the simple point-dipole approximation, the dielectrophoretic force $\mathbf{F}_{\mathrm{DEP}}$ can be expressed as:

$$\mathbf{F}_{\mathrm{DEP}} = \pi r_{\mathrm{p}}^3 \varepsilon_{\mathrm{m}} \mathrm{Re}\left(\frac{\tilde{\varepsilon}_{\mathrm{p}} - \tilde{\varepsilon}_{\mathrm{m}}}{\tilde{\varepsilon}_{\mathrm{p}} + 2\tilde{\varepsilon}_{\mathrm{m}}}\right) \nabla |\mathbf{E}|^2, \tag{1}$$

with r_{p} representing the particles radius, $\nabla|\mathbf{E}|^2$ the electric field gradient squared, and $\tilde{\varepsilon}_{\mathrm{p}}$ the complex permittivity of the particles and the medium ($\tilde{\varepsilon}_{\mathrm{m}}$), respectively. The velocity due to

dielectrophoresis, $\mathbf{v}_{\mathrm{DEP}}$, in a stationary fluid can be calculated by dividing the dielectrophoretic force by the friction factor f^*:

$$\mathbf{v}_{\mathrm{DEP}} = \mu_{\mathrm{DEP}} \nabla |\mathbf{E}|^2 = \frac{\pi r_{\mathrm{p}}^3 \varepsilon_{\mathrm{m}} \mathrm{Re}\left(\frac{\tilde{\varepsilon}_{\mathrm{p}} - \tilde{\varepsilon}_{\mathrm{m}}}{\tilde{\varepsilon}_{\mathrm{p}} + 2\tilde{\varepsilon}_{\mathrm{m}}}\right) \nabla |\mathbf{E}|^2}{f^*}. \tag{2}$$

Here, μ_{DEP} is the dielectrophoretic mobility, which not only provides the direction of the movement of the microparticles, but incorporates the radius of the particles and fluid properties additionally. The direction of the DEP force can be determined by calculating the real part of the Clausius–Mossotti factor $\mathrm{Re}(CM)$:

$$CM = \frac{\tilde{\varepsilon}_{\mathrm{p}} - \tilde{\varepsilon}_{\mathrm{m}}}{\tilde{\varepsilon}_{\mathrm{p}} + 2\tilde{\varepsilon}_{\mathrm{m}}}. \tag{3}$$

The complex permittivity expands the permittivity ε of a material and incorporates the material's conductivity σ and the angular frequency ω of the electric field:

$$\tilde{\varepsilon} = \varepsilon_0 \varepsilon_{\mathrm{r}} - i\frac{\sigma}{\omega}. \tag{4}$$

For low frequencies, Re(CM) is dominated by the conductivity of the material. With increasing frequency, the permittivity becomes more important. When particles are less polarizable than the surrounding medium ($\mathrm{Re}(CM) < 0$, negative DEP), they move against the electric field gradient and towards low field regions. On the contrary, more polarizable particles ($\mathrm{Re}(CM) > 0$, positive DEP) are directed with the gradient towards field maxima. In the current setup, field maxima are located close to the edges of the interdigitated electrodes at the bottom, and local field minima can be found at the top of the channel. Depending on the polarization, particles are either attracted to the edges of the electrode (positive, pDEP) or to the top (negative, nDEP). Therefore, the movement direction will be strongly affected by the applied field's frequency due to the frequency dependence of Re(CM) (Equation (4)). Particles can become trapped in potential wells (field extrema) due to DEP and can adhere to the walls of the device when they reach them.

The conductivity of small insulating particles (such as the polystyrene particles that are used in this study as a model) is dominated by their surface conductance K_{S} [34]:

$$\sigma_{\mathrm{p}} = \frac{2K_{\mathrm{S}}}{r_{\mathrm{p}}}. \tag{5}$$

Usually, K_{S} is assumed to be around 1 nS for polystyrene particles [35]. Equation (5) leads to a (with increasing particle diameter decreasing) net conductivity of polystyrene particles ($1\,\mu\mathrm{m} < d_{\mathrm{P}} < 10\,\mu\mathrm{m}$) of around $4\,\mu\mathrm{S\,cm^{-1}}$ to $40\,\mu\mathrm{S\,cm^{-1}}$, which is higher than some low conductive DEP buffers. This allows for positive DEP manipulation at low frequencies of even electrically insulating particles, when they are smaller than a certain threshold diameter.

To evaluate the resolution of a chromatographic separation, R_{S} can be calculated [28],

$$R_{\mathrm{s}} = \frac{\Delta t}{\frac{1}{2}(w_1 + w_2)}, \tag{6}$$

with Δt as the separation time between the maximum values (I_{max}) of two peaks and w_{x}, the width of the two residence time distributions. The width is defined as the distance in time between the half maximum values (FWHM).

2.2. Device Operation

The device proposed here, a microfluidic channel with interdigitated electrodes at the bottom of the channel (Figure 1b), uses periodic changes from pDEP to nDEP or vice versa to separate

particles with respect to their polarizability. Since the polarizability of a particle directly depends on the frequency of the electric field, constant frequency changes (Equation (7)) can be used to manipulate the particles' position in the separator. To achieve a retardation, due to either nDEP or pDEP, particles are dragged out of the fast streamlines in the center of the channel to streamlines with low fluid velocity at the bottom or top. Then, when the frequency changes, the pDEP or nDEP effect is reversed, and particles are pushed back into the faster streamlines in the center of the channel. Depending on the strength of the interaction of a particle with the field (i.e., the absolute value of Equation (3)), particles with different polarizabilities experience different retardation. Unlike DEP field-flow fractionation, there is no particle equilibrium position. Here, the periodic change of frequency leads to a constant change of the particles position and, therefore, depending on the polarizability of a particle, to a different average velocity.

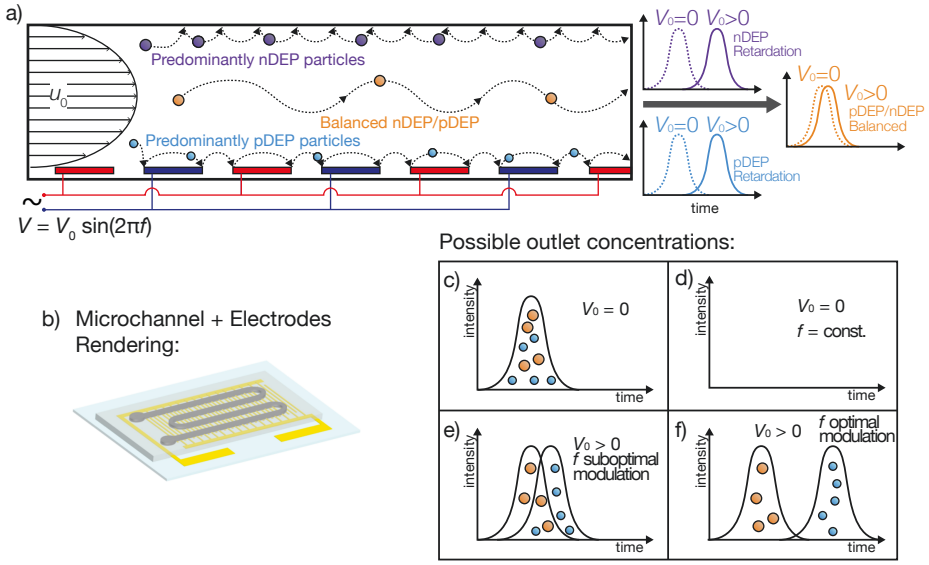

Figure 1. (**a**) Sketch of the DPC separation experiments. (**b**) Sketch of the DPC separation column. Meandering PDMS microchannel sealed by interdigitated electrodes on a glass chip. (**c**–**f**) Different possible outlet concentrations for DPC. (**c**) Without voltage, no retardation of the particles occurs, and both fractions elute at the same time. (**d**) When a voltage is applied and the frequency is fixed, the particles are trapped in the column due to DEP and will not exit the channel. If the frequency is modulated, a chromatographic separation occurs (**e**), which can be optimized by changing the frequencies and voltage (**f**).

In case a particle gets trapped in potential wells because of dielectrophoresis or adheres to the surface of the channel due to non-specific adsorption, a particle resuspension requires a force pointing away from the wall, which is in our case again DEP. Naturally, to reverse the trapping movement, particles trapped by pDEP now have to experience nDEP and vice versa (Figure 1a). Especially for particles trapped at the bottom of the channel, a resuspension via an external force becomes important, since no gravitational force contributes to their remobilization. Further, as the particles' diameter decreases, the gravitation force becomes less important and therefore may not be sufficient to resuspend small particles close to the ceiling of the channel. To achieve a retardation of the particles and consequently a chromatographic separation, it is in general not necessary to fixate particles at the bottom or ceiling. To generate an increase in retention time, particles are just required to be transported into regions of low fluid velocity, which are present at the bottom (transport via pDEP) or the ceiling (nDEP) of the channel. Apart from the approach taken here, which is to modulate the frequency to reverse the particle polarization and the DEP force vector's direction, in principle, it would also be possible to change the polarization by changing the medium's conductivity.

Depending on the particle's Clausius–Mossotti factor as a function of frequency (Equation (3)), three different scenarios can be distinguished (Figure 1a): (I) A particle shows substantial more pDEP than nDEP during the modulation spectrum and therefore predominantly moves towards the bottom of the channel, where the electrodes induce a high electric field strength. Since the fluids' velocity close to the bottom is low, particles are slowed down by the lower fluid velocity or by getting reversibly trapped at the electric field maxima. The particles are then pushed away from the electrodes by nDEP when the frequency changes. This scenario effectively increases the particle's residence time. (II) When a particle exhibits a balanced pDEP and nDEP movement, the retardation is less pronounced. These microparticles travel towards high field regions when the CM factor is positive and away from them when it is negative. Due to their constant movement orthogonal to the fluid-flow direction, they spend less time in regions with low fluid velocities and therefore are eluted fast. (III) If nDEP outweighs pDEP, particles are predominantly pushed towards low field regions, which here are present at the channel's ceiling. Like in Scenario I, only low fluid-flow is present at the field minima, and the particle's residence time is going to be enlarged. Although the polarizability of particles from Scenarios I and III is different, retention times can be the same. Nevertheless, since the extent of retardation depends on the chosen process parameters (e.g., frequency, voltage), a separation can be possible with a different set of parameters (Figure 1e,f).

Here, the frequency of the applied sinusoidal voltage was modulated using a triangle-shaped function. This allows changing the frequency of the electric field constantly between two values in a controllable time. Consequently, the frequency f can be described as a function of time t:

$$f(t) = f_{\mathrm{A}}\,\mathrm{tri}(2tf_{\mathrm{mod}}) + f_0 \tag{7}$$

with f_{A} as the amplitude of frequency modification, $\mathrm{tri}(x)$ as the triangle function, f_{mod} representing the modulation frequency, and f_0 for the offset of the frequency modulation. As an example, for achieving frequencies between 30 and 270 kHz. the following set of parameters was used: $f_{\mathrm{A}} = 120\,\mathrm{kHz}$, $f_{\mathrm{mod}} = 300\,\mathrm{mHz}$, and $f_0 = 150\,\mathrm{kHz}$. Other modulation functions may also be suitable for achieving a separation.

In this study, we used polystyrene (PS) particles to demonstrate the functionality of the proposed technique. Due to their surface conductance (Equation (5)), PS particles show pDEP at low frequencies and nDEP at high frequencies. With the usually assumed $K_{\mathrm{S}} = 1\,\mathrm{nS}$ [34–36] and a medium conductivity of $\sigma_{\mathrm{M}} = 1.2\,\mu\mathrm{S\,cm^{-1}}$, the cross-over frequency from negative to positive DEP ($\mathrm{Re}(CM) = 0$ in Equation (3)) depends only on particle size (see Figure S1). The frequency dependent polarizability of the particles forms the fundamental aspect of this separation technique and can be used by varying the frequency over time periodically, as shown in Figure 2. These periodical changes from pDEP to nDEP generate multiple trapping and release cycles. The separation technique can also be used for other particle types that show frequency dependent polarizability.

Larger polystyrene particles showed pDEP in a smaller frequency bandwidth and, consequently, when varying the frequency as shown, for a shorter duration. Four different polystyrene particle sizes were chosen to demonstrate the separation effect. With our chosen frequency modulation from 30 kHz to 270 kHz, 3 µm particles showed predominantly positive DEP, 6 µm particles a balanced pDEP/nDEP behavior, and 10 µm particles predominantly negative DEP. Further, we used 2 µm particles to assess the possibility to separate two particle types that both experienced predominantly pDEP.

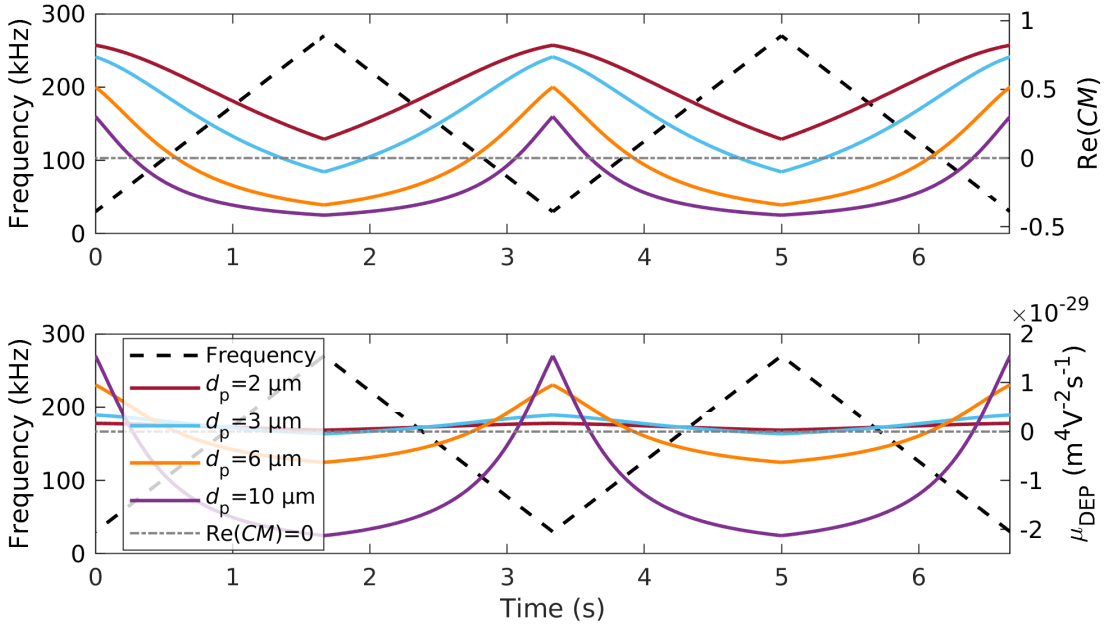

Figure 2. Real part of the Clausius–Mossotti factor Re(*CM*) (top) and dielectrophoretic mobility μ_{DEP} (bottom) of four different polystyrene particles over time for two full cycles (right ordinate axis of diagram). The modulated frequency is shown as well (left ordinate axis). Particles suspended in DI water with $\sigma_{\mathrm{m}} = 1.2\,\mu\mathrm{S\,cm^{-1}}$, $K_{\mathrm{S}} = 1\,\mathrm{nS}$, and $\varepsilon_{\mathrm{m}} = 78.5$, calculated with Equations (3) and (4).

2.3. Device Fabrication

The microfluidic device consisted of two main parts. The column was formed by a 2 mm wide meandering PDMS channel (height 80 µm, length 17 cm), which provided the walls and the top of the channel (Figure 1b). The bottom was formed by the electric field generating electrode chip. Both parts were bonded using an intermediate layer as described later. The PDMS channel were produced using an SU8 master mold (soft lithography). The interdigitated electrodes (electrode arm width and gap width 100 µm) were fabricated using standard cleanroom techniques. Full details of the fabrication method can be found in Section S2.

The electrode covered glass slide was bonded to the PDMS channel using liquid PDMS (10:3, base:curing agent). PDMS was selected as the intermediate layer, because of its well known spinning curves, low toxic potential, and easy accessibility [37–39]. The PDMS mixture was spin coated at 6000 rpm for 330 s on the electrodes. Using these parameters, the thickness of the uncured PDMS layer should be below 3 µm [38]. Subsequently, the cleaned PDMS channel was manually aligned over the electrodes and placed onto them. The bonding was finalized by curing the intermediate layer at 80 °C for an additional two hours. The PDMS did not only allow bonding the electrodes to the channel, which proved to be unsuccessful in our lab using corona bonding; it also reduced the unspecific adhesion of the particles to the electrodes [40]. Since using PDMS as the intermediate layer creates a reversible bonding and PDMS channels are inexpensive to replace, several channels were used during the experiments, and no significant changes between them could be observed.

2.4. Experimental Setup

Two syringe pumps were connected to a manually actuated 4 way valve (H&S V-101D, IDEX Health & Science, LLC, Oak Harbor, WA, USA). One syringe pump (KDS-100-CE, KD Scientific Inc., Holliston, MA, USA) controlled the volume flow of the carrier fluid; the other pump (LEGATO 270, KD Scientific Inc., Holliston, MA, USA) provided the flow of the particle suspension (both $5\,\mathrm{mL\,h^{-1}}$). In the normal position, the carrier flow was connected to the inlet of the separation

column. To initiate the experiment, the valve was manually turned to allow a 2 s pulse of particle suspension to flow into the separator (Figure 1a). The injection in all experiments happened at $t = 10$ s. The carrier fluid was pure water containing 0.02 vol % Tween20 (Sigma-Aldrich, Steinheim, Germany) to reduce particle–wall interactions, 0.003 vol % 0.01 mol L^{-1} potassium hydroxide in deionized water to adjust pH, and potassium chloride to adjust the electrical conductivity to the desired value (1.2 µS cm^{-1}). The particles were suspended in the same suspension as the carrier flow, but without adding potassium chloride.

Monodisperse fluorescent polystyrene particles (Fluoresbrite, Polysciences Europe GmbH, Hirschberg, Germany) of different sizes and colors (2 µm polychromatic red, 3 µm yellow-green, 6 µm polychromatic red, and 10 µm yellow-green plain particles) were mixed and diluted in the described solution.

The inlet of the channel was connected to the manually actuated 4 way valve via a capillary (inner diameter: 100 µm) with a length of about 17 mm. To allow a controlled injection of the particles (i.e., to avoid dispersion of the peak), the internal volume of the connection from valve to channel inlet should be kept as small as possible. The chosen (short and with small diameter) inlet capillary resulted in a volume of 135 nL, resulting in an average residence time of less than 100 ms in this capillary.

The electrodes were connected to a voltage amplifier (PZD2000A, TREK, Lockport, New York, NY, USA) controlled by a signal generator (Rigol DG4062, Rigol Technologies EU GmbH, Puchheim, Germany). The signal generator provided the functionality of frequency modulation inherently. The amplifier's output signal was monitored using an oscilloscope (RIGOL DS2072A, Rigol Technologies EU GmbH, Puchheim, Germany). The amplification factor of the amplifier was not constant, but decreased with increasing frequency. The output decreased by 4.3 % per 10 kHz, which resulted in exponential decay in the applied voltage. All stated voltages were measured at 30 kHz. This circumstance may be overcome by using a different amplifier in future experiments.

The different fluorescent stains of the particles allowed to easily distinguish between them. To observe the particles, an inverted microscope (ECLIPSE Ts2R-FL, Nikon Instruments Europe BV, Amsterdam, The Netherlands) was used. For observation, a 40,6-diamidino-2-phenylindole/fluorescein isothiocyanate/tetramethylrhodamine isothiocyanate (DAPI/FITC/TRITC, excitation: 387/478/555 nm, emission: 433/517/613 nm) triple bandpass was selected, which allowed observing at least three different types of particles at once. However, only two particle colors could be observed simultaneously, since the current optics inhibited the DAPI excitation. Videos of the fluorescence were recorded at the outlet of the channel using a color CMOS camera (GS3-U3-51S5C-C, FLIR Systems Inc., Wilsonville, OR, USA), which were further processed using MATLAB (see Section S2, for further information). In MATLAB, the frames were segmented, resulting in different pictures for each particle and background. Finally, the intensity of each picture was counted and plotted over time.

3. Results and Discussion

Three different main experiments were conducted to demonstrate the different capabilities of the proposed separator: We firstly demonstrate the possibility to separate particles experiencing predominantly pDEP from particles with a balanced pDEP/nDEP behavior. This was done by separating 3 µm particles from 6 µm particles. We further show the separation of predominantly nDEP experiencing particles (10 µm) from particles experiencing balanced pDEP/nDEP (again, 6 µm particles). Finally, we show that even particles that both experience mostly pDEP in the modulated frequency spectrum can be separated by separating 3 µm particles from 2 µm particles. Figure S9 provides Particle Image Velocimetry (PIV) data of 10 µm particles at 100 V_{pp} and 0 V to demonstrate the fluctuation of the velocity due to the nDEP effect. Further, Videos S2 and S3 visualize the separation of 3 µm and 6 µm particles at 80 V_{pp} and 0 V. For such small particles, it was not possible to extract the velocity reliably from the video using PIV. Nevertheless, the velocity fluctuations due to the action of DEP were clearly visible for the 3 µm particles. Unfortunately, from the observation perspective

and with the experimental methods at hand, it was not possible to infer if particles were slowed down because they were attracted to or pushed away from the electrode array.

For the 3 and 6 µm particles, without an electric field, both particles showed typical retention time distributions for a laminar flow without observing separation (as expected; Figure 3a). When applying a voltage with frequency modulation, we could observe a clear chromatographic separation for all investigated voltages, i.e., 60 V_{pp}, 80 V_{pp}, 100 V_{pp}, and 120 V_{pp} (see Figure S4 for the full dataset). To achieve separation, the frequency was varied between 30 kHz and 270 kHz in 3.33 s (full cycle length, 300 mHz). Various parameters for frequency modulation were tested in advance, but this set of parameters worked best. However, the influence of each parameter is not fully understood and needs to be investigated further. While we could observe separation at all voltages, the best resolution for the separation of 3 µm and 6 µm particles could be achieved at a voltage of 80 V_{pp}, resulting in an average resolution of $R_s = 3.60 \pm 0.31$ (number of experiments $N = 4$) (Figure 3b). To provide a visual impression of the separation of 3 µm and 6 µm at 0 V_{pp} and 80 V_{pp}, see Videos S2 and S3.

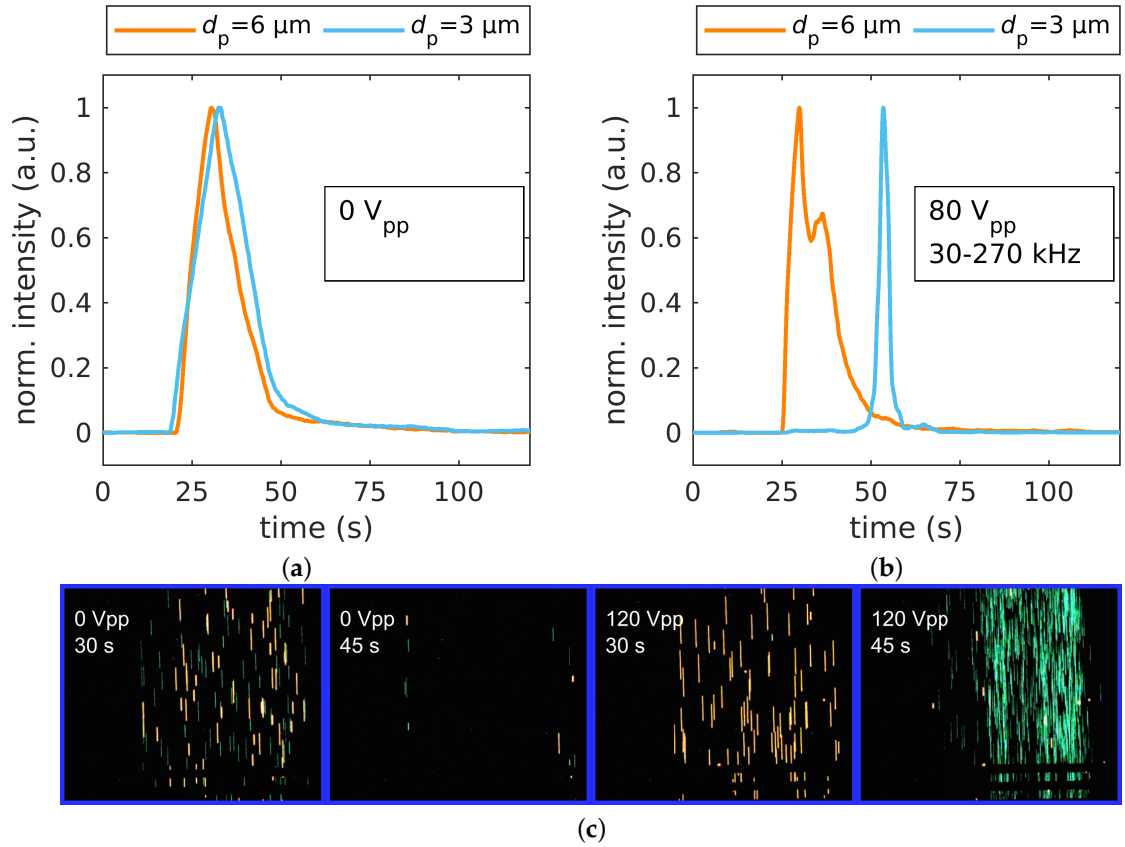

Figure 3. (**a**) Separation of 3 and 6 µm polystyrene particles: fluorescence intensity over time for no applied voltage, $R_s = 0.17 \pm 0.06$ ($N = 4$), and (**b**) when applying 80 V_{pp} at 30 kHz–270 kHz with a modulation frequency of 300 mHz, $R_s = 3.60 \pm 0.31$ ($N = 4$). (**c**) Single frames of different times of 3 µm (yellow-green) and 6 µm (orange/red) fluorescent polystyrene particles (brightness and contrast are adjusted for better visibility).

At all investigated voltages (see Figure S4 and Figure 3b), the 6 µm particles eluted earlier than the smaller particles, which showed a substantial delay with respect to measurements without the electric field. This was because the 3 µm particles showed predominately pDEP in the frequency modulation range and thus were substantially retarded due to the DEP interaction (Figure 2, blue line). Interestingly, the peak size of the 3 µm particles decreased significantly, which suggested that their retention time was dominated by DEP and not by their initial height in the channel, as was visible

in the experiments without applied voltage. In contrast, the peak size and position of the 6 µm stayed almost the same, which was due to the balanced nDEP/pDEP ratio (Figure 2, orange line). This balanced nDEP/pDEP led to a negligible movement orthogonal to the fluid-flow direction over one cycle. Consequently, at low to moderate voltages, particles were only slightly retarded in the channel caused by moving along the different streamlines of the parabolic flow profile. Since the dielectrophoretic velocity increased with increasing electric field strength (Equation (2)) and therefore with increasing applied potential, we assumed that particles traveled greater distances orthogonal to the flow, eventually hitting either the electrode array or channel ceiling, as the voltage increased. We thus assumed that with increasing voltage, also 6 µm particles would experience retardation.

The calculations suggested (Figure 2) that the retardation of the 3 µm PS particles was based on their movement towards the interdigitated electrodes (pDEP). To investigate the effect of nDEP on the retention time, we separated 10 µm particles, which showed predominantly nDEP in the chosen frequency modulation spectrum (Figure 2), from the balanced 6 µm particles (Figure 4). This switch from pDEP dominated behavior, to an nDEP/pDEP -balanced behavior, to an nDEP dominated behavior with increasing particle size was due to the decreasing conductivity of polystyrene particles with increasing diameter (Equation (5)). We observed a chromatographic separation of 10 µm from 6 µm particles (see Figure S5 for the full dataset) for 80 V_{pp}, 100 V_{pp}, and 120 V_{pp} at 30 kHz–270 kHz. As before, the 6 µm particles showed almost no change in their retention time, whereas the larger and less polarizable 10 µm particles showed substantial delay, which indicated a retardation due to nDEP. Figure S9 shows PIV data of the 10 µm particles at 0 V and at 100 V_{pp} to demonstrate how their velocity periodically decreased and increased due to the nDEP effect. This periodic velocity fluctuation corresponded exactly to the applied frequency modulation.

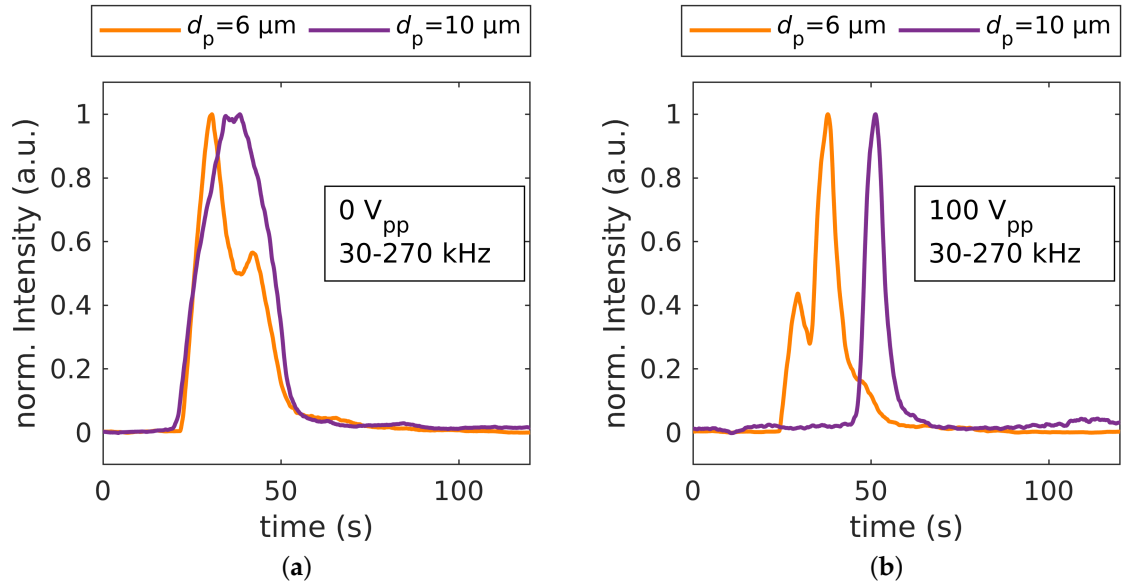

Figure 4. (**a**) Separation of 6 and 10 µm particles: fluorescence intensity over time of without applied voltage, $R_s = 0.21 \pm 0.19$ ($N = 4$), and (**b**) with application of 80 V_{pp} at 30 kHz–270 kHz with a modulation frequency of 300 mHz, $R_s = 1.95 \pm 0.33$ ($N = 4$).

Before we address the more challenging task of separating 2 µm and 3 µm particles that both experience pDEP in the modulation spectrum, we discuss the resolution for the separation of 6 µm from 3 µm and 6 µm from 10 µm (Figure 5). The resolution of the separation of 3 and 6 µm (Figure 5a, green) particles increased with voltage in all conducted experiments until a maximum at 80 V_{pp} was reached, after which the resolution decreased. This was because the retention time of bigger particles increased further with voltage (80 V_{pp}: 27.92 s ± 1.74 s to 160 V_{pp}: 40.8 s ± 3.33 s, both $N = 4$), while the time of the maximum fluorescence intensity for the smaller particles was constant for all voltages investigated,

as long as a voltage was applied. We suspect the increase of the retention time of the 6 µm particles was because of the increased covered distances orthogonal to the fluid-flow. As previously discussed, the higher field strength caused the particles to reach the walls or at least enter regions close to a wall with low fluid velocity (at the top and bottom of the channel) and to be retarded as a consequence.

This decrease in resolution was not observed for the separation of 6 µm and 10 µm particles (Figure 5a, turquoise). Although the retention times of the 6 µm increased monotonically with voltage, the resolution simultaneously increased with applied voltage. The even stronger increase in retention time of the 10 µm particles (80 V_{pp}: 45.61 s ± 5.24 s to 120 V_{pp}: 57.71 s ± 1.6 s, both $N = 4$) compensated the increase from the 6 µm particles. We assumed that the 10 µm particles spent even more time in areas with low fluid velocity, and therefore, the retention time increased. Our PIV measurements (see Figure S9) indicated a periodic interaction of the particles with the electric field. However, the change in velocity was below 20 %, which showed additional potential for increasing the retention time of the 10 µm particles.

To investigate the effect of the voltage on the resolution of the separation process further, particles with diameters of 2 µm and 3 µm were selected. As the mobility of both particles was close to each other, this posed a more ambitious separation problem. Using the same set of parameters as before, we could again observe a voltage dependence of the peak time (see Figure 5b and also Figures S6–S8, for intensity profiles as a function of time). In contrast to the 3 vs. 6 µm and 6 vs. 10 µm experiments, the separation was low for all investigated voltages. This was because μ_{DEP} for both particle types was low and very close to each other.

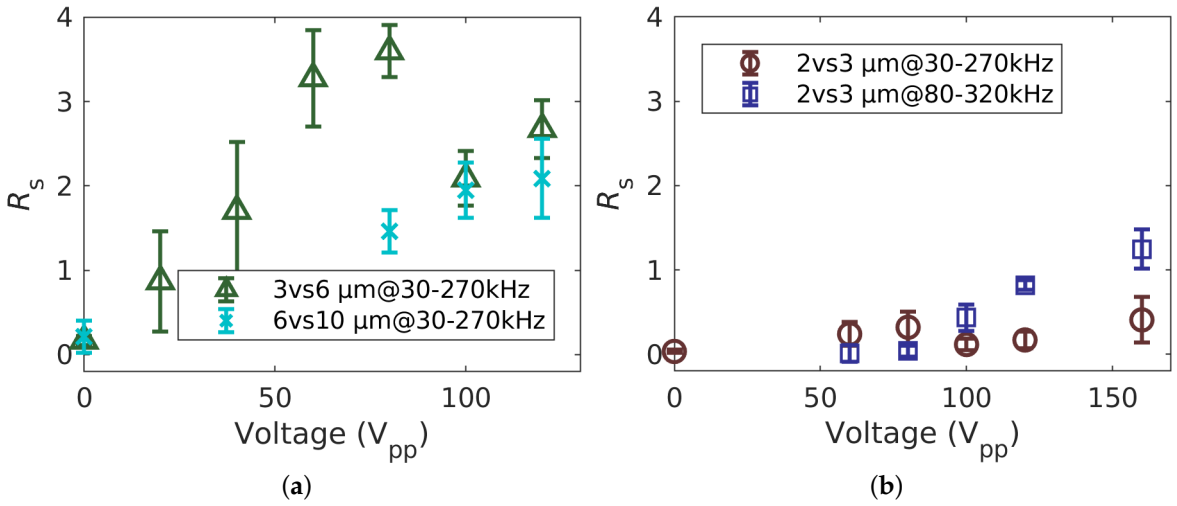

Figure 5. Resolution R_s of DPC over applied voltage for different particle suspensions and frequencies. (**a**) 3 µm vs. 6 µm and 6 µm vs. 10 µm PS particles at 30 kHz to 270 kHz. (**b**) 2 µm vs. 3 µm PS particles at 30 kHz to 270 kHz and 80 kHz to 320 kHz.

The separation of the 2 and 3 µm particles was improved, concerning peak width and peak distance, by changing the frequency between which was varied. Applying an offset of 50 kHz (now: 80 kHz to 320 kHz), the retention times of each particle type became more homogeneous (FWHM decreased) and the distance between the peaks increased (Figure 5b). Interestingly, the resolution was similarly low for both sets of frequencies for all voltages except for 120 V_{pp} and 160 V_{pp}, but the retention times were significantly different. At 120 V_{pp}, where the highest resolution using 30 kHz–270 kHz was achieved, the particles eluted almost 15 s later than when using 80 kHz–320 kHz at the same voltage (2 µm: 55.22 s ± 6.94 s vs. 40.73 s ± 0.75 s, 3 µm: 49.06 s ± 5.32 s vs. 36.86 s ± 0.84 s, both $N = 4$).

We propose that at the lower frequency (30 kHz to 270 kHz), both particles were dominated by pDEP (Figure 2) and thus showed a significant increase in retention time with increasing voltage.

When the frequency set switched to 80 kHz–320 kHz, the pDEP/nDEP behavior was more balanced, i.e., both particles exhibited less pDEP and more nDEP in the modulation spectrum, causing them to interact less with the field and thus to elute earlier. As expected, the subtle differences in polarizability of 2 µm and 3 µm particles in this frequency bandwidth were more pronounced, resulting in a better resolution. Although the residence time of the particles was much shorter when applying 80 kHz-320 kHz, the resolution stayed the same at 100 V_{pp} and increased even further to $R_s = 1.25 \pm 0.23$, $(N = 4)$, when the voltage was set to 160 V_{pp}, which did not occur using the lower frequency set. This highlights one of the potentials of our separation technique, i.e., the possibility to separate particles with very equal polarizabilities by tuning the frequency modulation according to the target particle's polarizabilities. Again, the particles larger in diameter eluted earlier, and in contrast to the 6 µm particles, both particles showed an increase in retention time with respect to the measurements without the electric field and therefore without superimposed dielectrophoretic movement. No maximum in retention time was found for the 2 vs. 3 µm mixture at higher frequency, indicating that a further increase in voltage led to a further increase in resolution.

Since the dielectrophoretic velocity depended quadratically on the particle's radius and the applied electric field, the size and voltage dependency was not surprising. Due to this, smaller particles accelerated less due to DEP. Additionally, the cross-over frequency at which the force switched from pDEP to nDEP was higher, i.e., small particles experienced pDEP for a longer duration per cycle. Consequently, small particles, once they came close to the interdigitated electrodes, remained there and thus in regions of low fluid velocity. The latter point should become more important as the residence time in the separation column increases (i.e., at a longer column length).

Both nDEP and pDEP can be utilized to induce a retardation of the suspended particles. As a consequence, particles with polarizability (e.g., one showing more pDEP, another one dominated by nDEP) can elute at the same time. However, as the frequencies and the modulation frequencies can be adjusted, the nDEP/pDEP ratio can be tuned, which should result in different retention times and lead to a chromatographic separation.

Despite the fact that the parameters were chosen by evaluating the mobility of the particles over the frequency and only model particles were evaluated, the technique can become a tool for chromatographic separation of arbitrary particles that show a frequency dependent polarizability. One major advantage of this technique is that the columns' parameters were adjustable without actually changing the column itself. As shown, the electric field strength and the frequency bandwidth had an impact on the retention times and the peak width. Joule heating could disturb the separation when mediums with higher conductivities are used (e.g., cell buffer) [41]. To reduce the required voltage, by maintaining a similar electric field strength, the thickness of the isolating layer on the electrodes could be reduced. Promising alternatives to PDMS to achieve thinner coatings are polymers with a lower viscosity (e.g., SU-8). Additionally, since the electric field decreases with the height of the channel significantly, channels with a reduced height could be used.

4. Conclusions

We experimentally showed the separation of three binary mixtures of suspended particles using dielectrophoretic particle chromatography with a modulated electric field frequency. The current data further suggested that a separation of three different particle types (for example 2, 3 and 6 µm) in a single experiment should be possible. Unfortunately, it was not possible to observe all three different kinds of particles at the same time with the current hardware. We believe that an increasing column length led to a better separation. In addition to this, when the injection valve was operated automatically (in contrast to the current manual operation), standard deviations should decrease significantly. The influence of other parameters such as the modulating frequency, the medium's electrical conductivity, the linearity of amplification, and the carrier fluids' volume flow are complex and not yet understood in detail. Comprehensive studies regarding their impact using experiments and simulations are under way. Nevertheless, we demonstrated the

principle and discussed the effect of the applied voltage. We further showed how adapting the modulation frequency to the target particle's polarizabilities further increased the resolution. In the proposed chromatography column, no single trap-and-release mechanism was used to achieve a chromatographic separation, but the particles showed different interactions with the permanently present and adjustable stationary phase. Although we only studied model particles in this study, the presented method allowed chromatographically separating arbitrary particles with frequency dependent polarizabilities. We believe that the presented technique can potentially separate particle mixtures that are traditionally difficult to separate, for instance cell separation in liquid biopsy or the recovery of precious materials from waste streams.

Supplementary Materials: The following are available online at http://www.mdpi.com/2072-666X/11/1/38/s1, Section S1: Method; Section S2: Device Fabrication; Section S3: Post-Processing; Section S4: Further Experimental Results; Figure S1: Real part of Clausius-Mossotti factor and DEP mobility; Figure S2: Gold electrodes and photomask; Figure S3: Result of segmentation process; Figure S4: Fluorescence intensity over time of 3 µm and 6 µm particles; Figure S5: Fluorescence intensity over time of 6 µm and 10 µm particles; Figure S6: Fluorescence intensity over time of 2 µm and 3 µm particles at 120 V_{pp}; Figure S7: Fluorescence intensity over time of 2 µm and 3 µm particles at 160 V_{pp}; Figure S8: Fluorescence intensity over time of 2 µm and 3 µm particles at different voltages; Figure S9: PIV data of 10 µm PS particles; Video S1: 10um_100Vpp_PIVdata.mp4, Video of periodic velocity changes of 10 µm particles; Video S2: DPC_0Vpp_3vs6umPS.mp4, Video of 3 µm and 6 µm particles without applied voltage; Video S3: DPC_80Vpp_3vs6umPS.mp4, Video of 3 µm and 6 µm particles at 80 V_{pp}.

Author Contributions: J.G., G.R.P., M.B., and J.T. conceived of the experiments. J.G. conducted the experiments. M.-P.S. fabricated the electrodes and SU8 master and contributed their layout. J.G., G.R.P., L.W., M.B., and J.T. analyzed the results. G.R.P. and M.B. supervised the project. J.G. wrote the manuscript with input from all other authors. All authors have read and agreed to the published version of the manuscript.

Funding: This work was funded by the German Research Foundation (DFG) within the priority program, "MehrDimPart—Highly specific and multidimensional fractionation of fine particle systems with technical relevance" (SPP2045, Grant Numbers BA 1893/2-1, TH 893/20-1, and project number 382064650).

Acknowledgments: The authors thank Jonathan Kottmeier (IMT, TUBraunschweig) for the help in manufacturing the components of the separation column and Fei Du (CVT, Universität Bremen) for fruitful discussions.

Conflicts of Interest: The authors declare no conflict of interest.

Abbreviations

The following abbreviations are used in this manuscript:

AC	alternating current
CM	Clausius–Mossotti factor
DEP	dielectrophoresis
DPC	dielectrophoretic particle chromatography
FWHM	full width at half maximum
nDEP	negative dielectrophoresis
pDEP	positive dielectrophoresis
PDMS	polydimethylsiloxane
PS	polystyrene

References

1. Vahey, M.D.; Voldman, J. An equilibrium method for continuous-flow cell sorting using dielectrophoresis. *Anal. Chem.* **2008**, *80*, 3135–3143, doi:10.1021/ac7020568. [CrossRef] [PubMed]
2. Moon, H.S.; Kwon, K.; Kim, S.I.; Han, H.; Sohn, J.; Lee, S.; Jung, H.I. Continuous separation of breast cancer cells from blood samples using multi-orifice flow fractionation (MOFF) and dielectrophoresis (DEP). *Lab Chip* **2011**, *11*, 1118, doi:10.1039/c0lc00345j. [CrossRef] [PubMed]
3. Henslee, E.A.; Sano, M.B.; Rojas, A.D.; Schmelz, E.M.; Davalos, R.V. Selective concentration of human cancer cells using contactless dielectrophoresis. *Electrophoresis* **2011**, *32*, 2523–2529, doi:10.1002/elps.201100081. [CrossRef] [PubMed]

4. Wang, X.B.; Yang, J.; Huang, Y.; Vykoukal, J.; Becker, F.F.; Gascoyne, P.R.C. Cell separation by dielectrophoretic field-flow-fractionation. *Anal. Chem.* **2000**, *72*, 832–839, doi:10.1021/ac990922o. [CrossRef] [PubMed]
5. Washizu, M.; Suzuki, S.; Kurosawa, O.; Nishizaka, T.; Shinohara, T. Molecular dielectrophoresis of bio-polymers. In Proceedings of the Conference Record of the 1992 IEEE Industry Applications Society Annual Meeting, Houston, TX, USA; pp.1446–1452, doi:10.1109/IAS.1992.244397. [CrossRef]
6. Spengler, T.; Ploog, M.; Schröter, M. Integrated planning of acquisition, disassembly and bulk recycling: A case study on electronic scrap recovery. *OR Spectr.* **2003**, *25*, 413–442. [CrossRef]
7. Du, F.; Baune, M.; Kück, A.; Thöming, J. Dielectrophoretic gold particle separation. *Sep. Sci. Technol.* **2008**, *43*, 3842–3855, doi:10.1080/01496390802365779. [CrossRef]
8. Williams, S.K.R.; Runyon, J.R.; Ashames, A.A. Field-flow fractionation: Addressing the nano challenge. *Anal. Chem.* **2011**, *83*, 634–642, doi:10.1021/ac101759z. [CrossRef]
9. Hanauer, M.; Pierrat, S.; Zins, I.; Lotz, A.; Sönnichsen, C. Separation of nanoparticles by gel electrophoresis according to size and shape. *Nano Lett.* **2007**, *7*, 2881–2885, doi:10.1021/nl071615y. [CrossRef]
10. Wei, G.T. Shape separation of nanometer gold particles by size-exclusion chromatography. *Anal. Chem.* **1999**, *71*, 2085–2091, doi:10.1021/ac990044u. [CrossRef]
11. Wills, B.A.; Finch, J.A. Dewatering. In *Wills' Mineral Processing Technology*; Elsevier: Amsterdam, The Netherlands, 2016; Chapter 15, pp. 417–438, doi:10.1016/b978-0-08-097053-0.00015-7. [CrossRef]
12. Wills, B.A.; Finch, J.A. Classification. In *Wills' Mineral Processing Technology*; Number 1993; Elsevier: Amsterdam, The Netherlands, 2016; Chapter 9, pp. 199–221, doi:10.1016/B978-0-08-097053-0.00009-1. [CrossRef]
13. Contado, C. Field flow fractionation techniques to explore the "nano-world". *Anal. Bioanal. Chem.* **2017**, *409*, 2501–2518, doi:10.1007/s00216-017-0180-6. [CrossRef]
14. Pesch, G.R.; Lorenz, M.; Sachdev, S.; Salameh, S.; Du, F.; Baune, M.; Boukany, P.E.; Thöming, J. Bridging the scales in high-throughput dielectrophoretic (bio-)particle separation in porous media. *Sci. Rep.* **2018**, *8*, 10480, doi:10.1038/s41598-018-28735-w. [CrossRef] [PubMed]
15. Suehiro, J.; Zhou, G.; Imamura, M.; Hara, M. Dielectrophoretic filter for separation and recovery of biological cells in water. *IEEE Trans. Ind. Appl.* **2003**, *39*, 1514–1521, doi:10.1109/TIA.2003.816535. [CrossRef]
16. Modarres, P.; Tabrizian, M. Frequency hopping dielectrophoresis as a new approach for microscale particle and cell enrichment. *Sens. Actuators B Chem.* **2019**, *286*, 493–500, doi:10.1016/j.snb.2019.01.157. [CrossRef]
17. Wang, Y.; Du, F.; Pesch, G.R.; Köser, J.; Baune, M.; Thöming, J. Microparticle trajectories in a high-throughput channel for contact-free fractionation by dielectrophoresis. *Chem. Eng. Sci.* **2016**, *153*, 34–44, doi:10.1016/j.ces.2016.07.020. [CrossRef]
18. Park, S.; Zhang, Y.; Wang, T.H.; Yang, S. Continuous dielectrophoretic bacterial separation and concentration from physiological media of high conductivity. *Lab Chip* **2011**, *11*, 2893, doi:10.1039/c1lc20307j. [CrossRef] [PubMed]
19. Pesch, G.R.; Du, F.; Schwientek, U.; Gehrmeyer, C.; Maurer, A.; Thöming, J.; Baune, M. Recovery of submicron particles using high-throughput dielectrophoretically switchable filtration. *Sep. Purif. Technol.* **2014**, *132*, 728–735, doi:10.1016/j.seppur.2014.06.028. [CrossRef]
20. Weirauch, L.; Lorenz, M.; Hill, N.; Lapizco-Encinas, B.H.; Baune, M.; Pesch, G.R.; Thöming, J. Material-selective separation of mixed microparticles via insulator-based dielectrophoresis. *Biomicrofluidics* **2019**, *13*, 064112, doi:10.1063/1.5124110. [CrossRef]
21. Sano, H.; Kabata, H.; Kurosawa, O.; Washizu, M. Dielectrophoretic chromatography with cross-flow injection. In Proceedings of the Technical Digest. MEMS 2002 IEEE International Conference. Fifteenth IEEE International Conference on Micro Electro Mechanical Systems (Cat. No.02CH37266), Las Vegas, NV, USA, 24 January 2002; pp. 2–5, doi:10.1109/MEMSYS.2002.984043. [CrossRef]
22. Kikkeri, K.; Ngu, B.; Agah, M.; Engineering, C.; Tech, V. Submicron Dielectrophoretic Chromatography. In Proceedings of the 2018 IEEE Micro Electro Mechanical Systems (MEMS), Belfast, UK, 21–25 January 2018; pp. 1177–1180.
23. Umezawa, Y.; Kobayashi, O.; Kanai, S.; Hakoda, M. Development of Particle Packed Bed Type Chromatography Using Dielectrophoresis. *Key Eng. Mater.* **2013**, *534*, 88–92, doi:10.4028/www.scientific.net/KEM.534.88. [CrossRef]

24. Hakoda, M.; Otaki, T. Analytical Characteristic of Chromatography Device Using Dielectrophoresis Phenomenon. *Key Eng. Mater.* **2012**, *497*, 87–92, doi:10.4028/www.scientific.net/KEM.497.87. [CrossRef]
25. Gascoyne, P.R.; Noshari, J.; Anderson, T.J.; Becker, F.F. Isolation of rare cells from cell mixtures by dielectrophoresis. *Electrophoresis* **2009**, *30*, 1388–1398, doi:10.1002/elps.200800373. [CrossRef]
26. Gupta, V.; Jafferji, I.; Garza, M.; Melnikova, V.O.; Hasegawa, D.K.; Pethig, R.; Davis, D.W. ApoStream^{TM}, a new dielectrophoretic device for antibody independent isolation and recovery of viable cancer cells from blood. *Biomicrofluidics* **2012**, *6*, 024133, doi:10.1063/1.4731647. [CrossRef]
27. Shim, S.; Stemke-Hale, K.; Tsimberidou, A.M.; Noshari, J.; Anderson, T.E.; Gascoyne, P.R. Antibody-independent isolation of circulating tumor cells by continuous-flow dielectrophoresis. *Biomicrofluidics* **2013**, *7*, 011807, doi:10.1063/1.4774304. [CrossRef]
28. Aldaeus, F.; Lin, Y.; Amberg, G.; Roeraade, J. Multi-step dielectrophoresis for separation of particles. *J. Chromatogr. A* **2006**, *1131*, 261–266, doi:10.1016/j.chroma.2006.07.022. [CrossRef]
29. Green, N.G.; Hughes, M.P.; Monaghan, W.; Morgan, H. Large area multilayered electrode arrays for dielectrophoretic fractionation. *Microelectron. Eng.* **1997**, *35*, 421–424, doi:10.1016/S0167-9317(96)00122-0. [CrossRef]
30. Cheng, I.F.; Froude, V.E.; Zhu, Y.; Chang, H.C.; Chang, H.C. A continuous high-throughput bioparticle sorter based on 3D traveling-wave dielectrophoresis. *Lab Chip* **2009**, *9*, 3193–3201, doi:10.1039/b910587e. [CrossRef]
31. Sun, T.; Morgan, H.; Green, N.G. Analytical solutions of ac electrokinetics in interdigitated electrode arrays: Electric field, dielectrophoretic and traveling-wave dielectrophoretic forces. *Phys. Rev. E Stat. Nonlinear Soft Matter Phys.* **2007**, *76*, 046610, doi:10.1103/PhysRevE.76.046610. [CrossRef]
32. García-Sánchez, P.; Ramos, A.; González, A.; Green, N.G.; Morgan, H. Flow reversal in traveling-wave electrokinetics: An analysis of forces due to ionic concentration gradients. *Langmuir* **2009**, *25*, 4988–4997, doi:10.1021/la803651e. [CrossRef]
33. Hughes, M.P. Fifty years of dielectrophoretic cell separation technology. *Biomicrofluidics* **2016**, *10*, 032801, doi:10.1063/1.4954841. [CrossRef]
34. Pethig, R. Dielectrophoresis: Status of the theory, technology, and applications. *Biomicrofluidics* **2010**, *4*, 022811, doi:10.1063/1.3456626. [CrossRef]
35. Ermolina, I.; Morgan, H. The electrokinetic properties of latex particles: Comparison of electrophoresis and dielectrophoresis. *J. Colloid Interface Sci.* **2005**, *285*, 419–428, doi:10.1016/j.jcis.2004.11.003. [CrossRef]
36. Arnold, W.M.; Schwan, H.P.; Zimmermann, U. Surface conductance and other properties of latex particles measured by electrorotation. *J. Phys. Chem.* **1987**, *91*, 5093–5098, doi:10.1021/j100303a043. [CrossRef]
37. Satyanarayana, S.; Karnik, R.N.; Majumdar, A. Stamp-and-stick room-temperature bonding technique for microdevices. *J. Microelectromech. Syst.* **2005**, *14*, 392–399, doi:10.1109/JMEMS.2004.839334. [CrossRef]
38. Gajasinghe, R.W.; Senveli, S.U.; Rawal, S.; Williams, A.; Zheng, A.; Datar, R.H.; Cote, R.J.; Tigli, O. Experimental study of PDMS bonding to various substrates for monolithic microfluidic applications. *J. Micromech. Microeng.* **2014**, *24*, 075010, doi:10.1088/0960-1317/24/7/075010. [CrossRef]
39. Koschwanez, J.H.; Carlson, R.H.; Meldrum, D.R. Thin PDMS films using long spin times or tert-butyl alcohol as a solvent. *PLoS ONE* **2009**, *4*, e4572, doi:10.1371/journal.pone.0004572. [CrossRef]
40. Wang, X.B.; Vykoukal, J.; Becker, F.F.; Gascoyne, P.R. Separation of polystyrene microbeads using dielectrophoretic/gravitational field-flow-fractionation. *Biophys. J.* **1998**, *74*, 2689–2701, doi:10.1016/S0006-3495(98)77975-5. [CrossRef]
41. Castellanos, A.; Ramos, A.; González, A.; Green, N.G.; Morgan, H. Electrohydrodynamics and dielectrophoresis in microsystems: Scaling laws. *J. Phys. D Appl. Phys.* **2003**, *36*, 2584–2597, doi:10.1088/0022-3727/36/20/023. [CrossRef]

5 Dielectrophoretic particle chromatography II

This chapter consists of a manuscript that was published before as

Giesler, J.; Weirauch, L.; Thöming, J.; Baune, M.; Pesch, G. R. Separating Microparticles by Material and Size Using Dielectrophoretic Chromatography with Frequency Modulation. *Scientific Reports* **2021**, *11*, 16861, DOI: 10.1038/s41598-021-95404-w.

The publication in Chapter 4 focused on the proof-of-principle investigation. This chapter provides additional investigations of the proposed mechanism. The study was designed in such a way that we could show by experiment and simulation that all proposed migration mechanisms are indeed observable in the channel. The study shows that pDEP dominated, nDEP dominated and balanced types of migration through the channel exist. The type of migration profile does not only depend on the particle but also on the frequency modulation spectrum.

The supporting information are available at the journal's page at https://doi.org/10.1038/s41598-021-95404-w.

scientific reports

Check for updates

OPEN

Separating microparticles by material and size using dielectrophoretic chromatography with frequency modulation

Jasper Giesler[1], Laura Weirauch[1], Jorg Thöming[1,2], Michael Baune[1] & Georg R. Pesch[1,2]✉

Separation of (biological) particles (≪ 10 μm) according to size or other properties is an ongoing challenge in a variety of technical relevant fields. Dielectrophoresis is one method to separate particles according to a diversity of properties, and within the last decades a pool of dielectrophoretic separation techniques has been developed. However, many of them either suffer selectivity or throughput. We use simulation and experiments to investigate retention mechanisms in a novel DEP scheme, namely, frequency-modulated DEP. Results from experiments and simulation show a good agreement for the separation of binary PS particles mixtures with respect to size and more importantly, for the challenging task of separating equally sized microparticles according to surface functionalization alone. The separation with respect to size was performed using 2 μm and 3 μm sized particles, whereas separation with respect to surface functionalization was performed with 2 μm particles. The results from this study can be used to solve challenging separation tasks, for example to separate particles with distributed properties.

Separation of particles from each other is important in a wide variety of areas. For example, it is required in electronic waste recycling to recover valuable metals[1–3], to enrich desired minerals in the mining sector[4,5], to detect circulating cancer cells[6], in waste water treatment[5], and many other fields. For large particles (≫ 10 μm), inertia- or gravity-driven processes are one option to achieve a classification with respect to density or particle size. Since both, gravity and inertia scale with particle mass, their influence decreases with decreasing particle size and becomes negligible when particles reach nanometre scale[7]. In this range, other forces (e.g. electrostatic, van-der-Waals interaction or Brownian motion) can dominate the particle behaviour. Thus, to separate micro or sub-micron particles, other approaches become attractive. We like to note that many biological separation tasks[8–11] or valuable dust fractions[2] are within this size range. For such particle sizes, (gel-)electrophoresis[12,13], field-flow-fractionation (FFF)[14], or size-exclusion chromatography[15] are some common methods. Dielectrophoresis (DEP) is a versatile technique that is not only capable of addressing micro and sub-micron particles[16,17], it also offers the potential to be scaled up[18]. Further, DEP can be used to manipulate both biological[9,19,20] and non-biological particles[21,22].

DEP describes the movement that rises when a suspended polarizable particle is placed into an inhomogeneous electric field. The dielectrophoretic force $\mathbf{F}_{\mathrm{DEP}}$ acting on a spherical particle is commonly approximated as[16]

$$\mathbf{F}_{\mathrm{DEP}} = 2\pi r_{\mathrm{p}}^{3}\varepsilon_{\mathrm{m}}\mathrm{Re}(CM)\nabla|\mathbf{E}_{\mathrm{rms}}|^{2}, \tag{1}$$

with r_{p}, the particle radius, the vector of the electric field $\mathbf{E}_{\mathrm{rms}}$ and the permittivity of the surrounding medium ε_{m}. $\mathrm{Re}(CM)$ is the real part of the so-called Clausius–Mossotti factor, which incorporates the frequency-dependent polarization of the particle and the medium. Using the complex permittivity $\tilde{\varepsilon}$ it can be calculated for homogeneous spherical particles as

$$\mathrm{Re}(CM) = \mathrm{Re}\left(\frac{\tilde{\varepsilon}_{\mathrm{p}} - \tilde{\varepsilon}_{\mathrm{m}}}{\tilde{\varepsilon}_{\mathrm{p}} + 2\tilde{\varepsilon}_{\mathrm{m}}}\right), \tag{2}$$

[1]Chemical Process Engineering, Faculty of Production Engineering, University of Bremen, Leobener Straße 6, 28359 Bremen, Germany. [2]MAPEX Center for Materials and Processes, University of Bremen, PO box 330 440, 28334 Bremen, Germany. ✉email: gpesch@uni-bremen.de

with $\tilde{\varepsilon} = \varepsilon_0 \varepsilon_r - i\frac{\sigma}{\omega}$, where σ is the conductivity, ε_0 the vacuum permittivity and $\omega = 2\pi f$ represents the angular frequency of the applied electric field. This factor ranges between - 0.5 and 1 and determines the movement direction of the particle: When $\mathrm{Re}(CM) > 0$, particles experience positive dielectrophoresis (pDEP) and move towards local field maxima, when $\mathrm{Re}(CM) < 0$, particles experience negative dielectrophoresis (nDEP) and are repelled from field maxima. The frequency where $\mathrm{Re}(CM)$ equals zero is called crossover frequency. At this frequency, the particles do not experience a dielectrophoretic force. Due to its dependency on field frequency and medium properties, $\mathrm{Re}(CM)$ can change its value or sign during an experiment, which can result in a movement direction change of target particles. The net conductivity of a microparticle of non-conducting bulk material in an electrolyte suspension can be calculated as[16,23]

$$\sigma_p = \sigma_{bulk} + \frac{2K_s}{r_p}. \tag{3}$$

The conductivity is composed of the bulk material conductivity, σ_{bulk}, and a part caused by the intrinsic double layer that forms around suspended particles. The surface conductance K_s comes from the ions in the electric double layer of the particle and can increase the overall conductivity[16]. As a consequence, even particles with negligible bulk conductivity, such as the polystyrene (PS) particles used in this work, can show pDEP.

Equations (1), (2) and (3) show that the dielectrophoretic motion depends on material (e.g. conductivity and permittivity), process parameters (e.g. medium conductivity, field strength and frequency) and size. The diversity of influencing variables provides the opportunity to address different separation tasks. Depending on the process design, even specific multidimensional tasks could solved in one set-up. Simultaneously, DEP-based separation requires careful design to enable a functioning separation processes. In its 50 years of existence, many different techniques and designs have been established to perform a dielectrophoretic separation of particles. One way to categorize the existing DEP techniques is whether a continuous or a chromatographic separation is performed. Whereas continuous separation methods often focus on spatial separation or selective trapping[17,24–26], chromatographic methods are usually batch or semi-batch processes and result in particle type-dependent residence times in a separator. They are a promising approach to achieving separation of high purity or adjustability[27,28]. In this work, we use experiments and simulation to gain further insight into the retention mechanisms of a chromatographic separation based on a frequency-modulation method.

Dielectrophoretic particle chromatography (DPC) was introduced by Washizu et al.[9] in 1992 and has been used since[8,27–31]. A prominent example is the isolation of tumor cells from blood by Shim et al.[19]. DPC exploits different polarizabilities of target particles for separation. For example, a specific particle type shows pDEP ($\mathrm{Re}(CM) > 0$) and gets reversibly trapped in the separation column, whereas other particles show no DEP or nDEP and are consequently eluted from the column. By changing the frequency, the formerly trapped particles in the channel can be levitated by nDEP, resulting in their subsequent elution. Some approaches vary the frequency as a function time, to separate different cell types from one another[8,19] or achieve a separation with respect to size[32,33]. As Yang et al.[28] also pointed out, sweeping the frequency can be used to compensate distributed cell properties and consequently achieve more homogeneous retention times in dielectrophoretic field-flow fractionation (FFF) by also reducing particle adhesion at field maxima at the same time. The above mentioned studies show the potential of varying the frequency in DPC. Additionally, Aldaeus et al.[27] numerically showed the benefit of multiple trap-and-release cycles in DPC. In a previous publication, we demonstrated the capabilities of a design that combined multiple trap-and-release cycles with the advantage of changing the frequency[33]. The chromatographic separation allows to address particle mixtures with only small dielectric differences or distributed particle properties. Additionally, since all particles elute from the same outlet, the design of the device is simple and easy to scale.

The functionality of such an approach is explained in detail in the "Functionality of frequency-modulated DPC" section. Briefly, a number of particles is injected once into a flow chamber and transported across an interdigitated electrode array by a carrier flow with a laminar flow profile (Fig. 1A,B). The electrode array generates an inhomogeneous electric field and thus a DEP force on the particles. The frequency of the applied field is continuously modulated between two values. For each particle in an arbitrary particle mixture, three general responses are possible: particles experience mainly pDEP in the modulation spectrum and are drawn towards the field maxima found at the electrode edges. Due to their interaction with the field maxima and the low fluid velocity close to the walls of the channel, they experience a retardation in the channel (as discussed below) and elute later than they would without field. The difference in elution time depends on the applied voltage and frequency range. Particles that, in contrast, experience mainly nDEP in the modulation spectrum interact with the field minima found at the channel ceiling and also elute later. Particles that experience a balanced pDEP/nDEP response in the modulation spectrum are neither drawn to the ceiling nor bottom of the channel and thus experience almost no retardation. They elute almost at the same time as they would without applied field. Thus, this technique allows to separate a particle mixture that is injected intermittently (or once) at the inlet (Fig. 1E); as long as the different particles show differences in their crossover frequency.

In our previous publication[33], we demonstrated how the approach can be used to separate polystyrene microparticles based on size. Both design and drawn conclusions were based mostly on observations without detailed numerical calculations of the underlying physics. In this study, we will simulate the size-selective separation of polystyrene particles and verify the simulation results against experiments. We will further capitalize on the simulation to predict parameters for separating polystyrene particles of equal size based only on their surface conductance. Finally, we will compare the simulated and experimental results of this separation. According to Eq. (3), the conductivity and thus crossover frequency of polystyrene particles depends on their size and the yet unknown surface conductance K_s. Thus, to perform a simulation we need to determine the crossover frequency and the particle's K_s-value. To do this, we use a fixed-frequency method (Fig. 1C), which is explained in detail

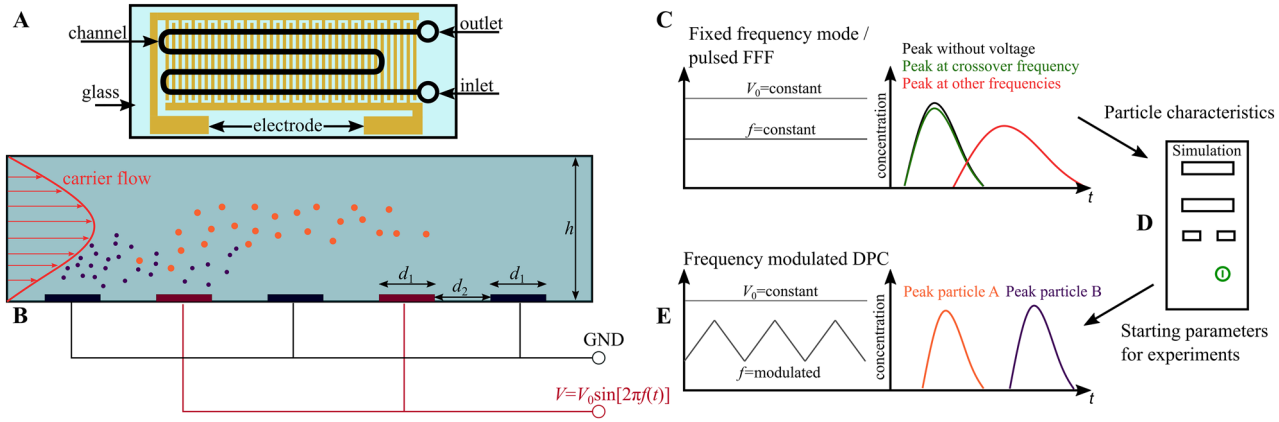

Figure 1. (**A**) Top view of the microfluidic device (sketch). (**B**) The microfluidic separation column (side view, height $h = 80\ \mu m$ and electrode width/spacing $d_1 = d_2 = 100\ \mu m$) is continuously flushed with a carrier fluid. Once per experiment a particle suspension is injected. The device is used for two different types of experiment. (I) The crossover frequency of particles is determined using field-flow fractionation (FFF) at a fixed frequency f by comparing the elution profiles with and without applied voltage (V_0) (**C**). The obtained particle characteristics where used as input parameters for a full-scale simulation model realized in COMSOL Multiphysics to find suitable process parameters (**D**). (II) Eventually, the set of process parameters is used as starting point for experiments to achieve a chromatographic separation by using frequency-modulated ($f = f(t)$) dielectrophoretic particle chromatography (DPC) (**E**).

in the "Determination of crossover frequency" section: Here, the frequency is kept constant per particle injection (but is changed between experiments) and the particle residence time is observed as a function of applied frequency. When the applied voltage is chosen carefully, particles will either be retarded by positive or negative DEP, or, in case the applied frequency closely matches the crossover frequency, particles will not be retarded. Thus, by comparing the elution time as a function of frequency and comparing it against the elution time without superimposed electric field, it is straight-forward to determine the crossover frequency. The determined K_s-value can be adjusted slightly to improve the match between experiments and simulation. To summarize our approach:

i. Find the crossover frequency and K_s of the particles by performing fixed-frequency experiments (Fig. 1C).
ii. Use the obtained K_s-value to determine suitable frequency ranges and perform frequency-modulated DPC experiments to separate particles by size (Fig. 1E).
iii. Simulate the particles movement and compare the elution profiles of the experiment and the simulation. Apply moderate changes to the simulation (e.g. simulated particle polarizability) to increase match with experiment (Fig. 1D).
iv. Use simulation to design a different separation task:

iii.a. Find crossover frequency of polystyrene particles with different surface functionalization but same size.
iii.b. Input crossover frequency into the simulation to find suitable center frequencies for separation in the experiment.
iii.c. Perform the separation experimentally with optimized parameters from iii.b.

Results and discussion

We first determine the surface conductance for the size-selective separation using fixed-frequency experiments (Fig. 1C). Based on these results, we perform DPC experiments using the frequency-modulation technique (Fig. 1E). We will then perform simulations, using the same process parameters, to see how the simulation matches the experiments. Finally, we use the simulation to find process parameters to separate a binary mixture of particles according to their surface modification.

Size-selective separation. Two monodisperse PS particle suspensions with diameters of 3.1 μm and 2.12 μm without an additional surface functionalization were selected for generating experimental data to compare with the simulation. Since the surface conductance is an important yet unknown characteristic of the particles, it was measured using fixed-frequency field-flow fractionation (see "Determination of crossover frequency" section). Choosing the right voltage for the experiments is important, as a too high voltage would cause immobilization and too low voltage would result in only slightly differences in the residence time distribution. For the larger particles a voltage of 120 V_{pp} was selected. The smaller particles required a higher voltage of 160V_{pp}, since the DEP force scales with particle volume. Frequencies between 180 and 310 kHz were tested. Figure 2 shows the concentration profiles at the outlet for 3.1 μm particles at different frequencies. At 210 kHz, the residence time is minimal and the concentration profile almost matches the profile without any applied voltage, indicating that the

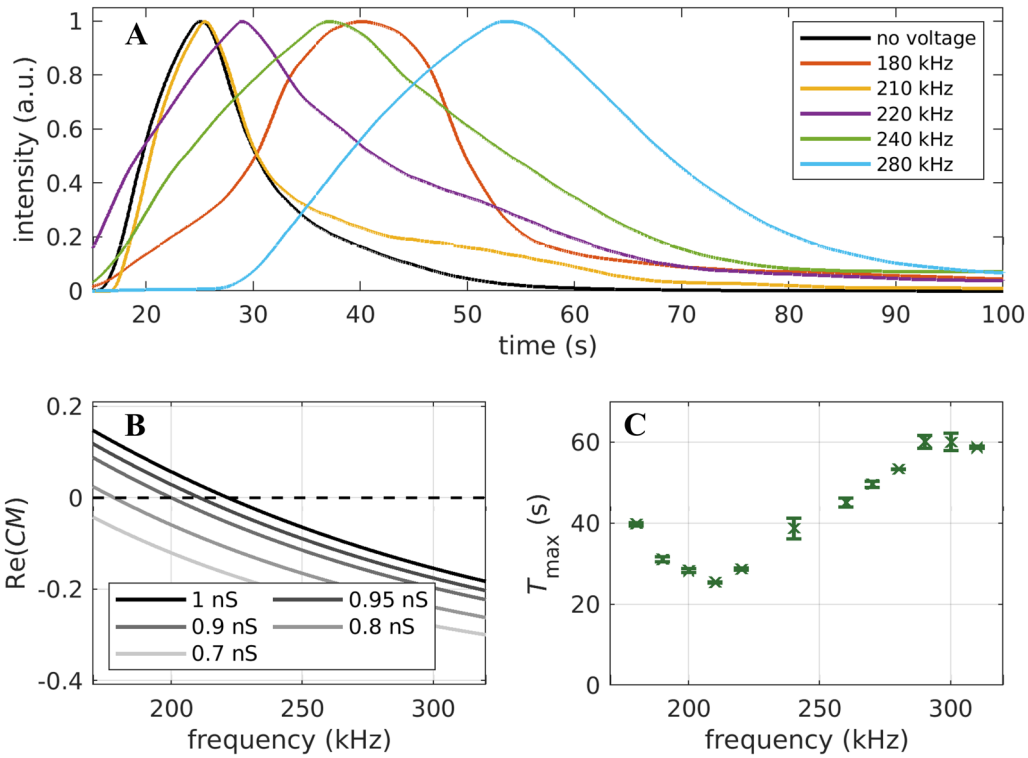

Figure 2. (**A**) Residence time distributions at 120 V_{pp} for different applied frequencies in fixed-frequency dielectrophoretic particle chromatography. (**B**) Calculated values of the real part of the Clausius–Mossotti equation for different surface conductances ($d_p = 3.1$ µm PS particles without surface functionalization in a 2 µS cm^{-1} suspension). The dashed line represents $\mathrm{Re}(CM) = 0$. (**C**) Maximum of the residence time distributions at 120 V_{pp} for all measured frequencies (extracted from the elution profiles). Experiments were repeated 3 times.

Center frequency	2.12 µm particles	3.1 µm particles
210 kHz	pDEP dominated	Balanced
245 kHz	pDEP dominated	nDEP dominated
280 kHz	Balanced	nDEP dominated

Table 1. Anticipated particle behaviour in the DPC experiments based on their crossover frequency. The 2.12 µm particles show their crossover at 290 kHz and the 3.1 µm particles at 210 kHz.

cross-over frequency is close to 210 kHz. At both, lower and higher frequencies, the concentration profiles are shifted towards longer times (i.e., particles elute later and are retarded to either nDEP in case of higher frequencies, or pDEP in case of lower frequencies). Combining the results with the real part of the Clausius–Mossotti factor (Eqs. (2) and (3) and Fig. 2), we calculate a surface conductance of $K_s = 0.95$ nS, which is in good accordance with the literature value of 1 nS[16,23,34]. The results for the 2.12 µm particles (Supplementary Fig. 2) show a minimum in residence time around 290 kHz. Since the dielectrophoretic mobility for smaller particles is lower, the crossover is less clear. Nevertheless, knowing the crossover is close to this value, a surface conductance of 0.9 nS was assumed for further steps.

Now that we know K_s and crossover frequency of both particles, we can select suitable frequency ranges for separation. Three frequency ranges were chosen. Two center frequencies f_c of the modulation spectrum ($f_c = 210$ kHz and $f_c = 280$ kHz) were selected because these frequencies are close to the respective crossover of the two particles. A third frequency was chosen in between (245 kHz). The bandwidth of 240 kHz in combination with a modulation frequency of 300 mHz were kept constant, because we know from previous experiments that these parameters allow a separation[33]. Both parameters are constant for all conducted experiments within this work. The selection of frequency windows allows to test the three predicted behaviours of the particle in the channel (see "Functionality of frequency-modulated DPC" section and Table 1). The spectrum centred at 210 kHz should produce no or only small retardation for the larger 3.1 µm particles, since they experience a balanced pDEP and nDEP force. In contrast to this, the movement of the 2.12 µm particles should be dominated by pDEP, resulting in a retardation. At 280 kHz, we expect an increase in residence time for the larger 3.1 µm particles

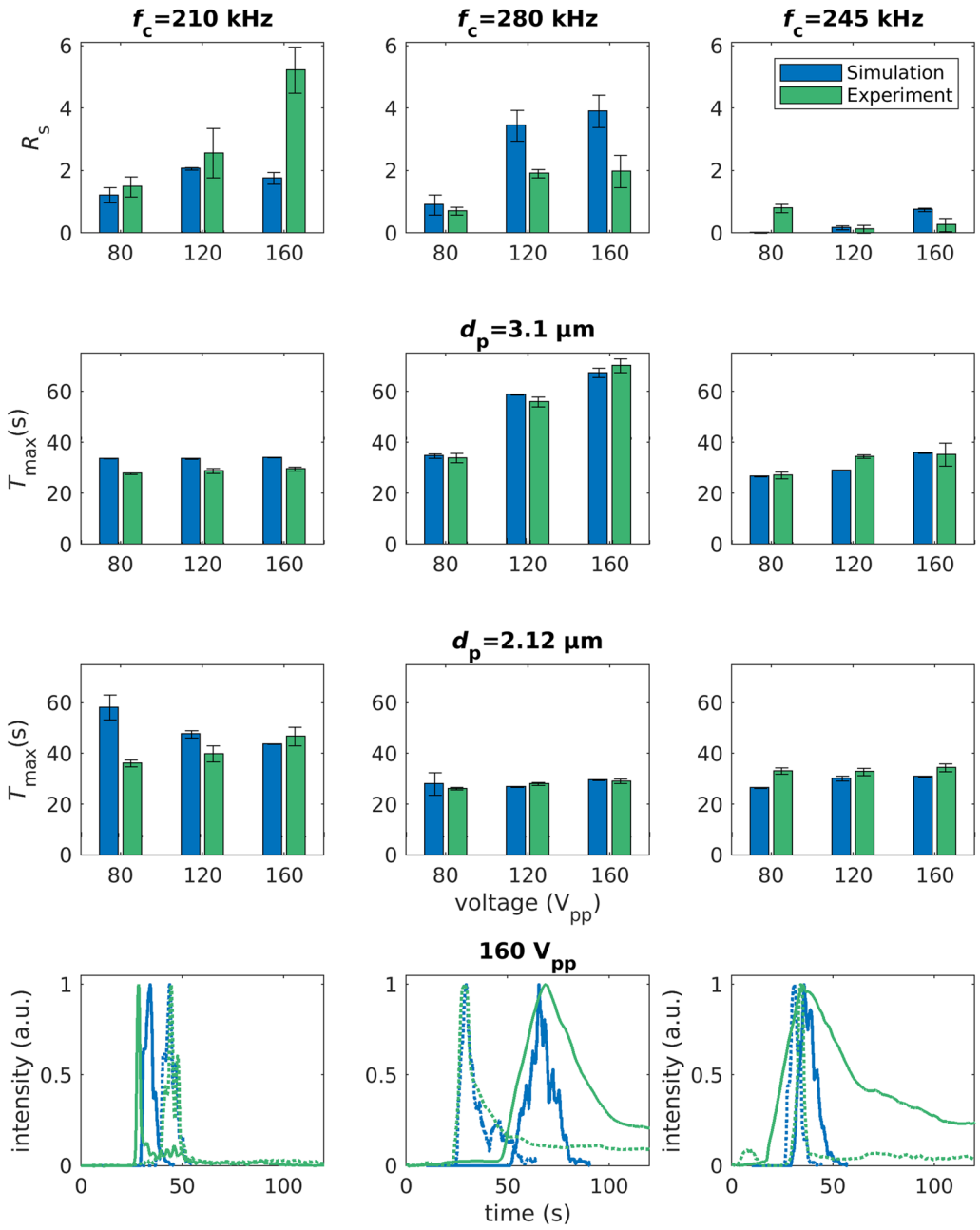

Figure 3. Top: Resolution and standard deviation of experimental and simulated frequency-modulated chromatography experiments at 80, 120 and 160 V_{pp} for three different modulation spectra. Surface conductance of the 2.12 µm and 3.1 µm particles are simulated with 0.775 nS and 1 nS, respectively. Middle two rows: Corresponding maxima of the residence time distributions and standard deviations for 3.1 µm and 2.12 µm particles. Bottom: Residence time distributions of experiment (green) and simulation (blue) for 3.1 µm (solid line) and 2.12 µm (dashed line) particles at different centre frequencies (210, 280 & 245 kHz) and 160V_{pp}. Simulations and experiments were repeated 5 times to check for statistical validity.

as they are retarded due to an nDEP dominated response. The smaller 2.12 µm particles experience balanced DEP and show no retardation. In the third spectrum (center frequency 245 kHz), which produces pDEP for the small and nDEP for the bigger particles, only poor separation is expected, as now both particles are retarded.

Figure 3 shows experimental and simulated chromatography results of the size-selective separation of 2.12 µm and 3.1 µm particles. As an example, the bottom row shows both experimental and simulated elution profiles at 160 V_{pp} and at the three different centre frequencies. From these profiles, we can extract the separation resolution R_s (see "Experimental details" section for a definition of R_s and top row for the results) as well as the maxima in the respective peaks (middle rows). For the experiments, the best resolution at all voltages is achieved at $f_c = 210$ kHz (top left). In this setting, the larger particles experience balanced pDEP and nDEP, thus almost no retardation, and are consequently eluted only about two seconds later than without an applied voltage (without

applied voltage $T_{max} = 26.91\ s \pm 0.28\ s$). The 2.12 µm particles, which experience more pDEP than nDEP, instead show a significant retardation. With increasing voltage, T_{max} of the 2.12 µm particles and thus the experimentally determined R_s increase. In contrast, at $f_c = 280$ kHz (middle panel), the 2.12 µm particles now experience balanced pDEP and nDEP behaviour and are eluted much earlier than the larger particles, which now experience an nDEP dominated movement. The T_{max} of the 3.1 µm particles and thus R_s here also increase with voltage, but the resolution is generally lower compared to $f_c = 210$ kHz. At $f_c = 245$ kHz, as expected, we observe only small retardation for both particle types, which consequently leads to a low experimental resolution among all voltages. These experiments show the three different types of particle movement in frequency modulated DPC. The set of experiments validates the theory stated before and is used for comparing chromatograms of experiment and simulation.

To achieve a good agreement in the residence time distributions between the experiments and our simulations, we applied empirical corrections to the surface conductance (see below). Especially maxima of the residence time distributions (T_{max}) agree quite well across all frequencies and voltages. For the 3.1 µm particles we applied an offset of 0.05 nS to the surface conductance (experimentally determined $K_s = 0.95$ nS vs. simulated $K_s = 1$ nS), which is within the uncertainty of the method to determine the surface conductance. To the smaller particles we applied an offset of −0.125 nS , resulting in a simulated K_s-value of 0.775 nS versus 0.9 nS found in the experiment. Since this would correspond with a crossover frequency of about 250 kHz, this can not be explained with the uncertainty of the surface conductance alone. Lowering the surface conductance in our simulation equals reducing the time the smaller particles spend adhered to the wall, resulting in a faster elution of the particles, which was observed experimentally. This is because they show predominately pDEP and by lowering the simulated conductivity of the particles, they show nDEP for longer periods of time. As the fixed-frequency experiments already suggest, not all particles adhere to the wall at fixed frequency, even when a frequency different from the crossover frequency is applied. Transferring this observation to the simulation, this means that the trapping of the particles at the wall is not as strong as predicted by the simulation. This is shown here for 2.1 µm particles (Fig. 3). We also tested this for 6.14 µm particles (see supplement). In general, corrections to the surface conductance are required so that they reduce the residence time in simulation. This means, particles that are predominantly experiencing pDEP require a correction so that the surface conductance is lowered. Particles that are experiencing more nDEP than pDEP require a correction that raises the surface conductance so that they experience nDEP for a shorter duration and thus spend less time adhered to the wall in the simulation. One explanation is that particles hop from one trapping location to another. (Electro-)thermal fluid movement and unspecific adhesion or hydrodynamic lift might be the reason behind this behaviour. Additionally, Adams et al.[35] showed, that the sweeping rate (frequency change per time) can affect the polarization of microspheres significantly, which may contribute to the observed effects. To account for the experimentally observed behaviour in the simulation, we chose to adjust the surface conductance of the particles to reduce the time particles spend adhering to the wall. The data of the size-selective experiments show that the particle-wall interactions should be studied in more detail in the future to remove the surface conductance of the particles as a fitting parameter from the simulation. By now, in addition to the experiments that we require to determine the surface conductance, we also require experiments providing retention behaviour of the particles during frequency modulation to calibrate the surface condutance offset. Based on this calibration experiments we perform extensive parametric studies.

Interestingly, at $f_c = 210$ kHz, the simulated T_{max} of the 2.12 µm particles decreases with voltage. Due to higher voltages, the 2.12 µm particles can travel larger distances away from the electrode array, reach regions with higher fluid velocity (parabolic flow profile) and can consequently cover more distance per frequency cycle. This results in a faster simulated elution. The significantly lower predicted R_s compared to the experiments is a combination due to diverging T_{max} of both particles in comparison to the experiments and broader peaks (higher FWHM, Supplementary Fig. 4) in the simulation. Further, at $f_c = 280$ kHz, the simulation predicts significantly higher resolutions compared to the experimentally determined R_s. T_{max} for both particle types match quite well across all voltages, leaving the width of the residence time distribution as diverging parameter (Eq. 4). Generally, a high resolution is achieved by a large time between the maxima of two peaks in combination with a small peak width. When the resident times show only small differences (small ΔT_{max}), the resolution becomes sensitive to small differences of the width of the residence time distributions (FWHM) when comparing experiment and simulation. Consequently, the reason for the disagreement concerning the R_s between experiment and simulation is the stronger peak broadening in the experiments and minor differences in T_{max}. As soon as the 3.1 µm particles experience retardation due to their nDEP dominated behaviour, their peaks begin to broaden (Supplementary Figs. 3 and 4). This peak broadening of the 3.1 µm particles can also be seen in the elution profiles (Fig. 3, bottom row, middle and right panel, solid green line). In the simulation the particles behaviour is not as inhomogeneous as in the experiments, resulting in narrower peaks. When the larger particles are showing predominantly negative dielectrophoresis, they migrate close to the ceiling of the channel. The electric field is here much lower compared to the bottom, which is the location of the electrode array. In combination with the lower dielectrophoretic force ($\mathbf{F}_{DEP} \propto \nabla|\mathbf{E}|^2$) this leads to inhomogeneous retention times, as now other effects such as unspecific particle-wall interactions or other fluid movements (e.g. electrothermal, buoyancy, AC electro-osmosis, hydrodynamic lift) can influence the particle movement. Additionally, as the DEP force decreases, particles travel shorter distances orthogonally to the wall due to DEP and consequently, cover less distance per frequency cycle. This could be compensated by adjusting the distribution with which the particles are released from the wall (see "Simulation model" section). Without detailed insight into the reasons behind these interactions, however, this seems like an arbitrary fit within the model. For achieving rapid separation with high resolution, consequently, pDEP dominated behaviour seems favourable according to the experiments.

Overall, the simulation gives valuable insight into the particle behaviour and trajectories in the channel and is able to support the process design. Additionally, it can be used to study the impact of side effects, since the

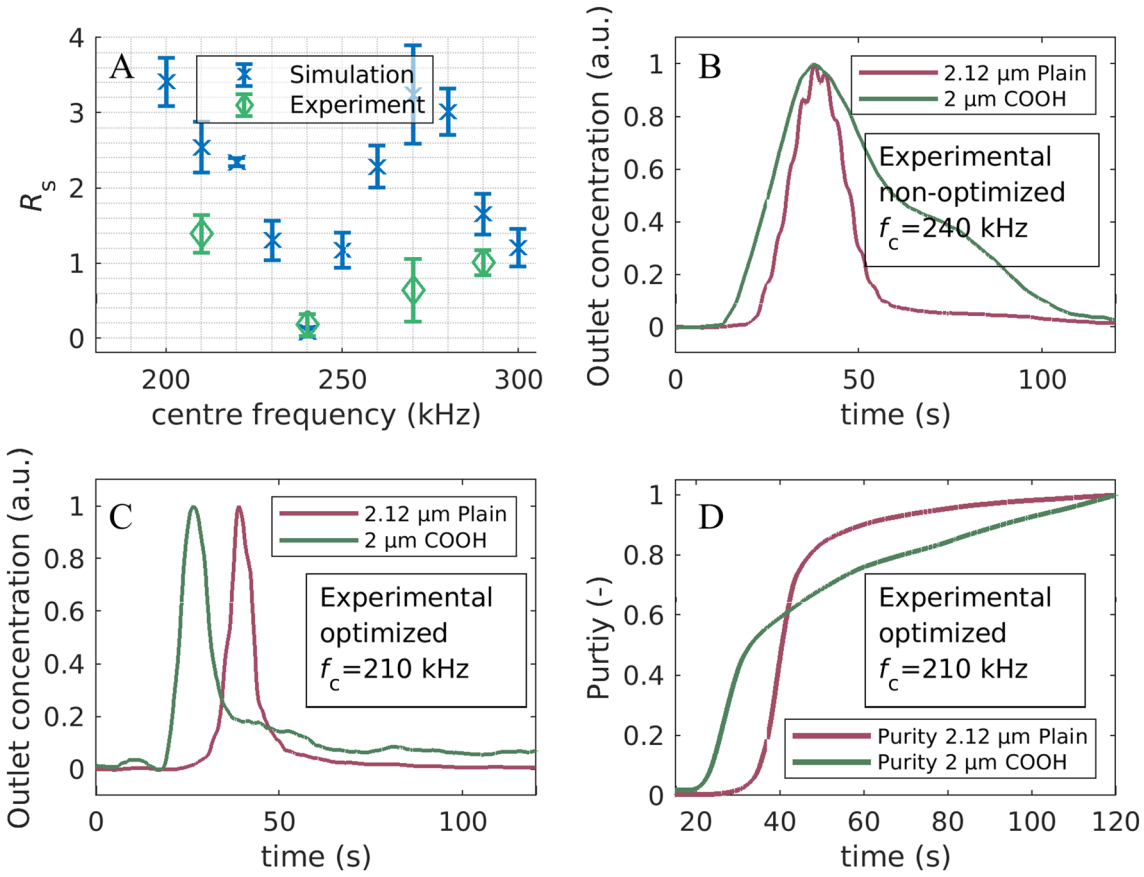

Figure 4. (**A**): Simulated (blue) and experimentally determined (green) resolution R_s at different center frequencies (f_c). Simulations were repeated 5 times. (**B**): Chromatogram of a non-optimized separation of 2 µm carboxy functionalized and 2.12 µm plain PS particles at a $f_c = 240$ kHz. (**C**) Chromatogram of an optimized separation of 2 µm carboxy functionalized and 2.12 µm plain PS particles at $f_c = 210$ kHz. (**D**) Purity as a function of time at $f_c = 210$ kHz.

simulation is able to isolate the movement due to drag, gravitation and dielectrophoresis and therefore a significant divergence between experiment and simulation suggests the presence of side effects.

Material-selective separation. In this section, we will demonstrate the separation of polystyrene particles of almost equal size based on their surface functionalization. Firstly, we determine the crossover frequency using fixed-frequency experiments. Then, we input the crossover frequency into the simulation to find ideal separation parameters. Finally, we will use these parameters to separate the particles efficiently in an experiment. The separation was conducted using the already characterized 2.12 µm PS particles without surface functionalization (plain) and 2 µm carboxy functionalized PS particles (COOH).

The fixed-frequency experiments (see Supplementary Fig. 2) suggest a crossover close to 210 kHz for the carboxylated particles, resulting in a surface conductance of $K_s = 0.6$ nS, significantly lower compared to K_s of the plain particles ($K_s = 0.9$ nS). The voltage for separating theses two particle types was fixed at $160V_{pp}$ because this voltage showed the highest separation efficiency before. Modulation frequency (300 mHz) and bandwidth (240 kHz) remain unchanged. Since no training data for the carboxy modified particles was available before the experiments, they were simulated with the experimentally determined surface conductance ($K_s = 0.6$ nS). Compared to the plain 2.12 µm particles, the surface conductance is lower. Therefore, the carboxy particles are expected to show balanced pDEP and nDEP movement or, with increasing center frequency, an nDEP dominated behaviour similar to the 3.1 µm plain particles at center frequencies between 200 kHz and 300 kHz. Although the crossover frequency of the carboxy 2 µm and plain 3.1 µm particles are comparable, the mobility deviates significantly ($F_{DEP} \propto d_p^3$) leading to a more challenging separation task.

The simulated resolutions (Fig. 4) show a first maximum at the lowest simulated center frequency. In this setting the carboxy particles show an almost balanced pDEP and nDEP movement and are therefore eluted first, while the better polarizable plain particles experience retardation due to pDEP. With increasing centre frequency the resolution reduces significantly as now both types of particles experience balanced pDEP/nDEP behaviour and thus, only small retardation. The minimum is reached at 240 kHz. Afterwards the resolution increases again, leading to a second peak at 270 kHz center frequency at which the plain particles experience a balanced pDEP/nDEP behaviour in contrast to the carboxylated particles which are now slowed down due to showing predominantly nDEP. At even higher center frequency, both particles show predominantly nDEP and the resolution is

again low. Compared to the separation with respect to size (Fig. 3), the resolution is generally lower, which is expected because the magnitude of the DEP force depends less strongly on surface functionalization than on size.

Experiments then were conducted for four different sets of frequencies to test the separation in the experiment. The selected center frequencies were 210, 240, 270 and 290 kHz. The best experimental separation resolution was achieved at a cetner frequency of 210 kHz with a value of $R_s = 1.39 \pm 0.25$. This is lower compared to the simulation but the setting allows a chromatographic separation as predicted by the simulation (Fig. 4, bottom row). The simulation suggested a minimum of the separation efficiency at a centre frequency of 240 kHz. At this frequency an experimental separation was also not possible, resulting in a resolution of $R_s = 0.18 \pm 0.15$ (Fig. 4, top right). To check whether with increasing frequency the resolution increases again, higher centre frequencies were tested. At a centre frequency of 270 kHz a resolution of $R_s = 0.64 \pm 0.42$ was measured, whereas 290 kHz as the centre of the modulation spectrum resulted in an increase of the resolution up to $R_s = 1.02 \pm 0.17$. Similar to the value at 210 kHz these values are below the simulative predicted ones, but the experiments do mirror the trends provided by the simulation.

In addition to the elution peaks, the purity (Eq. 5) is also plotted in Fig. 4. This provides another parameter besides retention time and resolution. Before a relevant amount of plain particles elute from the channel about 60 % of the carboxylated particles are crossing the measurement area. Furthermore, over 80% of the plain particles are eluted within a few seconds, which is crucial for a good separation.

Conclusion

To conclude, we have used simulation and experiments to demonstrate three different particle behaviors in frequency-modulated chromatography, i.e., retardation due to nDEP or pDEP-dominated behavior or a balanced behavior leading to no retardation. We have firstly addressed size-selective separation of two different PS particles to investigate the particle retention mechanisms. Here, the simulation model supported our previous hypothesis. We then addressed the more challenging material-selective separation of particles of equal size to show the power of the simulation method: We used the simulation to find suitable operating parameters which allow a separation of two equally sized 2 µm PS particles with different surface functionalization.

In the future, our simulation model can be used as a valuable tool to design operating schemes capable of addressing more complex separation tasks, for example shape sensitivity or heterogeneous samples, or to study how a reduction of the applied voltage would be possible for handling sensitive samples such as cells. To address biological particles we have to reduce the applied voltage while maintaining the ability to perform a chromatographic separation. This can be possible, for example, via geometrical optimization. Since biological systems typically have higher medium conductivities than used here, significant heat could develop if the voltage is not reduced. Additionally, high electric field strength could lead to irreversible electroporation of the suspended cells. The simulation does not always match the experiments exactly, which could only be achieved using extensive fitting considering the complex trap and release cycles. Nevertheless, the simulation can be used to perform design optimizations or to perform extensive parametric studies without the requirement to invest time and money on equipment and particles.

Methods

The principle behind the fixed-frequency and frequency-modulated experiments were presented in the "Introduction" section for readability of the manuscript. However, experimental and simulative details are presented in the following.

Functionality of frequency-modulated DPC. The suspended particles are injected into the channel and transported further by a carrier flow. During the experiments the particles are carried over an electrode array (Fig. 1A,B) and consequently subjected to an electric field. In this method, to generate trap and release or deceleration and acceleration cycles, the frequency of the electric field is not kept constant but modulated. In contrast to techniques published before, to the best of the authors knowledge, in this technique a modulation spectrum is chosen that generates pDEP and nDEP for all suspended particles during short periodic cycles rather than trapping one species first and releasing it after a different species was eluted from the channel. Therefore, the method does not dependent on strongly diverging polarizability of the particle mixtures for separation. Instead, it can be used to resolve minute or even overlapping distributions of the polarizability of particles. Using this approach a fast chromatographic separation can be achieved[33].

Modulating a sinusoidal voltage by a triangular function results in periodic changes of the frequency between two values (Fig. 1E). The centre of this frequency range is called centre frequency (f_c). During the modulation, particles may show pDEP in one part of the frequency range and nDEP in another one. Consequently, three different particle behaviours can be distinguished, as long as the crossover frequency is between the maximum and the minimum value of the modulation spectrum. Firstly, when particle shows more pDEP than nDEP in the applied frequency range, they tend to migrate towards the field maxima, which are located at the bottom of the channel at the electrode edges. Since in the channel a parabolic velocity profile is present due to the low Reynolds number, particles close to the wall are significantly slowed down either by low fluid velocity or by trapping. Consequently, their residence time in the channel is increased. Secondly, when a particle shows a balanced pDEP/nDEP response, the particles spend less time in low velocity regions due to the constant movement orthogonal to the fluid flow and therefore are only retarded minimal. Finally, when a particle predominately shows nDEP it migrates towards the ceiling of the channel and is slowed down there. Since the electric field gradients are smaller at the ceiling, trapping becomes more unlikely and migration velocities due to DEP are lower.

Determination of crossover frequency. As presented above, the direction dielectrophoretic movement is, among other things, influenced by the particles conductivity and its size. However, the conductivity of the particles is unknown and needs to be evaluated prior to the DPC experiments or simulations. In this work, model PS particles are used. Since their material conductivity is negligible, the surface conductance has a significant impact on the polarization (Eq. 3). At suitable medium conductivities, PS particles are know to show positive dielectrophoresis at low frequencies due to the surface conductance and negative dielectrophoresis at high frequencies since the permittivity is much smaller compared to the surrounding medium[17,23].

In the literature, multiple ways are presented to determine the dielectric properties and consequently the crossover frequency or vice versa. For example, the crossover can be measured by observing the particle movement when subjected to various frequencies[23,36] or using electrorotation[34]. Even commercial and label-free systems are available by now which provide a rapid analysis of the frequency response of (biological) particles[37].

An approach compatible with the DPC set-up was proposed by Sano et al.[29]. They stated that in dielectrophoretic particle chromatography a particle passes through a channel when the polarisation is negligible. This is valid for particles that are subjected to an electric field with a frequency which is close to the crossover frequency of the suspended particle and other effects such as hydrodynamic lift and gravitation are negligible. Gascoyne and coworkers [19,30] used a similar approach in batch-mode DEP field-flow fractionation and made it applicable for deformable particles.

By testing differed frequencies subsequently, the crossover frequency can be approximated by comparing the elution profiles of fixed-frequency DPC experiments to elution peaks where no voltage is applied (Fig. 1C).

Experimental details. The microfluidic device has been described in detail in a previous publication[33]. Briefly, the $h = 80\,\mu m$ high microfluidic channel is made from PDMS, has a width of 2 mm and a length of about 17 cm. The channel is bonded to an electrode array using PDMS as a thin intermediate layer, which also is meant to reduce particle adhesion to the electrodes. The electrodes have a width and a spacing of 100 µm and are connected to a single channel amplifier (A400, Pendulum Instruments, Sweden) which provides a constant amplification factor over a large bandwidth. The signal is generated by a signal generator (Rigol DG4062, Rigol Technologies EU GmbH, Puchheim, Germany) and controlled using a digital oscilloscope (Rigol DS2072A, Rigol Technologies EU GmbH, Puchheim, Germany). The particles were observed at the outlet using a Nikon TS2R-FL inverted fluorescence microscope (Nikon Instruments Europe BV, Amsterdam, The Netherlands), a white light source (XCite 120 PC, Excelitas Technologies Corp., USA), a triple-bandpass (DAPI/FITC/TRITC) and a USB RGB camera (GS3-U3-51S5C-C, FLIR Systems Inc., USA). Resident time distributions were obtained by segmenting and processing the video files from the experiments with MATLAB.

The particles were purchased from Polysciences, Inc. (USA) and suspended prior to the experiments in the medium. The suspension in all experiments has a conductivity of $2\,\mu S\,cm^{-1}$. To produce the medium per 100 ml pure water (OmniaTap 6 UV/UF, stakpure GmbH, Germany), we add 2 ml of 1 % Tween 20 and 3µL of 0.01 M KOH to adjust the pH value. Further, KCl was added to adjust the conductivity to a value of $2\,\mu S\,cm^{-1}$. The volume flow in all experiments was $5\,mL\,h^{-1}$ and the injection was conducted at $t = 10$ s by opening a manual 4 way valve (H&S V-101D, IDEX Health & Science, USA) for two seconds. The flow was generated by two syringe pumps (Legato 200 & 270, KD Scientific Inc., USA).

To quantify the outcome of the separation we use the resolution R_s, which can be defined as

$$R_s = \frac{\Delta T_{max}}{\frac{1}{2}(w_1 + w_2)}, \tag{4}$$

with T_{max} being the maximum of the residence time distributions and w_x the full width at half maximum (FWHM). In addition to the resolution the purity of each fraction can be used to describe the outcome of an separation, which here is defined as

$$\frac{\sum_0^t I_x(t)}{\sum_0^{t=120s} I_x(t)}, \tag{5}$$

by using t as time and $I_x(t)$ as fluorescence intensity at time t. This sum is normalized by its maximum cumulated intensity and therefore always reaches 1 at the end of the experiment ($t = 120$ s).

Simulation model. To investigate the particle movement and to isolate effects, we build a simulation model using COMSOL Multiphysics linked to MATLAB. Boundary conditions are necessary, which were selected in accordance with the literature[18,38] and are shown in Fig. 5. More details of the simulation model as well as a mesh independence study can be found in the supplement.

To compare experimental and simulative retention times of the particles quantitatively, a two-dimensional full scale model was chosen as basis for the simulation. Within the model three different sections, the static electric and velocity fields, particle tracing, and the MATLAB-COMSOL interaction, can be distinguished. The laminar flow ($Re \ll 1$) profile is calculated using the Stoke's approximation for low Reynolds numbers. The inlet velocity can be obtained by dividing the volume flow by the area of the microchannel. As outlet boundary condition a constant pressure (0 Pa) is used. In combination with a no slip condition at ceiling and bottom a parabolic flow profile is calculated.

The electric field in experiment and simulation is generated by an electrode array and simulated at the center frequency of the modulation spectrum. In these arrays an electrode with a applied potential of V_{RMS} is neighboured by two electrodes on GND (0 V) potential (Fig. 5). A thin PDMS layer is placed on top of the electrodes.

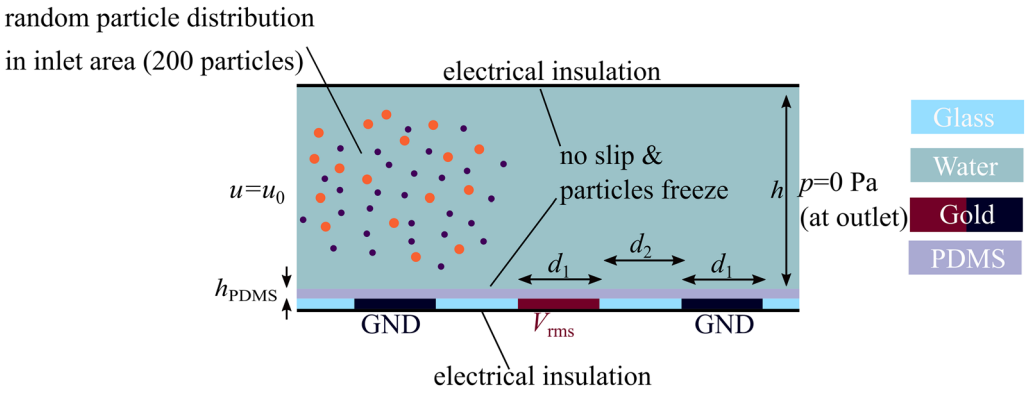

Figure 5. Important boundary conditions and materials of the simulative model. Important parameters: height of the channel $h = 80\,\mu m$, width d_1 and spacing d_2 of the electrodes is 100 µm. Inlet velocity 8.68 mm s^{-1} and insulation thickness $h_{PDMS} = 1.75\,\mu m$. At the inlet 200 particles were randomly distributed in a 1.5 cm × 60 µm area being 10 µm away from bottom and ceiling.

The thickness has not been determined experimentally but is significantly below 3 µm according to literature[39]. It has been used as a fitting factor and the best match between experiment and simulation was achieved when using $h_{PDMS} = 1.75\,\mu m$. Placing PDMS as dielectric material on top of the electrode array generates a high-pass filter. The effect was simulated and implemented into to the model (Supplementary Fig. 1). The medium was simulated with a conductivity of $\sigma_m = 2\,\mu S\ cm^{-1}$ and a relative permittivity of 78 whereas the particles were simulated with a substatially lower relative permittivity of 2.7 and a conductivity calculated according to Eq. (3) using $\sigma_{bulk} = 0$. Coupling of fluid field and electric field was not added, since the experiments were conducted at low medium conductivity and sufficiently high frequencies. The first point does reduce the effect of electrothermal movement (heat loss density $= \sigma_m \mathbf{E}^2$) whereas the latter suppresses the influence of AC electroosmosis[40,41].

However, in microfluidics unspecific adhesion, (electro-)thermal flow, hydrodynamic lift, particle-particle interactions and/or electrokinetic phenomena can play an important role, but are hard to quantify and therefore to implement. As a result, experimental training data was used to get a good match by adjusting some parameters of the simulation in a reasonable range. The adjusted parameters were PDMS isolation thickness and the surface conductance ("Size-selective separation" section) as well as the particle release offset (see below).

The second part of the simulation is the particle movement description. Particles are experiencing positive and negative dielectrophoresis, viscous drag, and gravitation. All particles are assumed to be massless, which is reasonable given their small stopping distance, to reduce the computational effort. Additionally, as soon as particles reach the ceiling or bottom they are assumed to be trapped, which is not always true in reality. Once particles are trapped in the simulation they stay at their location. This is not valid for a DPC experiment, which leads to the third part of the model which is formed by the COMSOL-MATLAB interaction. The Re(CM) needs to be calculated for each time step to implement the impact of the frequency modulation into the COMSOL model and consequently produce pDEP and nDEP movement of the particles with respect to their properties. To implement the frequency changes into the simulation a sawtooth function was used in COMSOL which then was used as feed for a calculation of the Clausius-Mossotti factor as a function of time/frequency. This procedure allows to reduce the computational cost of the simulation because is not needed to calculate the electric field in every single time step of the time dependent solver.

Using MATLAB, the movement of the particles through the channel is divided into multiple parts. In the experiment the valve to inject the particles is opened for two seconds. In this time period, particles are entering the channel at different heights (y-positions) and times. Due to the constant flow they are at different (x-)positions along the channel. Consequently to reproduce this kind of peak in the simulation, particles are initialized in an area rather than on one point or line. For this purpose we added an inlet area of 1.5 cm in front if the simulated channel where no electrodes are existent and $n = 200$ particles per type are randomly placed at the beginning in a range of heights between 10 and 70 µm.

After the particles are released they experience dielectrophoresis and may eventually reach a boundary where they freeze. Consequently, at sufficient high voltages no particles would exit the channel in the simulation. To overcome this issue, a MATLAB script checks Re(CM) for changes of its sign and stops the simulation as the value reaches zero. At this point the model checks for particles adhering to the wall and repositions them up to 10 µm orthogonal to the wall into the channel. The extend of the manipulation of the particles position is randomly chosen between 0 and 10 µm to incorporate the inhomogeneous nature of particle-wall interactions, which effectively can lead to broader, less pronounced elution peaks. Particle positions are logged to calculate residence time distributions. Since the model contains random components multiple runs are necessary to check for statistical validity (Supplementary Fig. 9).

Data availability

The datasets generated and/or analyzed during the current study are available from the corresponding author on reasonable request.

Received: 22 April 2021; Accepted: 26 July 2021
Published online: 19 August 2021

References

1. Louhadj, S. *et al.* Experimental analysis of the attraction force applied on metal particles using a double-side electrical curtain. *J. Electrostat.* **105**, 103448. https://doi.org/10.1016/j.elstat.2020.103448 (2020).
2. Wang, F. *et al.* Metals recovery from dust derived from recycling line of waste printed circuit boards. *J. Clean. Prod.* **165**, 452–457. https://doi.org/10.1016/j.jclepro.2017.07.112 (2017).
3. Spengler, T., Ploog, M. & Schröter, M. Integrated planning of acquisition, disassembly and bulk recycling: A case study on electronic scrap recovery. *OR Spectrum* **25**, 413–442 (2003).
4. Hansen, L., Wollmann, A., Weers, M., Benker, B. & Weber, A. P. Triboelectric charging and separation of fine powder mixtures. *Chem. Eng. Technol.* **43**, 933–941. https://doi.org/10.1002/ceat.201900558 (2020).
5. Peleka, E. N., Gallios, G. P. & Matis, K. A. A perspective on flotation: A review. *J. Chem. Technol. Biotechnol.* **93**, 615–623. https://doi.org/10.1002/jctb.5486 (2018).
6. Shim, S. *et al.* Antibody-independent isolation of circulating tumor cells by continuous-flow dielectrophoresis. *Biomicrofluidics*. https://doi.org/10.1063/1.4774304 (2013).
7. Friedlander, S. K. *Smoke, Dust, and Haze* 2nd edn. (Oxford University Press, New York, 2000).
8. Wang, X. B. *et al.* Cell separation by dielectrophoretic field-flow-fractionation. *Anal. Chem.* **72**, 832–839. https://doi.org/10.1021/ac990922o (2000).
9. Washizu, M., Suzuki, S., Kurosawa, O., Nishizaka, T. & Shinohara, T. Molecular dielectrophoresis of bio-polymers. In *Conference Record - IAS Annual Meeting (IEEE Industry Applications Society)* 1992-January, 1446–1452, https://doi.org/10.1109/IAS.1992.244397 (1992).
10. Moon, H.-S. *et al.* Continuous separation of breast cancer cells from blood samples using multi-orifice flow fractionation (MOFF) and dielectrophoresis (DEP). *Lab Chip* **11**, 1118. https://doi.org/10.1039/c0lc00345j (2011).
11. Michael, K. A., Hiibel, S. R. & Geiger, E. J. Dependence of the dielectrophoretic upper crossover frequency on the lipid content of microalgal cells. *Algal Res.* **6**, 17–21. https://doi.org/10.1016/j.algal.2014.08.004 (2014).
12. Hanauer, M., Pierrat, S., Zins, I., Lotz, A. & Sönnichsen, C. Separation of nanoparticles by gel electrophoresis according to size and shape. *Nano Lett.* **7**, 2881–2885. https://doi.org/10.1021/nl071615y (2007).
13. Barasinski, M. & Garnweitner, G. Restricted and unrestricted migration mechanisms of silica nanoparticles in agarose gels and their utilization for the separation of binary mixtures. *J. Phys. Chem. C* **124**, 5157–5166. https://doi.org/10.1021/acs.jpcc.9b10644 (2020).
14. Williams, S. K. R., Runyon, J. R. & Ashames, A. A. Field-flow fractionation: Addressing the nano challenge. *Anal. Chem.* **83**, 634–642. https://doi.org/10.1021/ac101759z (2011).
15. Wei, G. T. Shape separation of nanometer gold particles by size-exclusion chromatography. *Anal. Chem.* **71**, 2085–2091. https://doi.org/10.1021/ac990044u (1999).
16. Pethig, R. Dielectrophoresis: Status of the theory, technology, and applications. *Biomicrofluidics*. https://doi.org/10.1063/1.3456626 (2010).
17. Pesch, G. R., Du, F., Baune, M. & Thöming, J. Influence of geometry and material of insulating posts on particle trapping using positive dielectrophoresis. *J. Chromatogr. A* **1483**, 127–137. https://doi.org/10.1016/j.chroma.2016.12.074 (2017).
18. Pesch, G. R. *et al.* Bridging the scales in high-throughput dielectrophoretic (bio-)particle separation in porous media. *Sci. Rep.* **8**, 1–12. https://doi.org/10.1038/s41598-018-28735-w (2018).
19. Shim, S., Stemke-Hale, K., Noshari, J., Becker, F. F. & Gascoyne, P. R. Dielectrophoresis has broad applicability to marker-free isolation of tumor cells from blood by microfluidic systems. *Biomicrofluidics*. https://doi.org/10.1063/1.4774307 (2013).
20. Pethig, R. Review-where is dielectrophoresis (DEP) going?. *J. Electrochem. Soc.* **164**, B3049–B3055. https://doi.org/10.1149/2.0071705jes (2017).
21. Pesch, G. R. & Du, F. A review of dielectrophoretic separation and classification of non-biological particles. *Electrophoresis*. https://doi.org/10.1002/elps.202000137 (2020).
22. Weirauch, L. *et al.* Material-selective separation of mixed microparticles via insulator-based dielectrophoresis. *Biomicrofluidics* **13**, 20. https://doi.org/10.1063/1.5124110 (2019).
23. Ermolina, I. & Morgan, H. The electrokinetic properties of latex particles: Comparison of electrophoresis and dielectrophoresis. *J. Colloid Interface Sci.* **285**, 419–428. https://doi.org/10.1016/j.jcis.2004.11.003 (2005).
24. Lorenz, M. *et al.* High-throughput dielectrophoretic filtration of sub-micron and micro particles in macroscopic porous materials. *Anal. Bioanal. Chem.* **412**, 3903–3914. https://doi.org/10.1007/s00216-020-02557-0 (2020).
25. Calero, V., Garcia-Sanchez, P., Honrado, C., Ramos, A. & Morgan, H. AC electrokinetic biased deterministic lateral displacement for tunable particle separation. *Lab Chip* **19**, 1386–1396. https://doi.org/10.1039/c8lc01416g (2019).
26. Vahey, M. D. & Voldman, J. An equilibrium method for continuous-flow cell sorting using dielectrophoresis. *Anal. Chem.* **80**, 3135–3143. https://doi.org/10.1021/ac7020568 (2008).
27. Aldaeus, F., Lin, Y., Amberg, G. & Roeraade, J. Multi-step dielectrophoresis for separation of particles. *J. Chromatogr. A* **1131**, 261–266. https://doi.org/10.1016/j.chroma.2006.07.022 (2006).
28. Yang, J., Huang, Y., Wang, X. B., Becker, F. F. & Gascoyne, P. R. Differential analysis of human leukocytes by dielectrophoretic field- flow-fractionation. *Biophys. J.* **78**, 2680–2689. https://doi.org/10.1016/S0006-3495(00)76812-3 (2000).
29. Sano, H., Kabata, H., Kurosawa, O. & Washizu, M. Dielectrophoretic chromatography with cross-flow injection. In *Technical Digest. MEMS 2002 IEEE International Conference. Fifteenth IEEE International Conference on Micro Electro Mechanical Systems (Cat. No.02CH37266)* 2–5. https://doi.org/10.1109/MEMSYS.2002.984043 (2002).
30. Gascoyne, P. R. Dielectrophoretic-field flow fractionation analysis of dielectric, density, and deformability characteristics of cells and particles. *Anal. Chem.* **81**, 8878–8885. https://doi.org/10.1021/ac901470z (2009).
31. Wang, X. B., Vykoukal, J., Becker, F. F. & Gascoyne, P. R. Separation of polystyrene microbeads using dielectrophoretic/gravitational field-flow-fractionation. *Biophys. J.* **74**, 2689–2701. https://doi.org/10.1016/S0006-3495(98)77975-5 (1998).
32. Modarres, P. & Tabrizian, M. Frequency hopping dielectrophoresis as a new approach for microscale particle and cell enrichment. *Sensors Actuators B Chem.* **286**, 493–500. https://doi.org/10.1016/j.snb.2019.01.157 (2019).
33. Giesler, J. *et al.* Polarizability-dependent sorting of microparticles using continuous-flow dielectrophoretic chromatography with a frequency modulation method. *Micromachines* **11**, 1–14. https://doi.org/10.3390/mi11010038 (2020).
34. Arnold, W. M., Schwan, H. P. & Zimmermann, U. Surface conductance and other properties of latex particles measured by electrorotation. *J. Phys. Chem.* **91**, 5093–5098. https://doi.org/10.1021/j100303a043 (1987).
35. Adams, T. N., Leonard, K. M. & Minerick, A. R. Frequency sweep rate dependence on the dielectrophoretic response of polystyrene beads and red blood cells. *Biomicrofluidics*. https://doi.org/10.1063/1.4833095 (2013).
36. Liu, N. *et al.* Automated parallel electrical characterization of cells using optically-induced dielectrophoresis. *IEEE Trans. Autom. Sci. Eng.* **17**, 1084–1092. https://doi.org/10.1109/TASE.2019.2963044 (2020).
37. Hoettges, K. F. *et al.* Ten-second electrophysiology: Evaluation of the 3DEP Platform for high-speed, high-accuracy cell analysis. *Sci. Rep.* **9**, 1–13. https://doi.org/10.1038/s41598-019-55579-9 (2019).

38. Green, N. Numerical solution of the dielectrophoretic and travelling wave forces for interdigitated electrode arrays using the finite element method. *J. Electrostat.* **56**, 235–254. https://doi.org/10.1016/S0304-3886(02)00069-4 (2002).
39. Gajasinghe, R. W. *et al.* Experimental study of PDMS bonding to various substrates for monolithic microfluidic applications. *J. Micromech. Microeng.*. https://doi.org/10.1088/0960-1317/24/7/075010 (2014).
40. Green, N. G., Ramos, A., González, A., Castellanos, A. & Morgan, H. Electrothermally induced fluid flow on microelectrodes. *J. Electrostat.* **53**, 71–87. https://doi.org/10.1016/S0304-3886(01)00132-2 (2001).
41. González, A., Ramos, A., Green, N. G., Castellanos, A. & Morgan, H. Fluid flow induced by nonuniform ac electric fields in electrolytes on microelectrodes. II. A linear double-layer analysis. *Phys. Rev. E* **61**, 4019–4028. https://doi.org/10.1103/PhysRevE.61.4019 (2000).

Acknowledgements

The authors thank the German Research Foundation (DFG) within the priority program, "MehrDimPart—Highly specific and multidimensional fractionation of fine particle systems with technical relevance" (SPP2045, Grant Numbers BA 1893/2-1, PE 3015/3-2, TH 893/20-2) for funding. We thank Jonathan Kottmeier (IMT, Technische Universität Braunschweig) and Marc-Peter Schmidt (Technische Hochschule Brandenburg) for the help in manufacturing the components of the separation column and Fei Du (CVT, Universität Bremen) for fruitful discussions.

Author contributions

J.G., M.B., J.T. and G.R.P. conceived the experiments and simulations, J.G. conducted the experiments and simulations, J.G., M.B., J.T., L.W. and G.R.P. analyzed the results. J.G. wrote the manuscript with input from all other authors. All authors reviewed the manuscript.

Funding

Open Access funding enabled and organized by Projekt DEAL.

Competing interests

The authors declare no competing interests.

Additional information

Supplementary Information The online version contains supplementary material available at https://doi.org/10.1038/s41598-021-95404-w.

Correspondence and requests for materials should be addressed to G.R.P.

Reprints and permissions information is available at www.nature.com/reprints.

Publisher's note Springer Nature remains neutral with regard to jurisdictional claims in published maps and institutional affiliations.

6 Development of an high throughput electrode based dielectrophoretic separator I

This study was published as

Giesler, J.; Weirauch, L.; Thöming, J.; Baune, M.; Pesch, G. R. High-Throughput Dielectrophoretic Separator Based on Printed Circuit Boards. *ELECTROPHORESIS* **2023**, *44*, 72–81, DOI: 10.1002/elps.202200131.

This manuscript focuses on introducing large scale electrode arrays manufactured by a commercial PCB manufacturer at costs around 1 € per board. The area covered with electrodes and thus the throughput could be significantly increased compared to, the two previous chapters. In the same time the setups becomes less expensive and is easier to manufacture. In contrast to the chapters before, the study focuses of selective trapping at a fixed frequency and flow rates nearly two orders of magnitude larger than before.

The previously described DPC procedure (Chapter 4 and 5) requires high field strength in order to create multiple trap and release cycles. As the separator described in this chapter features significantly larger electrode arrays (array size 700 mm^2 vs. $\approx 2 \times 7000$ mm^2) such high voltages (80 to 160 V_{pp}) with a modulated frequency are challenging to obtain due to an increased current. Therefore, a fixed frequency approach seems reasonable as here the particles are experiencing pDEP or nDEP for a longer period of time what allows reducing the voltage significantly. Nonetheless, the setup presented in this study is in principle also suitable to achieve higher throughput in DPC experiments. Therefore, this setup should be considered as a potential basis for high throughput electrode based dielectophoretic separators in general which includes the approach presented in the previous two chapters.

Depending on the definition of microfluidics, the device in this chapter can be considered as a microfluidic channel or not. Nguyen [56] defines microfluidic devices as setups with dimensions of the channel from 1 µm to 1 mm, which is true in this case for the height but not the width of the channel.

For this publication not only supporting information exist, which can be found at the online version of the article, but also an online repository was created. The

online repository can be found at

Giesler, J. Online Repository for "High Throughput Dielectrophoretic Separator Based on Printed Circuit Boards" Zenodo, `https://doi.org/10.5281/zenodo.6806667`

and it contains not only measurement data but also evaluation scripts and manufacturing data for the printed circuit boards that make follow-up studies by other working groups easier.

Received: 20 May 2022 | Revised: 22 July 2022 | Accepted: 10 August 2022

DOI: 10.1002/elps.202200131

ELECTROPHORESIS

RESEARCH ARTICLE

High-throughput dielectrophoretic separator based on printed circuit boards

Jasper Giesler[1] | **Laura Weirauch**[1] | **Jorg Thöming**[1,2,3] | **Michael Baune**[1,3] | **Georg R. Pesch**[1,2]

[1]Chemical Process Engineering, Faculty of Production Engineering, University of Bremen, Leobener Straße 6,, 28359, Bremen, Germany

[2]MAPEX Center for Materials and Processes, University of Bremen 28359, Bremen, Germany

[3]Center for Environmental Research and Sustainable Technology (UFT), University of Bremen, Leobener Straße 6 28359, Bremen, Germany

Correspondence
Georg R. Pesch, Chemical Process Engineering, Faculty of Production Engineering, University of Bremen, Leobener Straße 6, 28359 Bremen, Germany.
Email: gpesch@uni-bremen.de

Color online: See the article online to view Figures 1–4 in color.

Funding information
Deutsche Forschungsgemeinschaft, Grant/Award Numbers: PE 3015/3-2, TH 893/20-2

Abstract

The separation of particles with respect to their intrinsic properties is an ongoing task in various fields such as biotechnology and recycling of electronic waste. Especially for small particles in the lower micrometer or nanometer range, separation techniques are a field of current research since many existing approaches lack either throughput or selectivity. Dielectrophoresis (DEP) is a technique that can address multiple particle properties, making it a potential candidate to solve challenging separation tasks. Currently, DEP is mostly used in microfluidic separators and thus limited in throughput. Additionally, DEP setups often require expensive components, such as electrode arrays fabricated in the clean room. Here, we present and characterize a separator based on two inexpensive custom-designed printed circuit boards (80 × 120 mm board size). The boards consist of interdigitated electrode arrays with 250 μm electrode width and spacing. We demonstrate the separation capabilities using polystyrene particles ranging from 500 nm to 6 μm in monodisperse experiments. Further, we demonstrate selective trapping at flow rates up to 240 ml/h in the presented device for a binary mixture. Our experiments demonstrate an affordable way to increase throughput in electrode-based DEP separators.

KEYWORDS
dielectrophoresis, high-throughput, lab-on-pcb, selective trapping, separation

1 | INTRODUCTION

Separating particles according to their properties is an important task in technical applications such as processing of minerals [1, 2] and recycling of electronic waste [3–5]. Separation is also a unit operation in biotechnological applications such as the detection of circulating tumor cells [6–8], processing of proteins or DNA [9–11], or the collection of micro algae with high lipid content [12–14]. Especially for particles with diameters in the micrometer or nanometer range, dielectrophoresis (DEP) is one promising candidate to solve challenging separation tasks. DEP is commonly used in the biomedical field [15, 16],

Abbreviations: DAPI, 4',6-diamidino-2-phenylindole; eDEP, electrode-based dielectrophoresis; FFF, field-flow fractionation; IDE, interdigitated electrodes; iDEP, insulator-based dielectrophoresis; nDEP, negative dielectrophoresis; PCB, printed circuit board; pDEP, positive dielectrophoresis; PS, polystyrene; TRITC, tetramethylrhodamine.

but also to separate non-biological particles [17–19]. Many existing approaches to separate particles are based on gravity or inertia. Both effects diminish with decreasing particle size. Therefore, alternatives for particle separation in the micrometer or nanometer range are in the focus of current research. Separators based on DEP usually show high selectivity, as it is for example necessary for the detection of circulating tumor cells [7].

Dielect describes the movement of a suspended polarizable particle in an inhomogeneous electric field. The dielectrophoretic force $\mathbf{F}_{\mathrm{DEP}}$ affecting a spherical particle can be approximated as [20]

$$\mathbf{F}_{\mathrm{DEP}} = 2\pi r_{\mathrm{p}}^3 \varepsilon_{\mathrm{m}} \mathrm{Re}(CM) \nabla |\mathbf{E}_{\mathrm{rms}}|^2 \tag{1}$$

with r_{p}, the radius of the particle, the electric field, $\mathbf{E}_{\mathrm{rms}}$, and the permittivity of the surrounding medium ε_{m}. Similar to gravitation or inertia, the magnitude of the dielectrophoretic force decreases with particle size. However, for strong electric fields, DEP can exceed the gravitational force by several orders of magnitude [21]. The frequency-dependent polarizability of a particle (subscript p) in a medium (subscript m) is reflected by $\mathrm{Re}(CM)$ which is the real part of the so-called Clausius–Mossotti factor [20]

$$\mathrm{Re}(CM) = \mathrm{Re}\left(\frac{\tilde{\varepsilon}_{\mathrm{p}} - \tilde{\varepsilon}_{\mathrm{m}}}{\tilde{\varepsilon}_{\mathrm{p}} + 2\tilde{\varepsilon}_{\mathrm{m}}}\right). \tag{2}$$

The complex permittivity $\tilde{\varepsilon}$ is defined as

$$\tilde{\varepsilon} = \varepsilon_0 \varepsilon_{\mathrm{r}} - i\frac{\sigma}{\omega}. \tag{3}$$

Here, σ represents the conductivity, ε_0 the vacuum permittivity, ε_{r} the relative permittivity of particle or medium, and $\omega = 2\pi f$ the angular frequency. When the sign of $\mathrm{Re}(CM)$ is positive, $\mathbf{F}_{\mathrm{DEP}}$ points toward local field maxima, which can be observed for particles that have higher polarizability than the surrounding medium. This is referred to as positive DEP (pDEP). When the sign of $\mathrm{Re}(CM)$ is negative, particles are less polarizable than the surrounding medium, which will result in negative DEP (nDEP). nDEP is a repulsive force pointing away from local field maxima. Both, pDEP [22–24] and nDEP [22, 25, 26] can be utilized to separate or trap particles specifically.

For small particles with low material conductivity σ_{bulk} in an aqueous suspension, the surface conductance K_{s} becomes an important parameter when calculating the overall particle conductivity σ_{p}. This conductivity can be approximated with [27]:

$$\sigma_{\mathrm{p}} = \sigma_{\mathrm{bulk}} + \frac{2K_{\mathrm{s}}}{r_{\mathrm{p}}}. \tag{4}$$

Most DEP separators are microfluidic devices and therefore handle volume flows in the µL/h or lower ml/h range [20, 28, 29]. For highly valuable products such as proteins or cells, this is sufficient and can be considered as high throughput [7, 30, 31]. Moreover, dielectrophoretic field-flow fractionation (DEP-FFF) setups can achieve a throughput in the 100 ml/h range but are challenging to scale up [32]. However, when high quantities or less valuable products are to be processed, a further increase of throughput is necessary. The DEP force scales with the gradient of the electric field squared (equation (1)). During device scale up, it is therefore important to keep the gradient of the electric field high, so that DEP is the dominant force in the separator. In microfluidic separators the gradient is often generated by using either interdigitated electrodes (IDE) [11, 29, 33, 34] or via disturbing an otherwise homogeneous electric field by adding insulating structures into the device [10, 35, 36]. These two approaches are referred to as electrode-based DEP (eDEP) and insulator-based DEP (iDEP). iDEP devices often use PDMS posts as insulating material. To scale up iDEP devices, our group proposed a setup consisting of a macroscopic ceramic foam which acts as insulator. The particle suspension flows through the foam that is sandwiched between two steel plates that act as electrodes [22, 28]. The insulating foam scatters the electric field and allows to apply flow rates above 0.5 L/h. Other approaches use for example glass spheres [37] or insulating polymer meshes [19, 38] to increase the volume of the separation chamber and hence the throughput.

In eDEP devices, the field strength is exponentially decreasing with distance from the IDE [39] making it difficult to increase the dimension orthogonal to the electrodes. Furthermore, electrodes in many cases are produced using a variety of clean-room techniques, making the production time consuming and expensive and therefore less accessible for many research groups [40]. One approach to reduce the costs of setups containing IDE is the lab-on-PCB approach [40, 41]. Here, printed circuit boards (PCB) are used as base material for lab-on-a-chip approaches. Because many commercial manufacturers exist that produce custom PCB and the process is highly automated and parallelized, this provides an inexpensive solution for groups wanting to design custom patterns on PCB [40]. These cannot only be utilized as electrodes but also as master molds for replica molding in microfluidics [42]. While clean rooms offer the opportunity to create electrodes with small width and spacing or three-dimensional structures that are required for highly sensitive separators and sensors [29, 43], commercially manufactured PCB are cheap and can be obtained without access to a clean room. Further, PCB can be produced with large surface areas (e.g., 46×61 cm [40]), while maintaining small enough elec-

trode spacing for many applications (minimum feature size around 100 μm) [40, 41]. Several groups showed the applicability of PCB in eDEP setups, mainly in the biotechnological field to manipulate and analyze cells [41, 44–46]. One of such applications is the commercially available 3DEP device [46]. However, these PCB-based approaches focus on analyzing or separating cells or particles from small volumes and are not designed for a continuous high-throughput separation. Williams et al. [23] proposed a setup with PCB structured by milling. The authors presented two different electrode configurations that can either concentrate PS particles in microfluidic channels utilizing nDEP or pDEP or analyze the frequency response of the particles. Other groups used PCB to fabricate customized electrical connections for their setups [47, 48]. PCB were also used to manipulate particles using so-called electric curtains for example for dust repulsion [49] or metal sorting [5].

To the best of the authors' knowledge, no eDEP device based on PCB with an application focus on high throughput separation has been published yet. The inexpensive manufacturing and easy scalability of PCB make these boards a good candidate to develop high throughput separators. In contrast to large-scale iDEP devices, devices based on eDEP are simpler to construct and easy to clean, as no additional material is blocking the fluid pathway. In this manuscript, we show an easy method to construct a scalable eDEP separator based on PCB. We also analyze the electrical properties of the separator and show its potential for selective particle separation. We present a low-cost device that can operate at high throughput and is aimed at the separation of non-biological particles. Corresponding application examples include the recovery of precious metals from electronic waste dust or the recovery of active materials during battery recycling. Apart from these applications, the setup presented here is in principal also suitable for applications in the biotechnological field.

2 | MATERIALS AND METHODS

2.1 | Channel fabrication

To create the inhomogeneous electric field necessary for DEP, we designed a PCB (manufactured by JLCPCB JiaLIChing (Hong Kong) Co. Ltd., China) with an interdigitated electrode array. The electrodes have a width and a spacing of 250 μm and are covered with a lead-free hot air solder leveling (HASL) surface layer. We performed a three-dimensional analysis of the electrode surface. The surface roughness was found to be 0.66 μm ± 0.23 μm (for further information please see Section S4, Supporting Information). We chose FR-4 as material for the board itself. The outer dimensions of the board are 80 × 120 mm and the costs of one board were below 1€ (March 2022), when ordering a quantity of 50 boards per order, which underlines the low-cost approach of this setup. We designed the PCB using KiCad 5.1.12, the manufacturing data can be downloaded at the online repository [50]. The board is shown in Figure 1A and a close up of the electrode array is given in Figure 1B. Two neighboring electrodes on the PCB are connected in an alternating order, so that one electrode is grounded and the other one provides the sinusoidal signal. The boards were embedded into a recess of the cover plates by using an inexpensive silicone sealant normally used in bath or kitchen environments (Sikasil E Plus, Sika Deutschland GmbH, Germany). The cover plates consist of polypropylene (PP). The PCB were connected to an amplifier using connection pads at the backside of the PCB and matching holes in the PP plates.

In this setup, two PCB face each other and therefore form ceiling and bottom of the flow chamber (Figure 1C). The boards are separated by a 0.5 mm silicone gasket which also acts as spacer (Figure 2B). The gasket was cut using a scalpel so that a meandering channel was created to avoid shortcuts from inlet to outlet and thus increase the residence time of the suspension in the setup (Figure 2B). By using this electrode configuration, particles showing pDEP will be attracted toward the electrode arrays and trapped at the local field maxima if the drag force is not exceeding the dielectrophoretic force. Particles experiencing nDEP, in contrast, will be repelled from them and are continuously flushed out of the channel (Figure 1C). This electrode configuration differs from traditional DEP-FFF setups where electrodes at the bottom of the device are used to levitate particles on specific flow lines to achieve characteristic retention time [26, 51, 52] or guide them into specific outlets [53]. In DEP-FFF setups, the drag force does not compete with the dielectrophoretic force. As the electrode material is opaque, the device has no optical accessibility to observe the particle movement in the device directly. For research projects where the observation of particles is important, transparent substrates as PET are available for flexible electrodes. In this study, optical access is not crucial as the behavior of PS particles over electrode arrays is well described in the literature [24–27, 33, 52, 54]. Drill holes with an M6 thread are used as inlets and outlets to which capillaries were connected using IDEX connectors (P-213, IDEX Health & Science, LLC, USA). The particle suspension was pumped by an Ismatec MCP-CPF IP65 piston pump with the pump head FMI 202 QP.Q0.SSY (Cole-Parmer GmbH, Germany, Figure 2A). The voltage was supplied by an F30PV (Pendulum Instruments, Sweden, Figure 2D) amplifier, which is capable of providing a current of 2 A up to the MHz range at a maximum

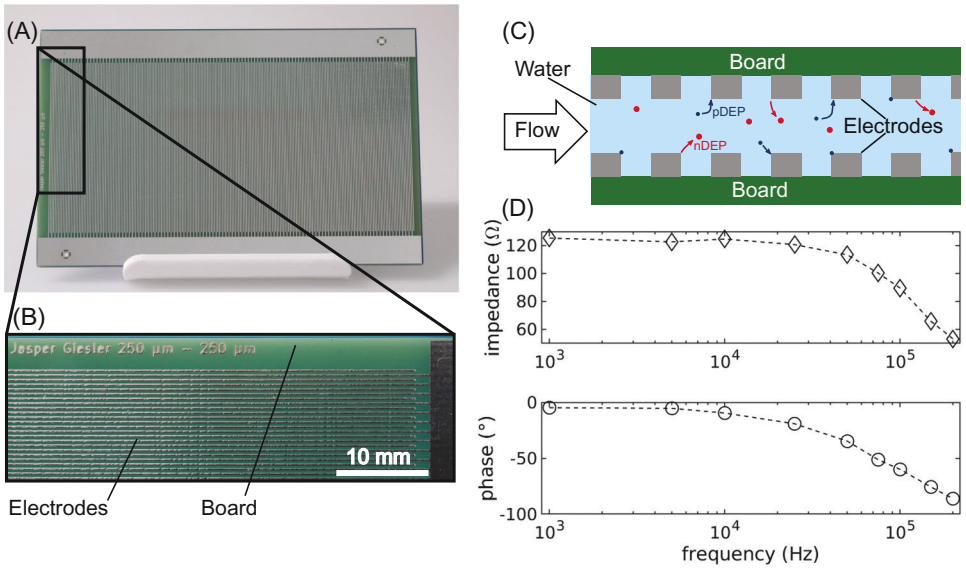

FIGURE 1 (A) Front view of the electrode array. Outer dimensions of the printed circuit board (PCB) are 80 × 120 mm. The substrate (green) is nonconductive and made out of FR-4, whereas the electrodes consist of copper. Additionally, a lead-free hot air solder leveling surface finish (silver) is applied. (B) Close-up of PCB. Width and spacing of the electrodes are 250 µm each. (C) Schematic representation of the device. PCBs are used as bottom and ceiling to form a channel through which a particle suspension is pumped. The electrodes generate an electric field that leads to positive (pDEP) and negative dielectrophoresis (nDEP) of the suspended particles. The boards are separated by a silicone gasket (not shown). (D) Measured impedance and phase shift of the device. During the measurement, water with a conductivity of 2.1 µS/cm was pumped through the channel.

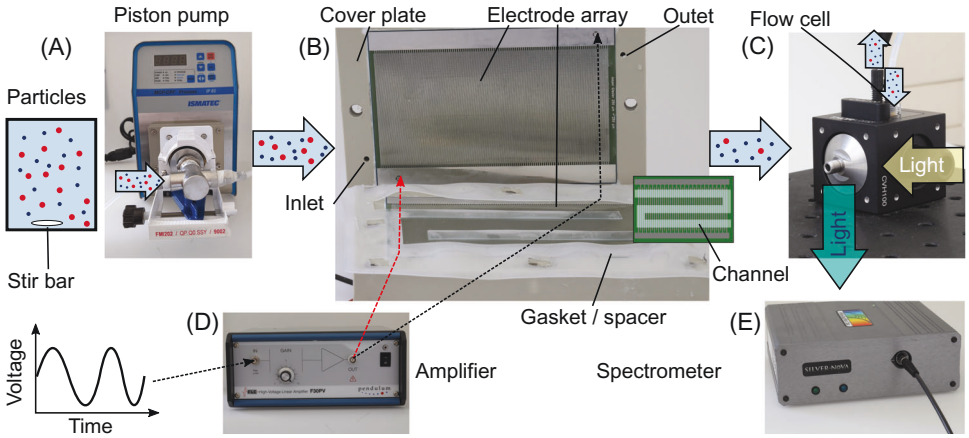

FIGURE 2 Overview of the experimental setup. The particles are suspended in water, stirred by a magnetic stirrer, and pumped by a piston pump (A) into the separation device (B). The separation chamber is formed by two PCBs on which the electrodes arrays are located. A silicone gasket (0.5 mm thickness) defines the flow path of the suspension as well as the height of the channel. Cover plates made of polypropylene and screws are used to press the components onto each other. The electrodes are connected to an amplifier which provides a sinusoidal voltage to operate the device (D). The suspension leaving the channel is flowing into a flow cell (C) that is coupled to a light source. The resulting fluorescence signal is recorded by a spectrometer (E) connected to a computer.

voltage of 75 V_{pp}. The sinusoidal voltage was generated by a signal generator (Rigol DG4062, Rigol Technologies EU GmbH, Germany) and monitored using a digital oscilloscope (Rigol DS2072A, Rigol Technologies EU GmbH, Germany).

We measured particle concentration using a fluorescence spectroscopy setup. A capillary was connected from the outlet of the setup to the inlet of a flow cell (HL176-760-85-40, Hellma GmbH & Co. KG, Germany, Figure 2C). A white-light source (XCite 120 PC, Excelitas

Technologies Corp., USA) was connected via a liquid light guide to the cuvette holder (CVH100/M, Thorlabs GmbH, Germany). In a 90° angle to the excitation light, a light guide adapter was mounted behind a triple-bandpass filter (DAPI/FITC/TRITC). The light guide was also connected to a spectrometer (Silver nova, StellarNet, Inc., USA, Figure 2E). The spectrometer measured the light intensity in the 190–1100 nm spectrum and the spectrum was stored every 250 ms using a LabVIEW script and subsequently evaluated using MATLAB.

We measured the impedance of the device with a 91 mΩ resistance in series to the setup using an oscilloscope, which measured both the voltage emitted from the amplifier and the voltage drop across the 91 mΩ ohmic resistance. A more detailed description of the impedance measurement can be found in the Section 2 of the Supporting Information. At a medium conductivity of 2.1 μS/cm, the impedance is about 120 Ω up to about 50 kHz leading to a current of about 0.6 A_{pp} at 75 V_{pp} (Figure 1D). As the frequency increases further the impedance decreases and the phase shift between voltage and current increases, indicating the presence of capacitive currents. At the highest measured frequency (200 kHz), a phase shift of 86.2° and an impedance of only 53 Ω was recorded. At low frequencies, the electronic double layer dominates the impedance of the setup, but with increasing frequency, the double layer, which acts as a capacitor, becomes less dominant. At higher frequencies, the voltage drop across the medium dominates the overall impedance of the device [55]. This measurement helps selecting the correct amplifier for the experiment.

2.2 | Particle suspension

We used fluorescent polystyrene (PS) particles (Polysciences Europe GmbH, Germany) that act as model particles for process development. They show good polarizability in low conductive media and are easy to detect due to their fluorescent labeling. Particles with diameters of 0.5, 1, and 3 μm were yellow-green labeled (excitation maximum = 441 nm, emission maximum = 486 nm), whereas the 6 μm particles were labeled with a dye called polychromatic red (excitation maximum = 525 nm, emission maximum = 565 nm) making it possible to distinguish between the two fluorescent dyes (see below). The particles (for the particle concentration see Section 1, supporting information) were suspended in a medium composed of pure water (Omniatap 6 UV/UF, stakpure GmbH, Germany) with 0.005 vol.% Tween20 (Sigma–Aldrich, Germany) to reduce particle-wall interactions and improve the wettability of the PCB boards. Additionally, we added 6 μM potassium hydroxide to adjust the pH value and potassium chloride to set the electrical conductivity of the suspension medium to 2.1 μS/cm. At this conductivity all selected particles are known to show pDEP at 15 kHz frequency (Figure S1).

2.3 | Experimental procedure

Prior to the experiments, we calibrated the volume flow using a measuring cylinder, since this type of pump is sensitive to air inside their pump heads. At the beginning of the experiment, no voltage was applied for 30 s to obtain the initial concentration c_0 of the particles. As a second step, we applied a voltage at a fixed frequency for 270 s. After the voltage was switched off, we continued recording the fluorescence intensity until the initial fluorescence intensity was regained. After three experiments, we flushed the channel at 10 ml/min to remove any air bubbles and stuck particles from the channel, flow cell, and pump head. During the entire experiment, we recorded the emission spectrum of the flow cell by the spectrometer that was connected to a computer. We used a LabVIEW program to store the data and MATLAB scripts to process them. These scripts and the recorded data can be found in the online repository [50]. We used a moving-average algorithm to reduce the noise of the fluorescence signal and to suppress the influence of air bubbles rushing through the flow cell as these produce high reflection and consequently spikes in the data. Once per day, medium without particles was used to measure the background signal i_b of the flow cell and the medium. This signal was subtracted from the data before further processing. We assume that the fluorescence intensity is proportional to the particle concentration. The trapping efficiency T was defined as the mean value of reduction of the intensity i from 200 s (t_1) to 300 s (t_2) after the background was subtracted:

$$T = 1 - \frac{1}{t_2 - t_1} \int_{t_1}^{t_2} \frac{i - i_b}{i_{c_0} - i_b} dt. \tag{5}$$

Between 200 and 300 s the trapping was observed to reach a steady-state and therefore used for defining the overall trapping efficiency. All intensities in the manuscript are normalized to the initial concentration i_{c_0} measured at the beginning of the experiment.

The procedure to obtain the concentrations of a mixture of polychromatic red and yellow-green particles is based on a linear combination of their two individual spectra. The best fit was found using a genetic algorithm in MATLAB. The procedure is published elsewhere in more detail [38].

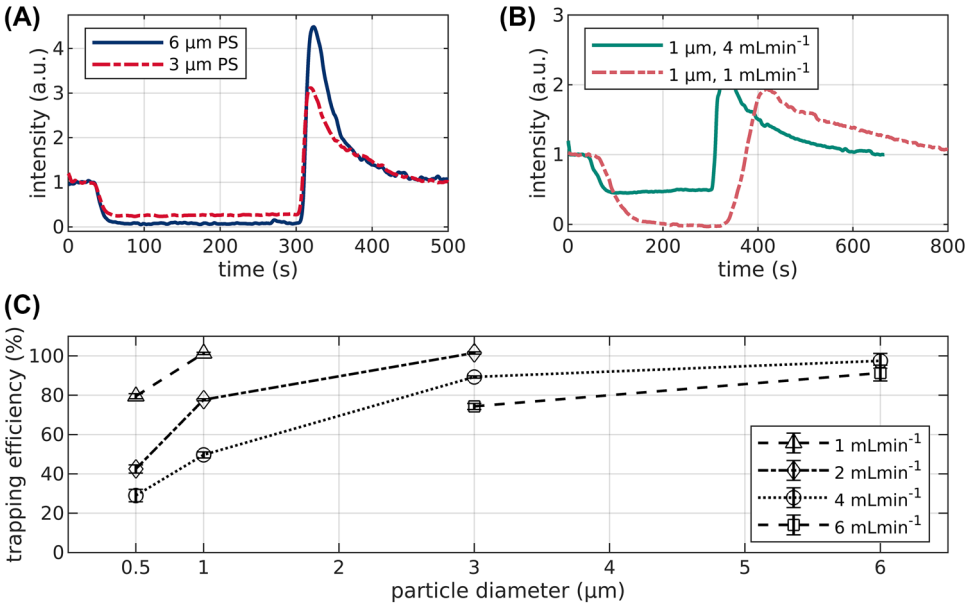

FIGURE 3 Trapping of monodisperse PS particles of different size and at different flow rates. All data are obtained at 15 kHz and 75 V_{pp}. Voltage was applied after 30 s and turned off at 300 s. (A) Fluorescence signal of 3 µm and 6 µm PS particles at 6 ml/min volume flow. (B) Fluorescence signal for 1 µm particles at 1 and 4 ml/min. (C) Monodisperse trapping efficiency as a function of particle size and flow rate.

3 | RESULTS AND DISCUSSION

Before assessing the possibility to perform selective separation, we perform trapping experiments with monodisperse PS particles ranging from 500 nm to 6 µm in diameter (Figure 3). To investigate the influence of the fluid velocity, we varied the volume flow in the range from 1 ml/min (60 ml/h) to 6 ml/min (360 ml/h). All experiments were conducted at a frequency of 15 kHz and voltage of 75 V_{pp} (26.5 V_{rms}) and at a medium conductivity of 2.1 µS/cm. The experiments for each parameter were conducted three to four times (for the exact number of repetitions per experiment, please consult the online repository [50]). All trapping and separation efficiencies are given as mean ± standard deviation. The standard deviation is calculated with data from all conducted experiments for this specific parameter.

In Figure 3A, we compare the fluorescence intensity as a function of time for 3 and 6 µm particles at 6 ml/min. We applied the voltage after 30 s and shortly after, the fluorescence intensity and therefore the amount of eluted particles begins to drop until a steady state is reached. Both, the 3 µm and 6 µm particles, show significant trapping (74.33 ± 1.54% and 91.33 ± 4.04%, respectively) during the experiments. After 300 s, we turn the voltage off. Shortly thereafter, previously trapped particles are leaving the channel and the fluorescence signal exceeds the initial signal for some time until it slowly converges towards the initial value. The overshoot of the particle concentration indicates a recovery of the trapped particles. The recovery rate in our experiments ranged from almost 100% to only 25% of the trapped particles (data not shown, for further information please see Section 1, Supporting Information). Optimizing the recovery rate of the device is out of the focus of this study and needs to be investigated in the future in more detail. Our results show, however, that using high flow rates for the recovery of particles is favorable, which is likely due to increasing drag force at higher fluid velocity.

Two experiments at different flow rates of equally sized (1 µm) particles are displayed in Figure 3B. Here, the influence of the volume flow becomes evident. As the residence time in the channel decreases with increasing volume flow, the trapping efficiency drops from 101.33 ± 0.58% at 1 ml/min to 49.67 ± 1.53% at 4 ml/min. A trapping efficiency above 100% seems odd, however, we observed this phenomena multiple times during the experiments. For example, it was observed for 3 µm at 2 ml/min (Figure 3C) with a calculated trapping efficiency of 101.5 ± 0.58%. We decided to include the data for full transparency. One reason for this behavior may be due the subtraction of the background signal. The setup is sensitive to reflective and fluorescent material inside the flow cell. During the measurement of the background no fluorescent particles should be present but we cannot exclude the presence of (small) air bubbles at all times. Small air bubbles tend to attach to the surface of the flow cell and then randomly detach from the surface. When they enter the flow cell, they scatter the emission light and consequently influence

the measurement. Another reason might be the position of the flow cell. During the experiments, we observed that even minor movements of the flow cell in the fluorescence measurement setup lead to a shift in measured intensity. In any case, the deviations are small and do not affect the drawn conclusions. In Figure 3B, it can also be seen that a lower volume flow leads to a slower drop in fluorescence intensity. This is because it takes longer time for the particles to reach the flow cell. The remobilization is also significantly slower at the lower flow rate.

Generally, at constant volume flow, trapping efficiency increases with particle size (Figure 3C). For example at 4 ml/min (240 ml/h), only $29 \pm 3.16\%$ of the 0.5 µm particles are retained in the channel. With increasing diameter, on the other hand, the trapping efficiency increases and reaches $49.67 \pm 1.53\%$, $89.33 \pm 0.58\%$, and $97.5 \pm 3.79\%$ for 1 µm, 3 µm, and 6 µm, respectively. As the dielectrophoretic force is proportional to the particle volume (equation (1)), this size dependency was expected and does agree with the theory.

To show that selective trapping is achievable with this setup, 3 µm and 6 µm particles, the same as used in the experiments described above, were selected to be separated. For this, we created a binary mixture of the particles. In a preliminary experiment, we tested the trapping efficiency for both particles at three different frequencies (see Section 3, Supporting Information). We found that the trapping efficiency for the 6 µm particles decreases sharply from 50 to 100 kHz from 80% to ca. 10%. The decrease of trapping efficiency with increasing frequency was significantly less for the 3 µm particle, from ca. 70% at 50 kHz to ca. 40% at 150 kHz. This behavior was expected, as the 6 µm particles have a lower net conductivity than the 3 µm particles. The surface conductance of the 3 µm particles was determined in a previous study as 0.95 nS, resulting in a cross over from pDEP to nDEP at a frequency of 210 kHz (see also Figure S1). Hence, 3 µm particles are expected to still show strong pDEP at 100 kHz. The 6 µm particles on the other hand seem to have a cross-over frequency close to $100 - 150$ kHz, which we deduce from the sharp decrease in separation efficiency at this frequency. The lower cross-over frequency for 6 µm particles is expected, as the particle net conductivity decreases with increasing particle size (equation (2)–(4)). We thus selected 100 kHz as a suitable frequency to demonstrate selective separation of the binary mixture as 6 µm particles show only weak pDEP or even nDEP at this frequency. We further performed the experiment at two different volume flows (2 and 4 ml/min) and at an applied voltage of 75 V_{pp}.

At both selected volume flows, substantial separation of the 3 µm particles can be observed (Figure 4), which decreases with increasing flow rate. At 100 kHz, $79 \pm 1.63\%$ (2 ml/min) and $60 \pm 1.15\%$ (4 ml/min), respectively, of

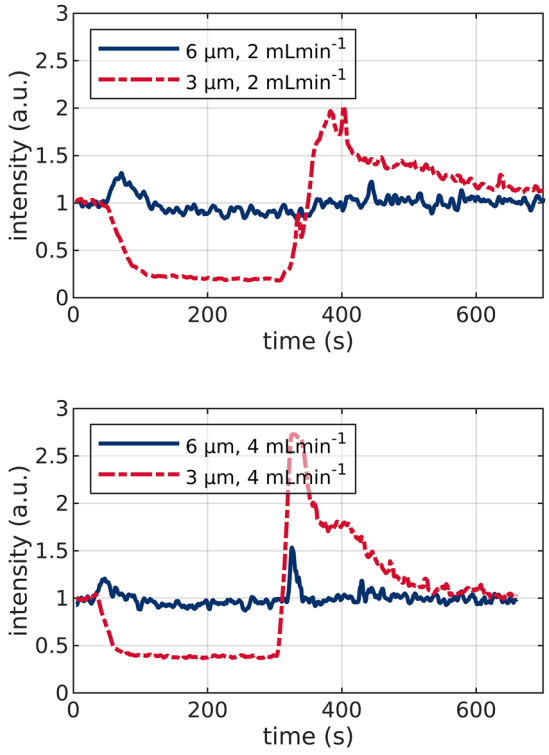

FIGURE 4 Exemplary experimental results for mixtures of 6 µm and 3 µm PS particles for 2 ml/min (top) and 4 ml/min (bottom) volume flow. Sinusoidal voltage (100 kHz and 75 V_{pp}) was applied after 30 s and turned off at 300 s.

the 3 µm particles are trapped. The trapping efficiency at 100 kHz is lower compared to those measured at 15 kHz. The trapping rate of the 3 µm particles during the separation is in good agreement with the trapping rate at 100 kHz, when no 6 µm particles are present in the channel (Figure S3). Since, for polystyrene particles, the polarizability decreases with increasing frequency (equation (2) and Figure S1), this agrees with the theory as well. The 6 µm show no significant trapping during the experiments at both flow rates. Trapping efficiencies were measured to be $2.25 \pm 4.19\%$ (2 ml/min) and $-2 \pm 5.57\%$ at 4 ml/min. A negative trapping efficiency corresponds to a higher particle concentration at the outlet as it is at the inlet. However, since no particles are produced within the experiments, this has to be due to other effects. One explanation is that the linear unmixing algorithm does not always produce completely accurate results. However, as we monitor the quality of the superposition of the peaks this might not be a major influence. More likely, either particles adhering to the electrodes or trapped between electrode array and gasket (see Figure 2B) are released due to the nDEP combined with the drag force exerted by the motion of the fluid. The gasket and the PCB base material (FR-4, green in Figure 2A) are separated by the electrodes that have a height of approximate 35 µm creating a dead spot

were particles could be trapped until released for example due to nDEP. This should be addressed for future studies and shows that in a next iteration of this setup, dead spots should be avoided. During monodisperse experiments with the 6 μm particles at 100 kHz, we observed a trapping efficiency of 11 ± 1%. This is higher than in the selective trapping experiment but also low compared to the trapping of the 3 μm particles. One possible reason for this divergence is particle–particle interactions either before particles enter the separation device or in the separation device itself. For example, the 3 μm particles do experience an attraction toward the local field maxima and could form pearl chains that influence the local field distribution and therefore reduce trapping of the 6 μm particles. This phenomenon is not fully understood by now and could be investigated by using transparent substrates or electrodes. Nevertheless, at 100 kHz the trapping of the larger particles seems to be low, whereas the 3 μm particles could be trapped selectively.

4 | CONCLUDING REMARKS

In this study, we presented and characterized a high throughput eDEP setup. We used inexpensive PCB to generate the electric field. We used fluorescent polystyrene microparticles of different diameter to show the capabilities of our setup. In monodisperse experiments with particles from 500 nm up to 6 μm good trapping could be observed at 15 kHz and 26.5 V_{rms} and at flow rates up to 6 ml/min. The volume flows in this study are significantly higher than in most microfluidic dielectrophoretic separators. In experiments with binary mixtures of 3 μm and 6 μm PS particles, we demonstrated selective trapping at 100 kHz of the smaller particles due to the difference in pDEP and nDEP. We consider the separator described here as a starting point for further developments of high throughput dielectrophoretic separators, that can be used to separate complex mixtures such as electronic waste.

ACKNOWLEDGMENTS

The authors thank the German Research Foundation (DFG) within the priority program, "MehrDimPart–Highly specific and multidimensional fractionation of fine particle systems with technical relevance" (SPP2045, Grant Numbers PE 3015/3-2, TH 893/20-2) for funding. The authors also thank Henning Hasselbruch from the IWT Bremen for helping to conduct the surface measurements of the electrode array.

CONFLICT OF INTEREST

The authors have declared no conflict of interest.

DATA AVAILABILITY STATEMENT

Experimental data, evaluation scripts and manufacturing data for the PCB can be found in an online repository [50]. Additional information is available from the corresponding author upon reasonable request.

ORCID

Jasper Giesler https://orcid.org/0000-0003-1334-3013
Georg R. Pesch https://orcid.org/0000-0003-4676-1908

REFERENCES

1. Peleka EN, Gallios GP, Matis KA. A Perspective on Flotation: A Review. J Chem Technol Biotechnol. 2018;93(3):615–23. https://doi.org/10.1002/jctb.5486
2. Hansen L, Wollmann A, Weers M, Benker B, Weber AP. Triboelectric Charging and Separation of Fine Powder Mixtures. Chem Eng Technol. 2020;43(5):933–41. https://doi.org/10.1002/ceat.201900558
3. Wang F, Zhao Y, Zhang T, Zhang G, Yang X, He Y, et al. Metals Recovery from Dust Derived from Recycling Line of Waste Printed Circuit Boards. J Cleaner Prod. 2017;165:452–7. https://doi.org/10.1016/j.jclepro.2017.07.112
4. Wang Y, Du F, Baune M, Thöing J. Predicting and Eliminating Joule Heating Constraints in Large Dielectrophoretic IDE Separators. Chem Eng Sci. 2015;137:235–42. https://doi.org/10.1016/j.ces.2015.06.042
5. Louhadj S, Hammadi N, Touhami S, Louati H, Hadjali A, Kimi IE, et al. Experimental Analysis of the Attraction Force Applied on Metal Particles Using a Double-Side Electrical Curtain. J Electrostat. 2020 May;105:103448. https://doi.org/10.1016/j.elstat.2020.103448
6. Gascoyne PRC. Dielectrophoretic-Field Flow Fractionation Analysis of Dielectric, Density, and Deformability Characteristics of Cells and Particles. Anal Chem. 2009;81(21):8878–85. https://doi.org/10.1021/ac901470z
7. Gupta V, Jafferji I, Garza M, Melnikova VO, Hasegawa DK, Pethig R, et al. ApoStream ™, a New Dielectrophoretic Device for Antibody Independent Isolation and Recovery of Viable Cancer Cells from Blood. Biomicrofluidics. 2012;6(2):024133. https://doi.org/10.1063/1.4731647
8. Shim S, Stemke-Hale K, Tsimberidou AM, Noshari J, Anderson TE, Gascoyne PRC. Antibody-Independent Isolation of Circulating Tumor Cells by Continuous-Flow Dielectrophoresis. Biomicrofluidics. 2013;7(1):011807. https://doi.org/10.1063/1.4774304
9. Liu Y, Hayes MA. Orders-of-Magnitude Larger Force Demonstrated for Dielectrophoresis of Proteins Enabling High-Resolution Separations Based on New Mechanisms. Anal Chem. 2021;93(3):1352–59. https://doi.org/10.1021/acs.analchem.0c02763
10. Jones PV, Salmon GL, Ros A. Continuous Separation of DNA Molecules by Size Using Insulator-Based Dielectrophoresis. Anal Chem. 2017;89(3):1531–39. https://doi.org/10.1021/acs.analchem.6b03369
11. Sano H, Kabata H, Kurosawa O, Washizu M. Dielectrophoretic Chromatography with Cross-Flow Injection. In: *Technical Digest. MEMS 2002 IEEE International Conference. Fifteenth*

IEEE International Conference on Micro Electro Mechanical Systems (Cat. No.02CH37266). Las Vegas, NV, USA: IEEE; 2002. pp. 11–4. https://doi.org/10.1109/MEMSYS.2002.984043
12. Abt V, Gringel F, Han A, Neubauer P, Birkholz M. Separation, Characterization, and Handling of Microalgae by Dielectrophoresis. Microorganisms. 2020;8(4):540. https://doi.org/10.3390/microorganisms8040540
13. Michael KA, Hiibel SR, Geiger EJ. Dependence of the Dielectrophoretic Upper Crossover Frequency on the Lipid Content of Microalgal Cells. Algal Res. 2014;6:17–21. https://doi.org/10.1016/j.algal.2014.08.004
14. Schor AR, Buie CR. Rapid Fabrication of Three-Dimensional Structures for Dielectrophoretic Sorting of Lipid-Containing Organisms. Journal of Micromechanics and Microengineering. 2016 Oct 1;26(10):105010. https://doi.org/10.1088/0960-1317/26/10/105010
15. Pethig R. Dielectrophoresis: Theory, Methodology, and Biological Applications. Hoboken, NJ: John Wiley & Sons, Inc; 2017. p. 428
16. Abd Rahman N, Ibrahim F, Yafouz B. Dielectrophoresis for Biomedical Sciences Applications: A Review. Sensors. 2017;17(3):449. https://doi.org/10.3390/s17030449
17. Pesch GR, Du F. A Review of Dielectrophoretic Separation and Classification of Non–biological Particles. Electrophoresis. 2021;42(1–2):134–52. https://doi.org/10.1002/elps.202000137
18. Weirauch L, Lorenz M, Hill N, Lapizco-Encinas BH, Baune M, Pesch GR, et al. Material-Selective Separation of Mixed Microparticles via Insulator-Based Dielectrophoresis. Biomicrofluidics. 2019;13(6):064112. https://doi.org/10.1063/1.5124110
19. Shen Y, Elele E, Khusid B. A Novel Concept of Dielectrophoretic Engine Oil Filter. Electrophoresis. 2011;32(18):2559–68. https://doi.org/10.1002/elps.201100072
20. Pethig R. Review Article—Dielectrophoresis: Status of the Theory, Technology, and Applications. Biomicrofluidics. 2010;4(2):022811. https://doi.org/10.1063/1.3456626
21. Castellanos A, Ramos A, González A, Green NG, Morgan H. Electrohydrodynamics and Dielectrophoresis in Microsystems: Scaling Laws. J Phys D: Appl Phys. 2003;36(20):2584–97. https://doi.org/10.1088/0022-3727/36/20/023
22. Lorenz M, Malangré D, Du F, Baune M, Thöming J, Pesch GR. High-Throughput Dielectrophoretic Filtration of Sub-Micron and Micro Particles in Macroscopic Porous Materials. Anal Bioanal Chem. 2020 Jun;412(16):3903–14. https://doi.org/10.1007/s00216-020-02557-0
23. Williams SJ, Romero N, Parkes L, Jackson DJ, Naber JF. Inexpensive Three-Dimensional Dielectrophoretic Microfluidic Devices Using Milled Copperclad Substrates. J Electrostat. 2015;75:49–53. https://doi.org/10.1016/j.elstat.2015.02.003
24. Modarres P, Tabrizian M. Frequency Hopping Dielectrophoresis as a New Approach for Microscale Particle and Cell Enrichment. Sens Actuators B. 2019;286:493–500. https://doi.org/10.1016/j.snb.2019.01.157
25. Kikkeri K, Kerr BA, Bertke AS, Strobl JS, Agah M. Passivated–electrode Insulator-based Dielectrophoretic Separation of Heterogeneous Cell Mixtures. J Sep Sci. 2020;43(8):1576–85. https://doi.org/10.1002/jssc.201900553
26. Wang XB, Vykoukal J, Becker FF, Gascoyne PRC. Separation of Polystyrene Microbeads Using Dielectrophoretic/Gravitational Field-Flow-Fractionation. Biophys J. 1998;74(5):2689–701. https://doi.org/10.1016/S0006-3495(98)77975-5
27. Ermolina I, Morgan H. The Electrokinetic Properties of Latex Particles: Comparison of Electrophoresis and Dielectrophoresis. J Colloid Interface Sci. 2005;285(1):419–28. https://doi.org/10.1016/j.jcis.2004.11.003
28. Pesch GR, Lorenz M, Sachdev S, Salameh S, Du F, Baune M, et al. Bridging the Scales in High-Throughput Dielectrophoretic (Bio-)Particle Separation in Porous Media. Sci Rep. 2018;8(1):10480. https://doi.org/10.1038/s41598-018-28735-w
29. Martinez-Duarte R. A Critical Review on the Fabrication Techniques That Can Enable Higher Throughput in Dielectrophoresis Devices. Electrophoresis. 2022;43(1–2):232–48. https://doi.org/10.1002/elps.202100179
30. Smith AJ, O'Rorke RD, Kale A, Rimsa R, Tomlinson MJ, Kirkham J, et al. Rapid Cell Separation with Minimal Manipulation for Autologous Cell Therapies. Sci Rep. 2017;7(1):41872. https://doi.org/10.1038/srep41872
31. Moon HS, Kwon K, Kim SI, Han H, Sohn J, Lee S, et al. Continuous Separation of Breast Cancer Cells from Blood Samples Using Multi-Orifice Flow Fractionation (MOFF) and Dielectrophoresis (DEP). Lab Chip. 2011;11(6):1118. https://doi.org/10.1039/c0lc00345j
32. Waheed W, Sharaf OZ, Alazzam A, Abu-Nada E. Dielectrophoresis-Field Flow Fractionation for Separation of Particles: A Critical Review. J Chromatogr A. 2021;1637:461799. https://doi.org/10.1016/j.chroma.2020.461799
33. Giesler J, Weirauch L, Thöming J, Baune M, Pesch GR. Separating Microparticles by Material and Size Using Dielectrophoretic Chromatography with Frequency Modulation. Sci Rep. 2021;11(1):16861. https://doi.org/10.1038/s41598-021-95404-w
34. Wang XB, Yang J, Huang Y, Vykoukal J, Becker FF, Gascoyne PRC. Cell Separation by Dielectrophoretic Field-flow-fractionation. Anal Chem. 2000 Feb 1;72(4):832–39. https://doi.org/10.1021/ac990922o
35. Hill N, Lapizco-Encinas BH. Continuous Flow Separation of Particles with Insulator-Based Dielectrophoresis Chromatography. Anal Bioanal Chem. 2020;412(16):3891–902. https://doi.org/10.1007/s00216-019-02308-w
36. Pesch GR, Du F, Baune M, Thöming J. Influence of Geometry and Material of Insulating Posts on Particle Trapping Using Positive Dielectrophoresis. J Chromatogr A. 2017;1483:127–37. https://doi.org/10.1016/j.chroma.2016.12.074
37. Suehiro J, Guangbin Z, Imamura M, Hara M. Dielectrophoretic Filter for Separation and Recovery of Biological Cells in Water. IEEE Trans Ind Appl. 2003;39(5):1514–21. https://doi.org/10.1109/TIA.2003.816535
38. Weirauch L, Giesler J, Baune M, Pesch GR, Thöming J. Shape-selective remobilization of microparticles in a mesh-based DEP filter at high throughput. Sep Purif Technol. 2022;300:121792. https://doi.org/10.1016/j.seppur.2022.121792
39. Green NG, Ramos A, Morgan H. Numerical Solution of the Dielectrophoretic and Travelling Wave Forces for Interdigitated Electrode Arrays Using the Finite Element Method. J Electrostat. 2002;56(2):235–54. https://doi.org/10.1016/S0304-3886(02)00069-4
40. Moschou D, Tserepi A. The Lab-on-PCB Approach: Tackling the TAS Commercial Upscaling Bottleneck. Lab Chip. 2017;17(8):1388–405. https://doi.org/10.1039/C7LC00121E

41. Park K, Suk HJ, Akin D, Bashir R. Dielectrophoresis-Based Cell Manipulation Using Electrodes on a Reusable Printed Circuit Board. Lab Chip. 2009;9(15):2224. https://doi.org/10.1039/b904328d
42. Tu J, Qiao Y, Feng H, Li J, Fu J, Liang F, et al. PDMS-based Microfluidic Devices Using Commoditized PCBs as Masters with No Specialized Equipment Required. RSC Adv. 2017;7(50):31603–9. https://doi.org/10.1039/C7RA03899B
43. Khoshmanesh K, Nahavandi S, Baratchi S, Mitchell A, Kalantar-zadeh K. Dielectrophoretic Platforms for Bio-Microfluidic Systems. Biosens Bioelectron. 2011;26(5):1800–14. https://doi.org/10.1016/j.bios.2010.09.022
44. Burt JPH, Al-Ameen TAK, Pethig R. An Optical Dielectrophoresis Spectrometer for Low-Frequency Measurements on Colloidal Suspensions. J Phys E: Sci Instrum. 1989;22(11):952–57. https://doi.org/10.1088/0022-3735/22/11/011
45. Altomare L, Borgatti M, Medoro G, Manaresi N, Tartagni M, Guerrieri R, et al. Levitation and Movement of Human Tumor Cells Using a Printed Circuit Board Device Based on Software-Controlled Dielectrophoresis. Biotechnol Bioeng. 2003;82(4):474–9. https://doi.org/10.1002/bit.10590
46. Hoettges KF, Henslee EA, Torcal Serrano RM, Jabr RI, Abdallat RG, Beale AD, et al. Ten–Second Electrophysiology: Evaluation of the 3DEP Platform for High-Speed, High-Accuracy Cell Analysis. Sci Rep. 2019;9(1):19153. https://doi.org/10.1038/s41598-019-55579-9
47. Vahey MD, Voldman J. High-Throughput Cell and Particle Characterization Using Isodielectric Separation. Anal Chem. 2009;81(7):2446–55. https://doi.org/10.1021/ac8019575
48. Jeong J, Chou N, Lee G, Kim S. Annealing Effects of Parylene-Caulked Polydimethylsiloxane as a Substrate of Electrodes. Sensors. 2016;16(12):2181. https://doi.org/10.3390/s16122181
49. Williams SJ, Schneider JD, King BC, Green NG. Particle-Induced Electrostatic Repulsion within an Electric Curtain Operating below the Paschen Limit. Micromachines. 2022;13(2):288. https://doi.org/10.3390/mi13020288
50. Giesler J. Online Repository for "High Throughput Dielectrophoretic Separator Based on Printed Circuit Boards". Zenodo. 2022 May. Available from: https://doi.org/10.5281/zenodo.6806667
51. Contado C. Field Flow Fractionation Techniques to Explore the "Nano-World". Anal Bioanal Chem. 2017;409(10):2501–18. https://doi.org/10.1007/s00216-017-0180-6
52. Giesler J, Pesch GR, Weirauch L, Schmidt MP, Thöming J, Baune M. Polarizability-Dependent Sorting of Microparticles Using Continuous-Flow Dielectrophoretic Chromatography with a Frequency Modulation Method. Micromachines. 2019;11(1):38. https://doi.org/10.3390/mi11010038
53. Balasubramanian P, Kinders RJ, Kummar S, Gupta V, Hasegawa D, Menachery A, et al. Antibody-Independent Capture of Circulating Tumor Cells of Non-Epithelial Origin with the ApoStream® System. PLoS One. 2017;12(4):e0175414. https://doi.org/10.1371/journal.pone.0175414
54. Dash S, Mohanty S. Dielectrophoretic Separation of Micron and Submicron Particles: A Review: Microfluidics and Miniaturization. Electrophoresis. 2014;35(18):2656–72. https://doi.org/10.1002/elps.201400084
55. Boldt NP, Malti DE, Damm S, Barai A, Birkholz M, Thewes R. Impedance Matching in Dielectrophoresis Experiments. In: *2021 IEEE Biomedical Circuits and Systems Conference (BioCAS)*. Berlin, Germany: IEEE; 2021. pp. 1–5. https://doi.org/10.1109/BioCAS49922.2021.9645025

SUPPORTING INFORMATION

Additional supporting information can be found online in the Supporting Information section at the end of this article.

How to cite this article: Giesler J, Weirauch L, Thöming J, Baune M, Pesch GR. High-throughput dielectrophoretic separator based on printed circuit boards. Electrophoresis. 2023;44:72–81. https://doi.org/10.1002/elps.202200131

7 Development of an high throughput electrode based dielectrophoretic separator II

The fourth publication was published as

Giesler, J.; Weirauch, L.; Rother, A.; Thöming, J.; Pesch, G. R.; Baune, M. Sorting Lithium-Ion Battery Electrode Materials Using Dielectrophoresis. *ACS Omega* **2023**, DOI: 10.1021/acsomega.3c04057.

and uses an improved version of the setup described in Chapter 6. As the prior publications focus on process development, this study evaluates the potential of the PCB based setup in order to tackle separation problems with particles of high technical relevance. In this study, the separation of graphite and lithium-ion phosphate microparticles via dielectrophoresis is tested and evaluated at high throughput. Battery-grade graphite and lithium-ion phosphate microparticles were chosen, as these are state-of-the-art active materials for the electrodes of lithium-ion batteries.

The design in this chapter features a flux of over 80 $Lh^{-1}m^{-2}$ when calculating with an area of 45 × 150 mm which equals size of one PCB and a volume flow of 10 mL/min. This is below the flux of microfiltration. Here, a flux over 1 $m^3m^{-2}h^{-1}$ can be reached [134, 135]. In contrast to microfiltration, the pressure drop should be lower in this setup as the *pore size* of this PCB based setup is high (500 µm×45 mm) compared to micofiltration setups (< 1 µm). However, the unique characteristics of DEP based techniques (e.g., address lipid content of cells or conductivity of particles) make comparisons only valid when the same goal is pursued (e.g., size exclusion) in the two separation processes.

Again, supporting information can be found at the journals' website for this publication. Additionally, an online repository was created.

Giesler, J. Online Repository for "Sorting Lithium-Ion Battery Electrode Materials Using Dielectrophoresis" Zenodo, https://doi.org/10.5281/zenodo.7593873.

It contains measurement data, evaluation scripts and manufacturing data for the refined printed circuit boards.

ACS OMEGA

http://pubs.acs.org/journal/acsodf

Article

Sorting Lithium-Ion Battery Electrode Materials Using Dielectrophoresis

Jasper Giesler, Laura Weirauch, Alica Rother, Jorg Thöming, Georg R. Pesch,*[,∥] and Michael Baune[∥]

Cite This: https://doi.org/10.1021/acsomega.3c04057

Read Online

ACCESS | Metrics & More | Article Recommendations | Supporting Information

ABSTRACT: Lithium-ion batteries (LIBs) are common in everyday life and the demand for their raw materials is increasing. Additionally, spent LIBs should be recycled to achieve a circular economy and supply resources for new LIBs or other products. Especially the recycling of the active material of the electrodes is the focus of current research. Existing approaches for recycling (e.g., pyro-, hydrometallurgy, or flotation) still have their drawbacks, such as the loss of materials, generation of waste, or lack of selectivity. In this study, we test the behavior of commercially available $LiFePO_4$ and two types of graphite microparticles in a dielectrophoretic high-throughput filter. Dielectrophoresis is a volume-dependent electrokinetic force that is commonly used in microfluidics but recently also for applications that focus on enhanced throughput. In our study, graphite particles show significantly higher trapping than $LiFePO_4$ particles. The results indicate that nearly pure fractions of $LiFePO_4$ can be obtained with this technique from a mixture with graphite.

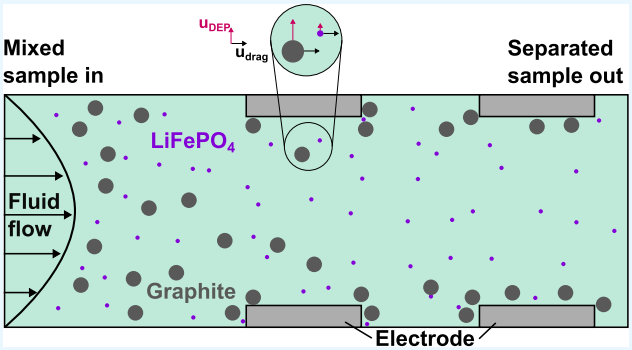

1. INTRODUCTION

Lithium-ion batteries (LIBs) are power electrical devices in nearly all parts of modern society. For example, LIBs are used in portable electronics and electric vehicles. Consequently, the demand for LIB resources is growing.[1] To recover materials of spent LIBs, the recycling of electrodes is a focus of current research. As about one-half of the weight of LIBs consists of the active material of anodes and cathodes, their recycling is desirable.[2] Cathode active materials typically are lithium metal oxides (e.g., $LiCoO_2$, $LiFePO_4$, or $LiNi_{1/3}Mn_{1/3}Co_{1/3}O_2$), whereas graphite is common for anodes.[1,2] Anodes and cathodes consist, among carbon black as a conductive additive and a polymer binder, of a current collector (Cu or Al foil) to which the active material adheres.[2−4] The current collector and the active material can be separated by both chemical and mechanical approaches, such as crushing and sieving.[1,3−5] Typically, one product of these processes is the so-called black mass, a mixture of anode and cathode active materials.[4] Current recycling techniques for black mass are, for example, pyro- or hydrometallurgical and focus on the recovery of the cathode active material because of its higher value than that of graphite. Graphite might be lost or burned as an energy source within the recycling process.[1,2,5−7] Yet processes exist where graphite can be recovered. In hydrometallurgical approaches, lithium metal oxides are dissolved in acid during a leaching step and recovered in subsequent unit operations. Graphite can simply be recovered by filtration after the leaching step.[4] But as significant amounts of liquid wastes are produced in this recycling pathway,[8] it would benefit from an efficient sorting step before the leaching to reduce the amount of chemicals needed. As the active materials are essentially microparticles,[9−11] direct recycling using particle separation techniques could play a vital role within the recycling process to enhance or replace existing recycling approaches of LIBs. One approach that is well established for particulate systems and capable of handling large amounts of product is flotation, which was also applied to separate black mass. This works because anode and cathode materials show different wettability.[5,7,12−14] However, according to Neumann et al.,[4] the process needs to be optimized further, as the achievable recovery rates are currently too low. Other direct approaches that utilize, for example, eutectic salts or ionic liquids can be found in two recent reviews[15,16] that elaborate these techniques in more detail than the scope of this study.

This paper investigates the possibility of addressing particles found within black mass using dielectrophoresis (DEP) at high throughput. DEP is the movement of a polarizable particle in an inhomogeneous electric field. Usually, it is used in the biomedical field and primarily in microfluidic devices.[17,18] Although DEP is label-free and has high selectivity and

Received: June 8, 2023
Accepted: June 29, 2023

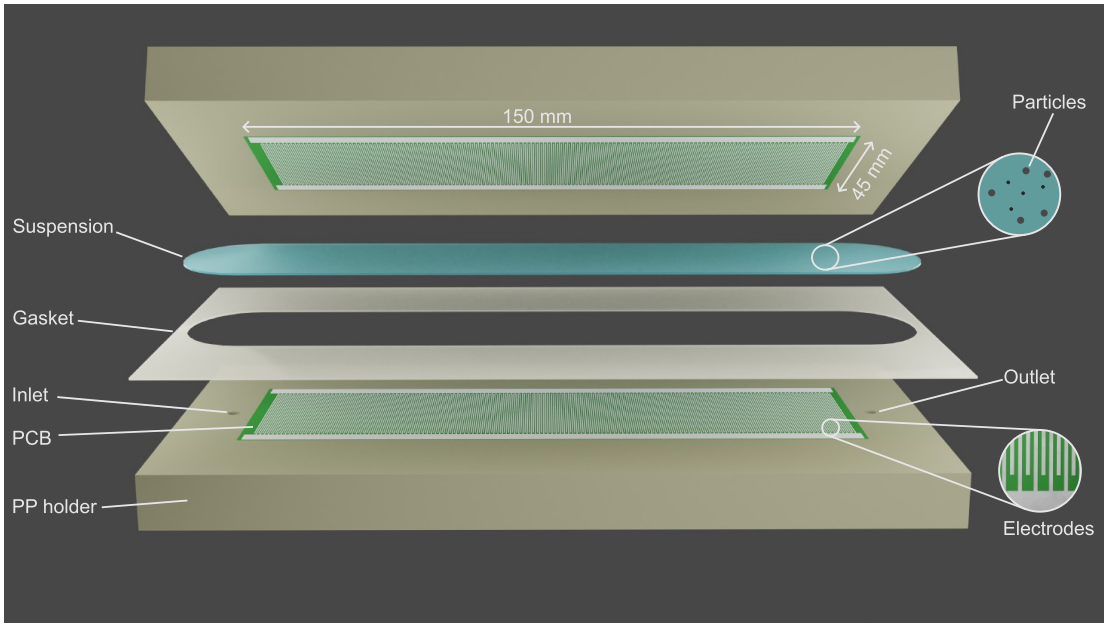

Figure 1. Rendered overview of the separator. The suspension is pumped from the inlet to the outlet through a channel formed by two printed circuit boards (PCBs), a silicon gasket, and polypropylene (PP) holders. The PCBs feature an interdigitated electrode structure (bottom right inset) that is used to generate a highly inhomogeneous electric field.

capability of addressing nanometer- to micrometer-scaled particles,[19−21] few studies have addressed recycling or the throughput that would be required for this.[22−27] While DEP is well studied with biological samples, such as DNA[28,29] and cells,[30−33] the separation of nonbiological particles, besides polystyrene particles, is rarely described in the literature.[18] This study is designed to expand this field by using artificial black mass to show that conductive particles can be addressed with an electrode-based DEP separator at high throughput. By using a setup based on printed circuit boards (PCBs), we assess the behavior of $LiFePO_4$ and graphite microparticles and their mixture under the influence of DEP. To the best of the authors' knowledge, the separation of LIB electrode materials using dielectrophoresis has not yet been addressed. This study aims to serve as a starting point for future research in this field by describing the possibilities and limitations of DEP as a separation technique for these materials.

2. MATERIALS AND METHODS

2.1. Dielectrophoretic Separator. The separator used in this study is an updated version of the one that was evaluated and published in ref 25 and is designed to selectively trap particles when an electric field is applied. An overview of the device can be seen in Figure 1. The key feature of this device is two inexpensive (<1 €/pc.) custom-designed PCBs (manufactured by JiaLiChuang (Hong Kong) Co., Limited, China) with a size of 45 × 150 mm, which is slightly different from the previous design.[25] The improved design showed similar performance with reduced PCB size and energy demand. The new design has an impedance of 20 Ω at 500 kHz in comparison to 13 Ω from the old design. The PCBs are covered by an interdigitated electrode array with the electrode width and spacing both being 250 μm. The two PCBs face each other and are separated by a 0.5 mm silicone gasket. The two PCBs together with the gasket form a channel. The gasket is manually cut to form a channel that is about 175 mm × 38 mm × 0.5 mm (L × W × H) and thus has a theoretical volume of 3.33 mL. We additionally measured the volume using a scale and found that the actual volume is 2.8 ± 0.1 mL, which is slightly lower and likely caused by a compression of the sealing. The calculated height of the sealing results to be 0.42 mm. This gives average residence times of 28 s at 6 mL/min and 17 s at 10 mL/min in the channel. Consequently, at 6 mL/min, an average velocity of 6.3 mm/s can be expected and that of 10.4 mm/s at 10 mL/min. The electrodes are connected to a power amplifier (F30PV, Pendulum Instruments, Sweden), which is capable of providing up to 75 V_{pp} at a maximum current of 2 A. The sinusoidal signal was generated by a signal generator (Rigol DG4062, Rigol Technologies EU GmbH, Germany), monitored using an oscilloscope (Rigol DS2072A, Rigol Technologies EU GmbH, Germany) and a power analyzer (PPA1510, Newtons4th Ltd, Leicester, United Kingdom). The suspension was pumped using a piston pump (Ismatec MCP-CPF IP65 with a pump head FMI 202 QP.Q0.SSY, Cole-Parmer GmbH, Germany).

The operating principle is described in detail elsewhere.[25] Briefly, DEP can be an attractive force (positive DEP/pDEP) if a particle is better polarizable than the surrounding medium or a repulsive force (negative DEP/nDEP) when the particle is less polarizable. Positive DEP guides particles toward local field maxima, whereas nDEP pushes particles away from them.[17] This can lead to a separation as was previously shown several times.[25,34,35] Whether a particle experiences pDEP or nDEP depends on the real part of the Clausius−Mossotti factor (CM), which is defined as[17]

$$\mathrm{Re}(CM) = \mathrm{Re}\left(\frac{\tilde{\varepsilon}_\mathrm{p} - \tilde{\varepsilon}_\mathrm{m}}{\tilde{\varepsilon}_\mathrm{p} + 2\tilde{\varepsilon}_\mathrm{m}}\right) \quad (1)$$

where the complex permittivity is $\tilde{\varepsilon} = \varepsilon_0\varepsilon_\mathrm{r} - i\frac{\sigma}{\omega}$. The complex permittivity incorporates not only the permittivity ε but also the angular frequency of the electric field ω and the conductivity of a material σ. $\mathrm{Re}(CM)$ is bound between −0.5

https://doi.org/10.1021/acsomega.3c04057
ACS Omega XXXX, XXX, XXX−XXX

and 1.0 and is negative in the case of nDEP and positive in the case of pDEP. Finally, the DEP force $\mathbf{F}_{DEP}$ for a spherical and homogeneous particle can be approximated as

$$\mathbf{F}_{DEP} = 2\pi r_p^3 \varepsilon_m \mathrm{Re}(CM) \nabla |\mathbf{E}_{rms}|^2 \quad (2)$$

where r_p is the radius of the particle, $\mathbf{E}_{rms}$ is the electric field, and ε_m is the permittivity of the surrounding medium. Conductive particles in a medium with low conductivity, as used in this study, will usually experience pDEP. $\mathbf{F}_{DEP}$ depends not only on the particle and medium polarizability but also on the particle volume (r_p^3), which is important in the following.

2.2. Particles. The particles investigated here all are commercially available and are specifically designed for battery research. We chose $LiFePO_4$ (Nanografi Nano Teknoloji AS, Turkey) as a cathode material, not only because it is widely used for LIBs but also because it is considered to have low toxicity, which makes it more convenient to work with.[11,36,37] $LiFePO_4$ as a cathode material is carbon coated to enhance its otherwise poor conductivity (about 1 nS/cm).[38,39] This leads, according to the distributor, to an electrical conductivity of 0.88 S/m. The used $LiFePO_4$ shows a distributed particle size from several hundred nm to a few μm (Table 1 and Figure 2A,D). The small size of $LiFePO_4$ particles and their high specific surface area is a result of design optimization, as this is favorable for the performance of batteries.[40] This is in the range of sizes mentioned in the literature for application in LIBs[41−44] and also in the range of sizes reported for some other cathode materials.[45] Additionally, two types of graphite particles were selected. Timrex KS6 (MSE Supplies LLC) is a synthetic graphite with high purity, which can be used as a conductive additive for anodes and cathodes. According to the manufacturer (Imerys Graphite & Carbon, Switzerland), it is larger than $LiFePO_4$ particles (Table 1 and Figure 2B,E). The second type of graphite C-NERGY Actilion GHDR 15-4 (provided by Imerys Graphite & Carbon, Switzerland), here referred to as Actilion, is an active material for anodes of LIBs and significantly larger than the other two materials (Table 1 and Figure 2C,F). The larger size of graphite that is used as an active material in anodes in LIBs was also described in the literature[10,11,44] and again is a result of optimizing the battery performance.[46] Both graphite and LFP are highly conductive compared to the suspension and thus will show pDEP at all frequencies used in this study (see Section S6 in the Supporting Information). Therefore, all particles move toward field maxima, which are located at the edges of the electrode array on PCBs. As the sizes of the particles here diverge significantly, we aim to exploit the linear volume dependence of $\mathbf{F}_{DEP}$ to achieve separation.

Table 1. Parameters Describing the Size Distribution of the Used Particles

particle	$d_{10}/\mu m$	$d_{50}/\mu m$	$d_{90}/\mu m$
$LiFePO_4$	0.6	1.5	6.0
KS6	1.5	3.4	6.1
actilion	13	17	23

The size differences in graphite and $LiFePO_4$ particles are critical for size-dependent sorting, as conducted in this study. This difference may be affected by an upstream liberation step that produces black mass. This, however, depends strongly on the liberation step itself. Mu et al.[47] described for a cathode material, here $LiCoO_2$, no apparent size changes when liberating the particles with calcination or supercritical CO_2. The liberation of particles from black mass during the recycling of spent LIBs is a separate field of research and not part of this study. Artificial black mass is used here to exclude the effects of upstream processes, focus on separability under ideal conditions, and facilitate reproducibility.

2.3. Measurement System. Two methods were used to measure the particle separation. Qualitatively, the total particle concentration was measured by white-light reflection in real time at the outlet. Quantitatively, the $LiFePO_4$ concentration was further evaluated using photometric detection of dissolved iron mass. The reflection measurement system is described in ref 25. Briefly, it consists of a spectrometer (Silver Nova, StellarNet, Inc.) and a flow cuvette (176-765-85-40 and 176-760-85-40, Hellma GmbH & Co. KG, Germany). A white-light

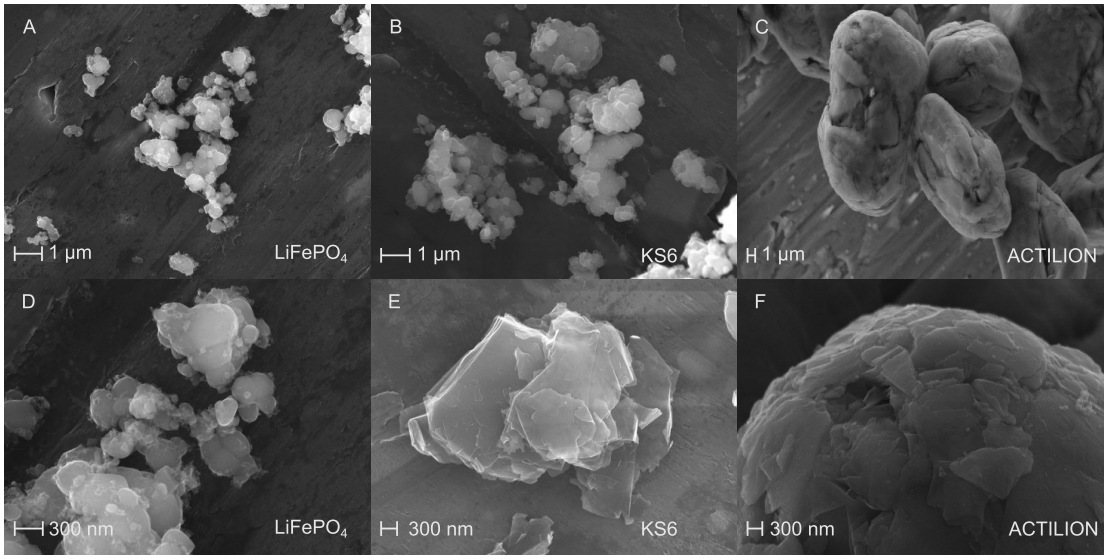

Figure 2. SEM images of $LiFePO_4$ (A&D), KS6 synthetic graphite (B&E), and C-NERGY Actilion GHDR 15-4 (C&F) microparticles. The scale bar in the top row equals 1 μm and 300 nm in the bottom row. Please note that the magnification and consequently the scale bar varies in size.

https://doi.org/10.1021/acsomega.3c04057
ACS Omega XXXX, XXX, XXX−XXX

source (XCite 120 PC, Excelitas Technologies Corp.) is connected at 90° with respect to the light guide of the spectrometer. Particles in the flow cuvette will scatter the light and produce a signal that can be recorded by the spectrometer. For size-distributed particle systems, it is important to keep in mind that the reflection intensity varies with particle size. For spheres in the size range of the particles used here and the wavelength of the light source, the scattering intensity is proportional to r_p^2.[48] As the particles here are not perfect spheres (Figure 2), the signal recorded by the spectrometer does not provide the information of the number or mass of eluted particles, which is different from those in monodisperse particulate systems as in refs 22 and 25. This certainly is a downside of the reflection measurement setup. We thus use the measured reflective light intensity reduction at the outlet as a qualitative real-time indicator of particle retention. To measure the retention of $LiFePO_4$ in the filter, we used a chemical procedure that allows a photometric determination of the iron mass. The procedure was derived from DIN 38406 (see Section S5 in the Supporting Information). Briefly, the $LiFePO_4$ particles are dissolved in an acid and the iron content is determined using a complexing agent and performing a photometric measurement afterward.[49]

2.4. Experimental Procedure. Experiments were carried out in a low-conductivity medium (2.1 μS/cm) consisting of pure water (Omniatap 6 UV/UF, Stakpure GmbH, Germany), 0.01 vol % Tween 20 (Sigma-Aldrich, Germany), and KCl to adjust the conductivity. A low-conductivity medium was selected, as this reduces the influence of thermal effects. For future applications, the impact of increased conductivity needs to be investigated, as this may have an impact on the separation. The black mass used in this study is artificial. Consequently, the impact of residuals from an upstream process that produces actual black mass is not considered and is beyond the scope of this study. To create particle stock suspensions, the particles were suspended in a 1 vol % aqueous Tween 20 suspension with 4 g/L for $LiFePO_4$ and KS6 and 12 g/L for Actilion. The $LiFePO_4$ suspension was renewed every three days as Li is known to dissolve to a low extent into aqueous solutions,[50] and we wanted to exclude this effect from our experiments. Prior to the experiments, we sonicated the particle stock suspensions and added 0.22 vol % of it, for $LiFePO_4$ and KS6, into the medium for the experiments. In order to achieve a sufficient reflection signal, we had to increase the Actilion concentration, resulting in a 10× higher total mass of Actilion in the final suspension than those of the other two particle types. The reason behind this might be the lower specific surface area of the larger Actilion particles and thus lower reflectance per added mass.

The suspensions were stirred throughout the entire experiment. To subtract the background signal, we recorded the intensity signal daily with no particles being present (Section S2 in the Supporting Information). At the beginning of the experiments, we measured the initial reflection signal of the particle suspension for 30 s. At 30 s, the electric field was turned on for 270 s. After the voltage was turned off, the experiment was further monitored until the initial intensity was obtained again. Sometimes, the initial signal was not fully reached due to effects such as sedimentation or bubble adhesion in the flow-through cuvette. As a consequence, we flushed the entire setup at a high flow rate after every two experiments. Every data point represents three experiments. Equation 1 in Section S1 of the Supporting Information is used to calculate the signal reduction.

To chemically determine the retention of the $LiFePO_4$ particles, we collected 4 mL of suspension in a 5 mL container. The samples were taken at the beginning of the experiment, starting after 5 s and during trapping, starting after 200 s. In order to obtain a sufficient sample volume at the beginning of the experiment, the voltage was turned on after 60 s.

All data from the reflection measurements, the evaluation script (MATLAB, for details, see Section S1 in the Supporting Information), and PCB manufacturing data are uploaded to an online repository (ref 51).

3. RESULTS AND DISCUSSION

3.1. Frequency-Dependent Behavior up to 500 kHz. All particles in this study are conductive and thus should show pDEP. To test this hypothesis, we conducted experiments at 30 V_{pp} from 1 to 500 kHz at a volume flow of 6 mL min^{-1} with only one particle type present per experiment (Figure 3).

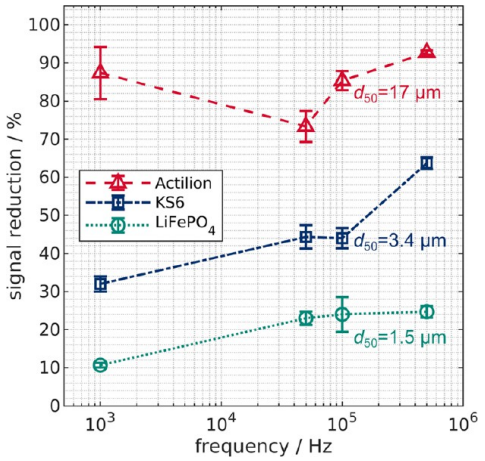

Figure 3. Frequency dependency of the signal reduction of Acilion, KS6, and $LiFePO_4$ suspensions at 6 mL min^{-1} and 30 V_{pp}. Frequencies were varied between 1 and 500 kHz.

Higher frequencies at the selected voltage were not applicable in this setup because the required current would exceed the maximum of the amplifier. For all particles, the trapping efficiency (measured qualitatively in terms of reduction of reflective light intensity signal, called signal reduction) was highest at 500 kHz and significantly higher than that at lower frequencies. This might be because disturbing electrokinetic effects like AC electroosmosis can be dominant at lower frequencies.[52] However, as the frequency significantly exceeds the electrothermal hydrodynamic relaxation frequency ($f = \sigma_m/(2\pi\varepsilon_m) \approx 48$ kHz), this effect should be negligible.[53] Currently, we are not sure what is causing the trapping increase/signal reduction when the frequency is increased; the effect is, however, reproducible. Nonetheless, a significant difference in signal reduction becomes apparent when comparing the particle types. This is likely caused by the differences in particle size as DEP scales with particle volume (eq 2). For example, at 30 V_{pp} and 500 kHz, Actilion shows a high signal reduction of 93 ± 0.6% but the signal of $LiFePO_4$ is only reduced by 26 ± 1.5%. To further investigate the behavior of the particles, we selected 500 kHz as the frequency for all

https://doi.org/10.1021/acsomega.3c04057
ACS Omega XXXX, XXX, XXX−XXX

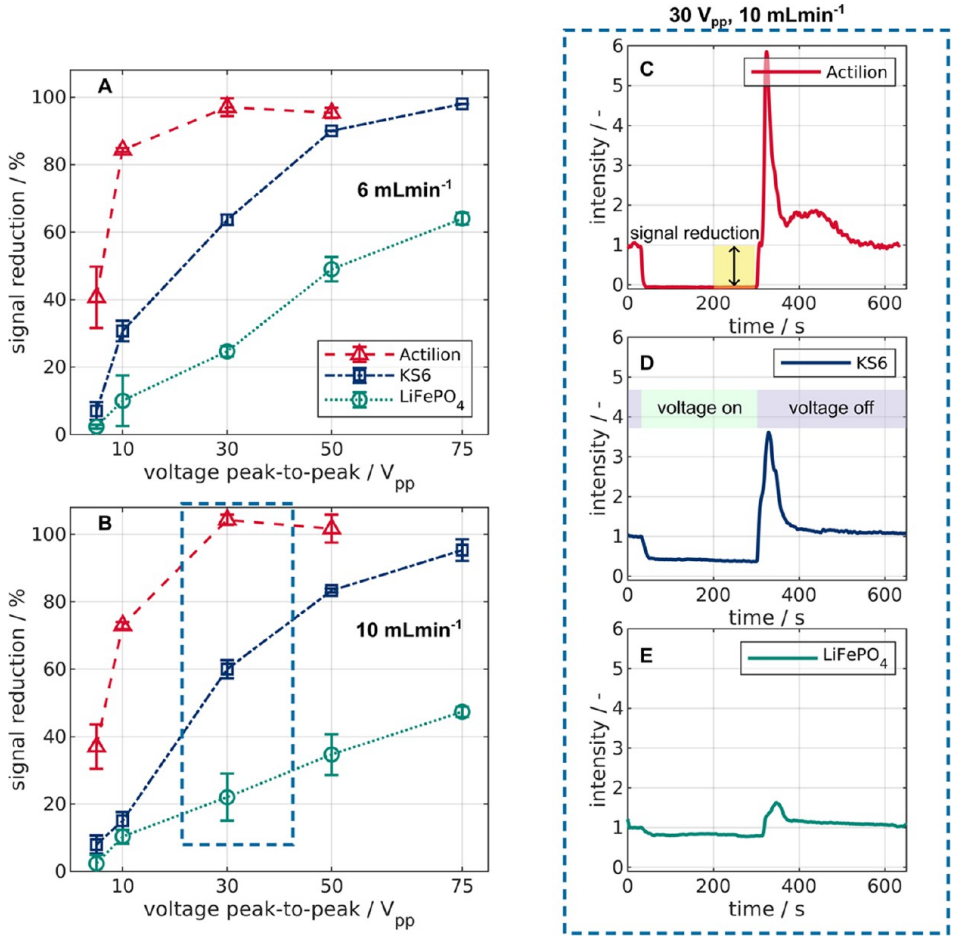

Figure 4. Voltage and volume flow dependency of the signal reduction for Actilion, KS6, and $LiFePO_4$ suspensions at a frequency of 500 kHz. The behavior was evaluated between 5 and 75 V_{pp} at 6 mL min^{-1} (A) and 10 mL min^{-1} (B). As an example, normalized reflection intensities over time for all materials at 30 V_{pp} and 10 mL min^{-1} are also shown (C−E). For all experiments, the signal reduction was measured between 200 and 300 s (C). The voltage was applied after 30 s for 270 s (D).

subsequent experiments because the performance of the device is the highest at this frequency, and DEP is the dominating force. We note that a direct quantitative comparison between the different particle types may be misleading. This is because the scatter properties between distributed particle samples may be different due to different shapes. The qualitative comparison, however, reveals significant differences that agree well with the proposed size selectivity. The application of 500 kHz also demonstrates that frequencies in this range can be applied in a high-throughput device. Compared to previous high-throughput approaches by our group[22−24] that were insulator-based DEP devices, the applicable frequency bandwidth was expanded from 75 to 500 kHz while maintaining the possibility of applying high-volume flows. A higher possible frequency can be beneficial when designing the process, as with increasing frequency, the polarizability can alter and enable separation. In a previous study, we could show that retention due to nDEP is small (<10%) in such a setup and therefore is not the reason for our observations.[25]

3.2. Influence of Voltage and Volume Flow. As a second step, we investigated the influence of voltage on signal reduction from 5 to 75 V_{pp} at 6 mL min^{-1} (Figure 4A) and 10 mL min^{-1} (Figure 4B). At both flow rates, all particles show an increased signal reduction or particle retention with increasing voltage. This is in line with the approximation of the DEP force (eq 2). Additionally, increasing volume flow decreases the signal reduction. This is due to the increased viscous drag and decreased residence time in the setup at the higher flow rate. The data at 6 mL min^{-1} and 30 V_{pp} are the same as in Figure 3, except for Actilion. Here, we used a different flow cuvette for this measurement to prevent sedimentation. However, the results are quite similar (here 97 ± 2.7% compared to 93 ± 0.6%). Figure 4C−E shows intensity plots over time for all particles at 30 V_{pp} and 10 mL min^{-1}. Three things become apparent from Figure 4. First, the signal reduction of Actilion is significantly higher than that of $LiFePO_4$. For example, at 30 V_{pp} and 10 mL min^{-1} (Figure 4B,C,E), the signal reduction of Actilion is over four times higher than that for $LiFePO_4$. Here, the recorded intensity for Actilion is close to zero, indicating complete removal. The relative difference in the signal reduction of $LiFePO_4$ and Actilion, however, decreases with increasing voltage (Figure 4A,B). Likely, this is because Actilion is already almost completely removed at voltages over 30 V_{pp} at both flow rates, whereas $LiFePO_4$ removal increases with voltage from 0 to 75 V_{pp}. Second, KS6 also shows significant trapping and gets fully removed at about 75 V_{pp} at both flow rates. Third, the reflection measurements can create signal reduction slightly higher than 100%, which is linked to the subtraction of the background signal and was observed before.[25] The highest recorded value was 104 ± 1.5%

https://doi.org/10.1021/acsomega.3c04057
ACS Omega XXXX, XXX, XXX−XXX

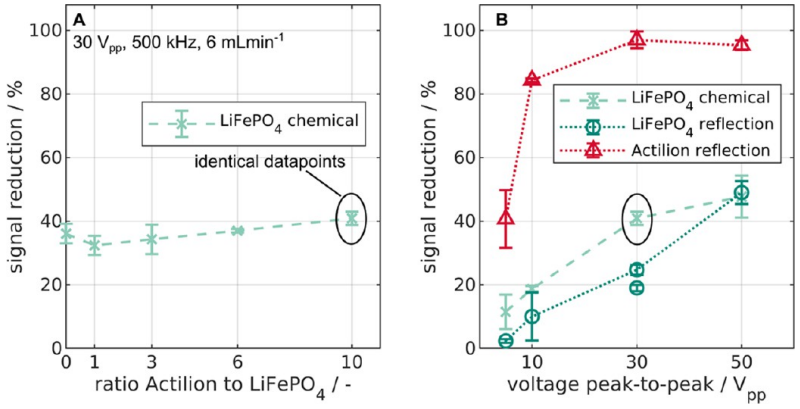

Figure 5. (A) Variation of the mass ratio of $LiFePO_4$ and Actilion graphite particles in the suspension at 30 V_{pp}, 500 kHz, and 6 mL min^{-1}. (B) Comparison of reflection measurements of suspensions with only one particle type present (dotted lines) and the chemical analysis of $LiFePO_4$ removal from a mixture with 10 times more mass of Actilion than that of $LiFePO_4$ (dashed line).

at 10 mL min^{-1} and 30 V_{pp}. As the deviation is explainable (Section S2 in the Supporting Information), relatively small, and showing complete removal of Actilion, we do not consider this problematic.

In summary, the size, voltage, and volume flow dependency of the signal reduction for these particles was as expected. In addition, we observed almost complete removal of Actilion from the suspension starting at 30 V_{pp}. For mixtures of $LiFePO_4$ and Actilion, this would correspond to a pure fraction of $LiFePO_4$ at the outlet and the enrichment of Actilion within the filter. Higher voltages than 30 V_{pp} would not lead to significantly increased trapping of Actilion but to more retained $LiFePO_4$. Therefore, we selected 30 V_{pp} for the separation experiments of Actilion and $LiFePO_4$.

3.3. Behavior in a Mixture of Graphite and $LiFePO_4$.

As a final step, we investigated the separability of a mixture of $LiFePO_4$ and Actilion. We did not include KS6 because conductive additives are only around 4% of the battery mass.[2] It would further increase the difficulty of analyzing the results because the reflection measurement is not material-sensitive. We tried to calculate separate reflection spectra for each component by superposition of the reflection spectra of pure $LiFePO_4$ and Actilion, as they are slightly different. For fluorescent particles, this can be achieved by coupling these reference spectra with global optimization to calculate separate intensities over time distributions as described in ref 24. Unfortunately, the results were not reliable for this mixture. Therefore, we had to rely on the information drawn from the experiments with only one particle type present (Figures 3 and 4). To determine the removal of $LiFePO_4$ from the mixture, we performed an additional chemical analysis of the mixture to measure the iron content. Prior to experiments with both particle types present, we compared the chemical- and reflection-based methods using 6 mL min^{-1}, 500 kHz, and 30 V_{pp} with only $LiFePO_4$ particles in our suspension. The reflection measurement revealed a signal reduction of 19 ± 1% (Figure 5B: $LiFePO_4$ reflection at 30 V_{pp}), whereas the chemical analysis showed a removal of 36 ± 3.0% (Figure 5A: ratio of 0). Please note that two slightly different signal reductions of two experimental runs, each representing three experiments, at 30 V_{pp} and 6 mL min^{-1} are shown (Figure 5B). One set of measurements showed a signal reduction of 25 ± 1.5%, whereas the other was 19 ± 1%. We collected the samples for the chemical analysis from the very same experiments in which we recorded 19 ± 1% signal reduction. It is therefore reasonable to compare these two values. The difference between chemical analysis and reflection measurement can be explained by the different principles of measurement. While the chemical analysis measures the mass of iron, the reflection does correspond to the particle surface area. Larger $LiFePO_4$ particles have high volume and mass but a low specific surface area. Due to their large size and thus higher DEP force, they are likely to be retained, whereas smaller particles are eluted and detected by the spectrometer. As the smaller particles have a higher specific surface area, they show higher reflection per mass. Consequently, these two measurement techniques are likely to obtain different yet valid results. In Section S4 in the Supporting Information, we provide more data, including calculations concerning the mass- and surface-weighted distributions of the $LiFePO_4$ material, which can explain the deviation.

Additionally, we conducted a series of experiments to investigate the influence of the mass ratio of Actilion and $LiFePO_4$ (Figure 5A). The ratio is defined as $m_{Actilion}/m_{LiFePO_4}$. The mass ratio does not influence the retention significantly at our set of parameters. Assuming a complete removal of graphite above 30 V_{pp} as measured for the pure graphite, we can assume an almost pure fraction of $LiFePO_4$ at the outlet at voltages above 30 V_{pp} and a retention of about 35−40% by mass of $LiFePO_4$ in the filter.

The encircled data in Figure 5A are also shown in Figure 5B in comparison with results at other voltages. We included the reflection data from Figure 4A of pure Actilion and $LiFePO_4$ for comparison (dotted lines). The chemical analysis again shows increasing retention of $LiFePO_4$ with voltage (Figure 5B), as observed before. Consequently, the conclusions drawn from the suspensions with only one particle type present remain valid, meaning that higher voltages than 30 V_{pp} would not enhance the separation any further. It is likely that the retention of Actilion in the mixed sample is similar to the previously measured retention of pure Actilion, mainly because of two effects. First, we could not observe any saturation effects within our experiments. Even after almost 1000 s of trapping, the signal remained constant (Section S3 in the Supporting Information). Second, the addition of $LiFePO_4$ particles could even increase the trapping efficiency. This is because trapped particles can create additional field inhomogeneous that would increase trapping efficiency by forming so-called pearl chains.[54]

https://doi.org/10.1021/acsomega.3c04057
ACS Omega XXXX, XXX, XXX−XXX

Nonetheless, the results would benefit from a further investigation of the particles and their mixture before and after the separation to show which particle sizes are retained in the channel and whether there is a cutoff diameter. Also, it needs to be investigated how residuals on the particles (e.g., binder or electrolyte) or changes in particle size due to upstream processes interfere with the DEP behavior of the particles and what space-time yield this method can achieve. However, this is beyond the scope of this study.

Concluding, we presented the first study on the separation of commercially available electrode active materials using dielectrophoresis. The sorting of the particles could lead to a direct recycling step that can be combined with other recycling techniques which then can reduce the amount of chemicals or energy needed. The results strengthen the assumption that separability using DEP increases with the difference in particle size. As some cathode active materials are even smaller than $LiFePO_4$ used in this study,[45] it is worth investigating this pathway of recycling further. DEP can also be an option for larger cathode active materials, since the separation could be improved by selective removal of graphite (several nm thickness[38]) from the cathode particles while not dissolving the anode graphite in the black mass completely. This would decrease the conductivity of the cathode particles and result in a weaker pDEP or even nDEP response of the particles. This would allow material- rather than size-selective separation, which is more robust to size changes in the particle mixture. With this study, we gave a starting point to direct future research on the direct recycling of particle systems using dielectrophoresis. We further demonstrated the applicability of dielectrophoresis besides microfluidic applications.

■ ASSOCIATED CONTENT

Supporting Information

The Supporting Information is available free of charge at https://pubs.acs.org/doi/10.1021/acsomega.3c04057.

Details of signal processing and background intensity; filter saturation analysis; analysis of the influence of particle distribution on measurement procedures; experimental details of the chemical analysis; and calculations of the Clausius−Mossotti factor (PDF)

■ AUTHOR INFORMATION

Corresponding Author

Georg R. Pesch − *School of Chemical and Bioprocess Engineering, University College Dublin, Dublin 4, Ireland;* orcid.org/0000-0003-4676-1908; Email: georg.pesch@ucd.ie

Authors

Jasper Giesler − *Chemical Process Engineering, Faculty of Production Engineering, University of Bremen, Bremen 28359, Germany;* orcid.org/0000-0003-1334-3013

Laura Weirauch − *Chemical Process Engineering, Faculty of Production Engineering, University of Bremen, Bremen 28359, Germany*

Alica Rother − *Center for Environmental Research and Sustainable Technology (UFT), University of Bremen, Bremen 28359, Germany*

Jorg Thöming − *Chemical Process Engineering, Faculty of Production Engineering, University of Bremen, Bremen 28359, Germany; Center for Environmental Research and Sustainable Technology (UFT), University of Bremen, Bremen 28359, Germany;* orcid.org/0000-0002-5374-114X

Michael Baune − *Chemical Process Engineering, Faculty of Production Engineering, University of Bremen, Bremen 28359, Germany; Center for Environmental Research and Sustainable Technology (UFT), University of Bremen, Bremen 28359, Germany*

Complete contact information is available at: https://pubs.acs.org/10.1021/acsomega.3c04057

Author Contributions

‖G.R.P. and M.B. contributed equally to this work.

Notes

The authors declare no competing financial interest.

■ ACKNOWLEDGMENTS

The authors thank the German Research Foundation (DFG) within the priority program, "MehrDimPart—Highly specific and multidimensional fractionation of fine particle systems with technical relevance" (SPP2045, Grant Numbers PE 3015/3-2, TH 893/20-2) for funding. The authors also thank Krischan Sandmann and Dilyan Kamenov from the IWT Bremen for helping to conduct particle size analysis.

■ ABBREVIATIONS

CM	Clausius-Mossotti factor
DEP	Dielectrophoresis
LIB	Lithium-ion battery
nDEP	negative Dielectrophoresis
PCB	printed circuit board
pDEP	positive Dielectrophoresis

■ REFERENCES

(1) Lv, W.; Wang, Z.; Cao, H.; Sun, Y.; Zhang, Y.; Sun, Z. A Critical Review and Analysis on the Recycling of Spent Lithium-Ion Batteries. *ACS Sustainable Chem. Eng.* **2018**, *6*, 1504−1521.

(2) Natarajan, S.; Divya, M. L.; Aravindan, V. Should We Recycle the Graphite from Spent Lithium-Ion Batteries? The Untold Story of Graphite with the Importance of Recycling. *J. Energy Chem.* **2022**, *71*, 351−369.

(3) Wu, X.; Ma, J.; Wang, J.; Zhang, X.; Zhou, G.; Liang, Z. Progress, Key Issues, and Future Prospects for Li-Ion Battery Recycling. *Global Challenges* **2022**, *6*, No. 2200067.

(4) Neumann, J.; Petranikova, M.; Meeus, M.; Gamarra, J. D.; Younesi, R.; Winter, M.; Nowak, S. Recycling of Lithium-Ion Batteries—Current State of the Art, Circular Economy, and Next Generation Recycling. *Adv. Energy Mater.* **2022**, *12*, No. 2102917.

(5) Vanderbruggen, A.; Hayagan, N.; Bachmann, K.; Ferreira, A.; Werner, D.; Horn, D.; Peuker, U.; Serna-Guerrero, R.; Rudolph, M. Lithium-Ion Battery Recycling-Influence of Recycling Processes on Component Liberation and Flotation Separation Efficiency. *ACS ES&T Engg* **2022**2, DOI: 10.1021/acsestengg.2c00177.

(6) Abdollahifar, M.; Doose, S.; Cavers, H.; Kwade, A. Graphite Recycling from End-of-Life Lithium-Ion Batteries: Processes and Applications. *Adv. Mater.Technol.***2023** *8*, 2200368. DOI: 10.1002/admt.202200368.

(7) Werner, D.; Peuker, U. A.; Mütze, T. Recycling Chain for Spent Lithium-Ion Batteries. *Metals* **2020**, *10*, No. 316.

(8) Heath, G. A.; Ravikumar, D.; Hansen, B.; Kupets, E. A Critical Review of the Circular Economy for Lithium-Ion Batteries and Photovoltaic Modules − Status, Challenges, and Opportunities. *J. Air Waste Manage. Assoc.* **2022**, *72*, 478−539.

(9) Satyavani, T. V. S. L.; Ramya Kiran, B.; Rajesh Kumar, V.; Srinivas Kumar, A.; Naidu, S. V. Effect of Particle Size on Dc

Conductivity, Activation Energy and Diffusion Coefficient of Lithium Iron Phosphate in Li-ion Cells. *Eng. Sci. Technol. Int. J.* **2016**, *19*, 40−44.
(10) Dai, K.; Wang, Z.; Ai, G.; Zhao, H.; Yuan, W.; Song, X.; Battaglia, V.; Sun, C.; Wu, K.; Liu, G. The Transformation of Graphite Electrode Materials in Lithium-Ion Batteries after Cycling. *J. Power Sources* **2015**, *298*, 349−354.
(11) Kassem, M.; Delacourt, C. Postmortem Analysis of Calendar-Aged Graphite/LiFePO4 Cells. *J. Power Sources* **2013**, *235*, 159−171.
(12) Vanderbruggen, A.; Salces, A.; Ferreira, A.; Rudolph, M.; Serna-Guerrero, R. Improving Separation Efficiency in End-of-Life Lithium-Ion Batteries Flotation Using Attrition Pre-Treatment. *Minerals* **2022**, *12*, 72.
(13) Zhan, R.; Oldenburg, Z.; Pan, L. Recovery of Active Cathode Materials from Lithium-Ion Batteries Using Froth Flotation. *Sustainable Mater. Technol.* **2018**, *17*, No. e00062.
(14) Harper, G.; Sommerville, R.; Kendrick, E.; Driscoll, L.; Slater, P.; Stolkin, R.; Walton, A.; Christensen, P.; Heidrich, O.; Lambert, S.; Abbott, A.; Ryder, K.; Gaines, L.; Anderson, P. Recycling Lithium-Ion Batteries from Electric Vehicles. *Nature* **2019**, *575*, 75−86.
(15) Xu, P.; Tan, D. H. S.; Jiao, B.; Gao, H.; Yu, X.; Chen, Z. A Materials Perspective on Direct Recycling of Lithium-Ion Batteries: Principles, Challenges and Opportunities. *Adv. Funct. Mater.* **2023**, *33*, No. 2213168.
(16) Larouche, F.; Tedjar, F.; Amouzegar, K.; Houlachi, G.; Bouchard, P.; Demopoulos, G. P.; Zaghib, K. Progress and Status of Hydrometallurgical and Direct Recycling of Li-Ion Batteries and Beyond. *Materials* **2020**, *13*, 801.
(17) Pethig, R. Review Article—Dielectrophoresis: Status of the Theory, Technology, and Applications. *Biomicrofluidics* **2010**, *4*, No. 022811.
(18) Pesch, G. R.; Du, F. A Review of Dielectrophoretic Separation and Classification of Non-biological Particles. *Electrophoresis* **2021**, *42*, 134−152.
(19) Pethig, R. *Dielectrophoresis*; Wiley & Sons, Ltd: Chichester, UK, 2017; pp 309−379. https://onlinelibrary.wiley.com/doi/book/10.1002/9781118671443
(20) Balasubramanian, P.; Kinders, R. J.; Kummar, S.; Gupta, V.; Hasegawa, D.; Menachery, A.; Lawrence, S. M.; Wang, L.; Ferry-Galow, K.; Davis, D.; Parchment, R. E.; Tomaszewski, J. E.; Doroshow, J. H. Antibody-Independent Capture of Circulating Tumor Cells of Non-Epithelial Origin with the ApoStream System. *PLoS One* **2017**, *12*, No. e0175414.
(21) Sano, H.; Kabata, H.; Kurosawa, O.; Washizu, M. *Dielectrophoretic Chromatography with Cross-Flow Injection. Technical Digest*, MEMS 2002 IEEE International Conference. Fifteenth IEEE International Conference on Micro Electro Mechanical Systems (Cat. No. 02CH37266), Las Vegas, NV, USA, 2002; pp 11−14.
(22) Lorenz, M.; Malangré, D.; Du, F.; Baune, M.; Thöming, J.; Pesch, G. R. High-Throughput Dielectrophoretic Filtration of Sub-Micron and Micro Particles in Macroscopic Porous Materials. *Anal. Bioanal. Chem.* **2020**, *412*, 3903−3914.
(23) Pesch, G. R.; Lorenz, M.; Sachdev, S.; Salameh, S.; Du, F.; Baune, M.; Boukany, P. E.; Thöming, J. Bridging the Scales in High-Throughput Dielectrophoretic (Bio-)Particle Separation in Porous Media. *Sci. Rep.* **2018**, *8*, No. 10480.
(24) Weirauch, L.; Giesler, J.; Baune, M.; Pesch, G. R.; Thöming, J. Shape-Selective Remobilization of Microparticles in a Mesh-Based DEP Filter at High Throughput. *Sep. Purif. Technol.* **2022**, *300*, No. 121792.
(25) Giesler, J.; Weirauch, L.; Thöming, J.; Baune, M.; Pesch, G. R. High-Throughput Dielectrophoretic Separator Based on Printed Circuit Boards. *Electrophoresis* **2023**, *44*, 72−81.
(26) Shen, Y.; Elele, E.; Khusid, B. A Novel Concept of Dielectrophoretic Engine Oil Filter. *Electrophoresis* **2011**, *32*, 2559−2568.
(27) Suehiro, J.; Guangbin Zhou; Imamura, M.; Hara, M. Dielectrophoretic Filter for Separation and Recovery of Biological Cells in Water. *IEEE Trans. Ind. Appl.* **2003**, *39*, 1514−1521.
(28) Jones, P. V.; Salmon, G. L.; Ros, A. Continuous Separation of DNA Molecules by Size Using Insulator-Based Dielectrophoresis. *Anal. Chem.* **2017**, *89*, 1531−1539.
(29) Martinez-Duarte, R.; Camacho-Alanis, F.; Renaud, P.; Ros, A. Dielectrophoresis of Lambda-DNA Using 3D Carbon Electrodes: Microfluidics and Miniaturization. *Electrophoresis* **2013**, *34*, 1113−1122.
(30) Gascoyne, P. R. C.; Wang, X.-B.; Huang, Y.; Becker, F. F. Dielectrophoretic Separation of Cancer Cells from Blood. *IEEE Trans. Ind. Appl.* **1997**, *33*, 670−678.
(31) Gascoyne, P. R. C.; Noshari, J.; Anderson, T. J.; Becker, F. F. Isolation of Rare Cells from Cell Mixtures by Dielectrophoresis. *Electrophoresis* **2009**, *30*, 1388−1398.
(32) Shim, S.; Stemke-Hale, K.; Tsimberidou, A. M.; Noshari, J.; Anderson, T. E.; Gascoyne, P. R. C. Antibody-Independent Isolation of Circulating Tumor Cells by Continuous-Flow Dielectrophoresis. *Biomicrofluidics* **2013**, *7*, No. 011807.
(33) Hughes, M. P. Fifty Years of Dielectrophoretic Cell Separation Technology. *Biomicrofluidics* **2016**, *10*, No. 032801.
(34) Giesler, J.; Weirauch, L.; Thöming, J.; Baune, M.; Pesch, G. R. Separating Microparticles by Material and Size Using Dielectrophoretic Chromatography with Frequency Modulation. *Sci. Rep.* **2021**, *11*, No. 16861.
(35) Modarres, P.; Tabrizian, M. Frequency Hopping Dielectrophoresis as a New Approach for Microscale Particle and Cell Enrichment. *Sens. Actuators, B* **2019**, *286*, 493−500.
(36) Liang, Q.; Yue, H.; Wang, S.; Yang, S.; Lam, K.-h.; Hou, X. Recycling and Crystal Regeneration of Commercial Used LiFePO4 Cathode Materials. *Electrochim. Acta* **2020**, *330*, No. 135323.
(37) Qiu, X.; Zhang, B.; Xu, Y.; Hu, J.; Deng, W.; Zou, G.; Hou, H.; Yang, Y.; Sun, W.; Hu, Y.; Cao, X.; Ji, X. Enabling the Sustainable Recycling of LiFePO $_4$ from Spent Lithium-Ion Batteries. *Green Chem.* **2022**, *24*, 2506−2515.
(38) Chen, Z.; Zhang, Q.; Liang, Q. Carbon-Coatings Improve Performance of Li-Ion Battery. *Nanomaterials* **1936**, *12*, No. 1936.
(39) Doeff, M. M.; Wilcox, J. D.; Kostecki, R.; Lau, G. Optimization of Carbon Coatings on LiFePO4. *J. Power Sources* **2006**, *163*, 180−184.
(40) Yu, F.; Zhang, L.; Li, Y.; An, Y.; Zhu, M.; Dai, B. Mechanism Studies of LiFePO4 Cathode Material: Lithiation/Delithiation Process, Electrochemical Modification and Synthetic Reaction. *RSC Adv.* **2014**, *4*, 54576−54602.
(41) Lepage, D.; Sobh, F.; Kuss, C.; Liang, G.; Schougaard, S. B. Delithiation Kinetics Study of Carbon Coated and Carbon Free LiFePO4. *J. Power Sources* **2014**, *256*, 61−65.
(42) Zhang, H.; Wang, L.; Chen, Y.; Wen, X. Regenerated LiFePO4/C for Scrapped Lithium Iron Phosphate Powder Batteries by Pre-Oxidation and Reduction Method. *Ionics* **2022**, *28*, 2125−2133.
(43) Larouche, F.; Amouzegar, K.; Houlachi, G.; Bouchard, P.; Demopoulos, G. P. Conversion of LiFePO $_4$ to FePO$_4$ via Selective Lithium Bicarbonation: A Direct Pathway Towards Battery Recycling. *J. Electrochem. Soc.* **2022**, *169*, No. 073509.
(44) Zaghib, K.; Striebel, K.; Guerfi, A.; Shim, J.; Armand, M.; Gauthier, M. LiFePO4/Polymer/Natural Graphite: Low Cost Li-ion Batteries. *Electrochim. Acta* **2004**, *50*, 263−270.
(45) Li, J.; Daniel, C.; Wood, D. Materials Processing for Lithium-Ion Batteries. *J. Power Sources* **2011**, *196*, 2452−2460.
(46) Zaghib, K.; Brochu, F.; Guerfi, A.; Kinoshita, K. Effect of Particle Size on Lithium Intercalation Rates in Natural Graphite. *J. Power Sources* **2001**, *103*, 140−146.
(47) Mu, D.; Liang, J.; Zhang, J.; Wang, Y.; Jin, S.; Dai, C. Exfoliation of Active Materials Synchronized with Electrolyte Extraction from Spent Lithium-Ion Batteries by Supercritical CO2. *ChemistrySelect* **2022**, *7*, No. e202200841.
(48) Friedlander, S. K. *Smoke, Dust, and Haze: Fundamentals of Aerosol Dynamics*, 2nd ed.; Topics in Chemical Engineering; Oxford University Press: New York, 2000.

https://doi.org/10.1021/acsomega.3c04057
ACS Omega XXXX, XXX, XXX−XXX

(49) DIN 38406 Teil 1 - Deutsche Einheitsverfahren zur Wasser-, Abwasser- und Schlammuntersuchung. 1983.
(50) Porcher, W.; Moreau, P.; Lestriez, B.; Jouanneau, S.; Guyomard, D. Is LiFePO4 Stable in Water?: Toward Greener Li−Batteries. *Electrochem. Solid-State Lett.* **2007**, *11*, A4.
(51) Giesler, J. Online Repository for "Sorting Lithium-Ion Battery Electrode Materials Using Dielectrophoresis at Frequencies of up to 500 kHz". https://doi.org/10.5281/zenodo.7593873, 2023.
(52) Castellanos, A.; Ramos, A.; González, A.; Green, N. G.; Morgan, H. Electrohydrodynamics and Dielectrophoresis in Microsystems: Scaling Laws. *J. Phys. D: Appl. Phys.* **2003**, *36*, 2584−2597.
(53) Hong, F. J.; Cao, J.; Cheng, P. A Parametric Study of AC Electrothermal Flow in Microchannels with Asymmetrical Interdigitated Electrodes. *Int. Commun. Heat Mass Transfer* **2011**, *38*, 275−279.
(54) Kong, T. F.; Tan, P. Y.; Tay, B. Z.; Shen, X.; Marcos. Bacteria and Cancer Cell Pearl Chain under Dielectrophoresis. *Electrophoresis* **2021**, *42*, 1070−1078.

https://doi.org/10.1021/acsomega.3c04057
ACS Omega XXXX, XXX, XXX−XXX

8 Conclusion and Outlook

Within this thesis, two novel approaches for electrode-based dielectrophoretic separators were presented. Both devices are able to separate microparticles according to their size and polarizability. The frequency modulated dielectrophoretic particle chromatography offers rapid chromatographic separation but is limited in throughput as electrode-based dielectrophoretic separators commonly are. An approach based on printed circuit boards was developed to overcome this issue of electrode-based dielectrophoretic separators. Consequently, these two approaches, namely DPC and upscaling via PCBs, could be coupled in the future to allow fast chromatographic separation with high throughput.

For the frequency modulated dielectrophoretic particle chromatography, first, the procedure and afterward a comprehensive understanding of the mechanics inside the separator was developed and presented. By developing a simulation tool which was shown to be in good agreement with the experimental results, the proposed separation mechanics could be validated in a subsequent step. Additionally, it was shown that this technique is capable of separating particles not only by size but also by material (e.g., surface functionalization). The technique allows fast separation within a few minutes or even below one minute, depending on the process parameters and particles.

The frequency modulated particle chromatography needs to be seen in the area of fundamental research. However, as similar but more time-consuming approaches were successfully used to manipulate biological particles as cells, this could be a future application of this methodology. However, this is beyond the scope of the research presented here and the manuscripts describing frequency modulated particle chromatography can be a starting point for other researchers.

The development of the second approach that was presented in this thesis focused on increasing the throughput of electrode-based dielectrophoretic separators. We could not only show selective trapping of polystyrene model particles, but also its applicability for particles with significant technical relevance. The removal of graphite was successfully shown from a mixture with lithium iron phosphate particles. Both of them are common active materials in lithium-ion batteries.

The design does not only feature a high throughput compared to classical microfluidic setups, but also maintained selectivity and the ability of applying high frequencies at those flow rates. By increasing throughput and expanding the appli-

cable frequency range, this approach improves the feasibility of dielectrophoretic setups for real-world separation tasks. Also, it could help to address separation problems with less valuable products as costs with this setup decrease while throughput increases. A potential design to further enhance the throughput could be derived from plate heat exchangers, which would result in a stacking of the electrodes and a parallelization.

Further, the device has high adaptability for other groups of researchers, as the electrodes consist of commercially available printed circuit boards that can be purchased at low cost. The data to manufacture the printed circuit boards are published under a creative commons license (CC BY 4.0) and thus can be used by researchers without significant restrictions.

Bibliography

(1) Giesler, J.; Pesch, G. R.; Weirauch, L.; Schmidt, M.-P.; Thöming, J.; Baune, M. Polarizability-Dependent Sorting of Microparticles Using Continuous-Flow Dielectrophoretic Chromatography with a Frequency Modulation Method. *Micromachines* **2019**, *11*, 38, DOI: 10.3390/mi11010038.

(2) Giesler, J.; Weirauch, L.; Thöming, J.; Baune, M.; Pesch, G. R. Separating Microparticles by Material and Size Using Dielectrophoretic Chromatography with Frequency Modulation. *Scientific Reports* **2021**, *11*, 16861, DOI: 10.1038/s41598-021-95404-w.

(3) Giesler, J.; Weirauch, L.; Thöming, J.; Baune, M.; Pesch, G. R. High-Throughput Dielectrophoretic Separator Based on Printed Circuit Boards. *ELECTROPHORESIS* **2023**, *44*, 72–81, DOI: 10.1002/elps.202200131.

(4) Giesler, J.; Weirauch, L.; Rother, A.; Thöming, J.; Pesch, G. R.; Baune, M. Sorting Lithium-Ion Battery Electrode Materials Using Dielectrophoresis. *ACS Omega* **2023**, DOI: 10.1021/acsomega.3c04057.

(5) Weirauch, L.; Giesler, J.; Baune, M.; Pesch, G. R.; Thöming, J. Shape-Selective Remobilization of Microparticles in a Mesh-Based DEP Filter at High Throughput. *Separation and Purification Technology* **2022**, *300*, 121792, DOI: 10.1016/j.seppur.2022.121792.

(6) Peleka, E. N.; Gallios, G. P.; Matis, K. A. A Perspective on Flotation: A Review. *Journal of Chemical Technology & Biotechnology* **2018**, *93*, 615–623, DOI: 10.1002/jctb.5486.

(7) Hansen, L.; Wollmann, A.; Weers, M.; Benker, B.; Weber, A. P. Triboelectric Charging and Separation of Fine Powder Mixtures. *Chemical Engineering & Technology* **2020**, *43*, 933–941, DOI: 10.1002/ceat.201900558.

(8) Gascoyne, P. R. C. Dielectrophoretic-Field Flow Fractionation Analysis of Dielectric, Density, and Deformability Characteristics of Cells and Particles. *Analytical Chemistry* **2009**, *81*, 8878–8885, DOI: 10.1021/ac901470z.

(9) Gupta, V.; Jafferji, I.; Garza, M.; Melnikova, V. O.; Hasegawa, D. K.; Pethig, R.; Davis, D. W. ApoStream ™ , a New Dielectrophoretic Device for Antibody Independent Isolation and Recovery of Viable Cancer Cells from Blood. *Biomicrofluidics* **2012**, *6*, 024133, DOI: 10.1063/1.4731647.

(10) Shim, S.; Stemke-Hale, K.; Tsimberidou, A. M.; Noshari, J.; Anderson, T. E.; Gascoyne, P. R. C. Antibody-Independent Isolation of Circulating Tumor Cells by Continuous-Flow Dielectrophoresis. *Biomicrofluidics* **2013**, *7*, 011807, DOI: 10.1063/1.4774304.

(11) Wang, F.; Zhao, Y.; Zhang, T.; Zhang, G.; Yang, X.; He, Y.; Wang, L.; Duan, C. Metals Recovery from Dust Derived from Recycling Line of Waste Printed Circuit Boards. *Journal of Cleaner Production* **2017**, *165*, 452–457, DOI: 10.1016/j.jclepro.2017.07.112.

(12) Wang, Y.; Du, F.; Baune, M.; Thöming, J. Predicting and Eliminating Joule Heating Constraints in Large Dielectrophoretic IDE Separators. *Chemical Engineering Science* **2015**, *137*, 235–242, DOI: 10.1016/j.ces.2015.06.042.

(13) Louhadj, S.; Hammadi, N.; Touhami, S.; Louati, H.; Hadjali, A.; Kimi, I.-E.; Tilmatine, A. Experimental Analysis of the Attraction Force Applied on Metal Particles Using a Double-Side Electrical Curtain. *Journal of Electrostatics* **2020**, *105*, 103448, DOI: 10.1016/j.elstat.2020.103448.

(14) Vanderbruggen, A.; Hayagan, N.; Bachmann, K.; Ferreira, A.; Werner, D.; Horn, D.; Peuker, U.; Serna-Guerrero, R.; Rudolph, M. Lithium-Ion Battery Recycling-Influence of Recycling Processes on Component Liberation and Flotation Separation Efficiency. *ACS ES&T Engineering* **2022**, DOI: 10.1021/acsestengg.2c00177.

(15) Waheed, W.; Sharaf, O. Z.; Alazzam, A.; Abu-Nada, E. Dielectrophoresis-Field Flow Fractionation for Separation of Particles: A Critical Review. *Journal of Chromatography A* **2021**, *1637*, 461799, DOI: 10.1016/j.chroma.2020.461799.

(16) Al-Faqheri, W.; Thio, T. H. G.; Qasaimeh, M. A.; Dietzel, A.; Madou, M.; Al-Halhouli, A. Particle/Cell Separation on Microfluidic Platforms Based on Centrifugation Effect: A Review. *Microfluidics and Nanofluidics* **2017**, *21*, 102, DOI: 10.1007/s10404-017-1933-4.

(17) Katasonova, O. N.; Fedotov, P. S. Methods for Continuous Flow Fractionation of Microparticles: Outlooks and Fields of Application. *Journal of Analytical Chemistry* **2009**, *64*, 212–225, DOI: 10.1134/S1061934809030022.

(18) Hoettges, K. F.; Henslee, E. A.; Torcal Serrano, R. M.; Jabr, R. I.; Abdallat, R. G.; Beale, A. D.; Waheed, A.; Camelliti, P.; Fry, C. H.; van der Veen, D. R.; Labeed, F. H.; Hughes, M. P. Ten–Second Electrophysiology: Evaluation of the 3DEP Platform for High-Speed, High-Accuracy Cell Analysis. *Scientific Reports* **2019**, *9*, 19153, DOI: 10.1038/s41598-019-55579-9.

(19) Moon, H.-S.; Kwon, K.; Kim, S.-I.; Han, H.; Sohn, J.; Lee, S.; Jung, H.-I. Continuous Separation of Breast Cancer Cells from Blood Samples Using Multi-Orifice Flow Fractionation (MOFF) and Dielectrophoresis (DEP). *Lab on a Chip* **2011**, *11*, 1118, DOI: 10.1039/c0lc00345j.

(20) Guillory, J. L.; Placer, F. M.; Grace, D. S. Electrostatic Enhancement of Moving-Bed Granular Filtration. *Environment International* **1981**, *6*, 387–395, DOI: 10.1016/0160-4120(81)90051-9.

(21) Liu, Y.; Hayes, M. A. Orders-of-Magnitude Larger Force Demonstrated for Dielectrophoresis of Proteins Enabling High-Resolution Separations Based on New Mechanisms. *Analytical Chemistry* **2021**, *93*, 1352–1359, DOI: 10.1021/acs.analchem.0c02763.

(22) Jones, P. V.; Salmon, G. L.; Ros, A. Continuous Separation of DNA Molecules by Size Using Insulator-Based Dielectrophoresis. *Analytical Chemistry* **2017**, *89*, 1531–1539, DOI: 10.1021/acs.analchem.6b03369.

(23) Sano, H.; Kabata, H.; Kurosawa, O.; Washizu, M. In *Technical Digest. MEMS 2002 IEEE International Conference. Fifteenth IEEE International Conference on Micro Electro Mechanical Systems (Cat. No.02CH37266)*, Technical Digest. MEMS 2002 IEEE International Conference. Fifteenth IEEE International Conference on Micro Electro Mechanical Systems, IEEE: Las Vegas, NV, USA, 2002, pp 11–14, DOI: 10.1109/MEMSYS.2002.984043.

(24) Abt, V.; Gringel, F.; Han, A.; Neubauer, P.; Birkholz, M. Separation, Characterization, and Handling of Microalgae by Dielectrophoresis. *Microorganisms* **2020**, *8*, 540, DOI: 10.3390/microorganisms8040540.

(25) Michael, K. A.; Hiibel, S. R.; Geiger, E. J. Dependence of the Dielectrophoretic Upper Crossover Frequency on the Lipid Content of Microalgal Cells. *Algal Research* **2014**, *6*, 17–21, DOI: 10.1016/j.algal.2014.08.004.

(26) Schor, A. R.; Buie, C. R. Rapid Fabrication of Three-Dimensional Structures for Dielectrophoretic Sorting of Lipid-Containing Organisms. *Journal of Micromechanics and Microengineering* **2016**, *26*, 105010, DOI: 10.1088/0960-1317/26/10/105010.

(27) tagesschau.de Rohstoffe für E-Autos: Die Chancen des Batterie-Recyclings tagesschau.de, `https://www.tagesschau.de/wirtschaft/technologie/mercedes-batterierecycling-fabrik-101.html` (accessed 03/08/2023).

(28) Satyavani, T. V. S. L.; Ramya Kiran, B.; Rajesh Kumar, V.; Srinivas Kumar, A.; Naidu, S. V. Effect of Particle Size on Dc Conductivity, Activation Energy and Diffusion Coefficient of Lithium Iron Phosphate in Li-ion Cells. *Engineering Science and Technology, an International Journal* **2016**, *19*, 40–44, DOI: 10.1016/j.jestch.2015.05.011.

(29) Dai, K.; Wang, Z.; Ai, G.; Zhao, H.; Yuan, W.; Song, X.; Battaglia, V.; Sun, C.; Wu, K.; Liu, G. The Transformation of Graphite Electrode Materials in Lithium-Ion Batteries after Cycling. *Journal of Power Sources* **2015**, *298*, 349–354, DOI: 10.1016/j.jpowsour.2015.08.055.

(30) Kassem, M.; Delacourt, C. Postmortem Analysis of Calendar-Aged Graphite/LiFePO4 Cells. *Journal of Power Sources* **2013**, *235*, 159–171, DOI: 10.1016/j.jpowsour.2013.01.147.

(31) Kharlamova, M. V.; Burdanova, M. G.; Paukov, M. I.; Kramberger, C. Synthesis, Sorting, and Applications of Single-Chirality Single-Walled Carbon Nanotubes. *Materials* **2022**, *15*, 5898, DOI: 10.3390/ma15175898.

(32) Li, W.; Hennrich, F.; Flavel, B. S.; Dehm, S.; Kappes, M.; Krupke, R. Principles of Carbon Nanotube Dielectrophoresis. *Nano Research* **2021**, *14*, 2188–2206, DOI: 10.1007/s12274-020-3183-0.

(33) Castellanos, A.; Ramos, A.; González, A.; Green, N. G.; Morgan, H. Electrohydrodynamics and Dielectrophoresis in Microsystems: Scaling Laws. *Journal of Physics D: Applied Physics* **2003**, *36*, 2584–2597, DOI: 10.1088/0022-3727/36/20/023.

(34) Barasinski, M.; Garnweitner, G. Restricted and Unrestricted Migration Mechanisms of Silica Nanoparticles in Agarose Gels and Their Utilization for the Separation of Binary Mixtures. *The Journal of Physical Chemistry C* **2020**, *124*, 5157–5166, DOI: 10.1021/acs.jpcc.9b10644.

(35) Furat, O.; Masuhr, M.; Kruis, F. E.; Schmidt, V. Stochastic Modeling of Classifying Aerodynamic Lenses for Separation of Airborne Particles by Material and Size. *Advanced Powder Technology* **2020**, *31*, 2215–2226, DOI: 10.1016/j.apt.2020.03.014.

(36) Wullenweber, M. S.; Kottmeier, J.; Kampen, I.; Dietzel, A.; Kwade, A. Simulative Investigation of Different DLD Microsystem Designs with Increased Reynolds Numbers Using a Two-Way Coupled IBM-CFD/6-DOF Approach. *Processes* **2022**, *10*, 403, DOI: 10.3390/pr10020403.

(37) Kottmeier, J.; Wullenweber, M.; Blahout, S.; Hussong, J.; Kampen, I.; Kwade, A.; Dietzel, A. Accelerated Particle Separation in a DLD Device at Re $>$ 1 Investigated by Means of µPIV. *Micromachines* **2019**, *10*, 768, DOI: 10.3390/mi10110768.

(38) Calero, V.; Garcia-Sanchez, P.; Ramos, A.; Morgan, H. Combining DC and AC Electric Fields with Deterministic Lateral Displacement for Micro- and Nano-Particle Separation. *Biomicrofluidics* **2019**, *13*, 054110, DOI: 10.1063/1.5124475.

(39) Sandmann, K.; Fritsching, U. Selektive Partikelklassierung in ultraschallangeregten Aerosolen. *Chemie Ingenieur Technik* **2020**, *92*, 635–642, DOI: 10.1002/cite.201900158.

(40) Wu, Y.; Chattaraj, R.; Ren, Y.; Jiang, H.; Lee, D. Label-Free Multitarget Separation of Particles and Cells under Flow Using Acoustic, Electrophoretic, and Hydrodynamic Forces. *Analytical Chemistry* **2021**, *93*, 7635–7646, DOI: 10.1021/acs.analchem.1c00312.

(41) Sygusch, J.; Rudolph, M. A Contribution to Wettability and Wetting Characterisation of Ultrafine Particles with Varying Shape and Degree of Hydrophobization. *Applied Surface Science* **2021**, *566*, 150725, DOI: 10.1016/j.apsusc.2021.150725.

(42) Williams, S. J.; Schneider, J. D.; King, B. C.; Green, N. G. Particle-Induced Electrostatic Repulsion within an Electric Curtain Operating below the Paschen Limit. *Micromachines* **2022**, *13*, 288, DOI: 10.3390/mi13020288.

(43) Louati, H.; Tilmatine, A.; Ouiddir, R.; Alibida, A.; Zouzou, N. New Separation Technique of Metal/Polymer Granular Materials Using an Electrostatic Sorting Device. *Journal of Electrostatics* **2020**, *103*, 103410, DOI: 10.1016/j.elstat.2019.103410.

(44) Pethig, R. Review Article—Dielectrophoresis: Status of the Theory, Technology, and Applications. *Biomicrofluidics* **2010**, *4*, 022811, DOI: 10.1063/1.3456626.

(45) Pesch, G. R.; Lorenz, M.; Sachdev, S.; Salameh, S.; Du, F.; Baune, M.; Boukany, P. E.; Thöming, J. Bridging the Scales in High-Throughput Dielectrophoretic (Bio-)Particle Separation in Porous Media. *Scientific Reports* **2018**, *8*, 10480, DOI: 10.1038/s41598-018-28735-w.

(46) Lorenz, M.; Malangré, D.; Du, F.; Baune, M.; Thöming, J.; Pesch, G. R. High-Throughput Dielectrophoretic Filtration of Sub-Micron and Micro Particles in Macroscopic Porous Materials. *Analytical and Bioanalytical Chemistry* **2020**, *412*, 3903–3914, DOI: 10.1007/s00216-020-02557-0.

(47) Morgan, H.; Green, N. G., *AC Electrokinetics: Colloids and Nanoparticles*; Microtechnologies and Microsystems Series 2; Research Studies Press: Baldock, 2003; 324 pp.

(48) Pethig, R., *Dielectrophoresis: Theory, Methodology, and Biological Applications*; John Wiley & Sons, Inc: Hoboken, NJ, 2017; 428 pp.

(49) Hughes, M. P. Fifty Years of Dielectrophoretic Cell Separation Technology. *Biomicrofluidics* **2016**, *10*, 032801, DOI: 10.1063/1.4954841.

(50) Kirby, B. J., *Micro- and Nanoscale Fluid Mechanics: Transport in Microfluidic Devices*; Cambridge University Press: Cambridge, 2010, DOI: 10.1017/CBO9780511760723.

(51) Trombley, C. I.; Ekiel-Jeżewska, M. L. In *Flowing Matter*, Toschi, F., Sega, M., Eds.; Springer International Publishing: Cham, 2019, pp 35–50, DOI: 10.1007/978-3-030-23370-9_2.

(52) Friedlander, S. K., *Smoke, Dust, and Haze: Fundamentals of Aerosol Dynamics*, 2nd ed; Topics in Chemical Engineering; Oxford University Press: New York, 2000; 407 pp.

(53) Zhang, J.; Yan, S.; Yuan, D.; Alici, G.; Nguyen, N.-T.; Warkiani, M. E.; Li, W. Fundamentals and Applications of Inertial Microfluidics: A Review. *Lab on a Chip* **2016**, *16*, 10–34, DOI: 10.1039/C5LC01159K.

(54) Nasiri, R.; Shamloo, A.; Ahadian, S.; Amirifar, L.; Akbari, J.; Goudie, M. J.; Lee, K.; Ashammakhi, N.; Dokmeci, M. R.; Di Carlo, D.; Khademhosseini, A. Microfluidic-Based Approaches in Targeted Cell/Particle Separation Based on Physical Properties: Fundamentals and Applications. *Small* **2020**, *16*, 2000171, DOI: 10.1002/smll.202000171.

(55) Wang, X.-B.; Vykoukal, J.; Becker, F. F.; Gascoyne, P. R. Separation of Polystyrene Microbeads Using Dielectrophoretic/Gravitational Field-Flow-Fractionation. *Biophysical Journal* **1998**, *74*, 2689–2701, DOI: 10.1016/S0006-3495(98)77975-5.

(56) Nguyen, N.-T., *Mikrofluidik*; Vieweg+Teubner Verlag: Wiesbaden, 2004, DOI: 10.1007/978-3-322-80069-5.

(57) Gustrau, F., *Hochfrequenztechnik*, 2nd ed.; Hanser Verlag GmbH & Co. KG: Leipzig, 2013.

(58) Masliyah, J. H.; Bhattacharjee, S., *Electrokinetic and Colloid Transport Phenomena*; Wiley-Interscience: Hoboken, N.J, 2006; 707 pp.

(59) Kaatze, U. Complex Permittivity of Water as a Function of Frequency and Temperature. *Journal of Chemical & Engineering Data* **1989**, *34*, 371–374, DOI: 10.1021/je00058a001.

(60) Shaik, S.; Mandal, D.; Ramanan, R. Oriented Electric Fields as Future Smart Reagents in Chemistry. *Nature Chemistry* **2016**, *8*, 1091–1098, DOI: 10.1038/nchem.2651.

(61) Calvaresi, M.; Martinez, R. V.; Losilla, N. S.; Martinez, J.; Garcia, R.; Zerbetto, F. Splitting CO2 with Electric Fields: A Computational Investigation. *The Journal of Physical Chemistry Letters* **2010**, *1*, 3256–3260, DOI: 10.1021/jz101005u.

(62) Kurzweil, P., *Chemie: Grundlagen, Aufbauwissen, Anwendungen und Experimente*, 10., überarb. Aufl; Chemie; Springer Vieweg: Wiesbaden, 2015.

(63) Iwamoto, M. In *Encyclopedia of Nanotechnology*, Bhushan, B., Ed.; Springer Netherlands: Dordrecht, 2012, pp 1276–1285, DOI: 10.1007/978-90-481-9751-4_5.

(64) Pohl, H. A.; Crane, J. S. Dielectrophoretic Force. *Journal of Theoretical Biology* **1972**, *37*, 1–13, DOI: 10.1016/0022-5193(72)90112-9.

(65) Beneduci, A. Which Is the Effective Time Scale of the Fast Debye Relaxation Process in Water? *Journal of Molecular Liquids* **2008**, *138*, 55–60, DOI: 10.1016/j.molliq.2007.07.003.

(66) Wang, X.; Wang, X.-B.; Gascoyne, P. R. General Expressions for Dielectrophoretic Force and Electrorotational Torque Derived Using the Maxwell Stress Tensor Method. *Journal of Electrostatics* **1997**, *39*, 277–295, DOI: 10.1016/S0304-3886(97)00126-5.

(67) Ermolina, I.; Morgan, H. The Electrokinetic Properties of Latex Particles: Comparison of Electrophoresis and Dielectrophoresis. *Journal of Colloid and Interface Science* **2005**, *285*, 419–428, DOI: 10.1016/j.jcis.2004.11.003.

(68) Gierhart, B. C.; Howitt, D. G.; Chen, S. J.; Smith, R. L.; Collins, S. D. Frequency Dependence of Gold Nanoparticle Superassembly by Dielectrophoresis. *Langmuir* **2007**, *23*, 12450–12456, DOI: 10.1021/la701472y.

(69) Ramos, A.; García-Sánchez, P.; Morgan, H. AC Electrokinetics of Conducting Microparticles: A Review. *Current Opinion in Colloid & Interface Science* **2016**, *24*, 79–90, DOI: 10.1016/j.cocis.2016.06.018.

(70) Kong, T. F.; Tan, P. Y.; Tay, B. Z.; Shen, X.; Marcos Bacteria and Cancer Cell Pearl Chain under Dielectrophoresis. *ELECTROPHORESIS* **2021**, *42*, 1070–1078, DOI: 10.1002/elps.202000277.

(71) Kadaksham, J.; Singh, P.; Aubry, N. Dielectrophoresis Induced Clustering Regimes of Viable Yeast Cells. *ELECTROPHORESIS* **2005**, *26*, 3738–3744, DOI: 10.1002/elps.200500133.

(72) Green, N. G.; Ramos, A.; González, A.; Castellanos, A.; Morgan, H. Electrothermally Induced Fluid Flow on Microelectrodes. *Journal of Electrostatics* **2001**, *53*, 71–87, DOI: 10.1016/S0304-3886(01)00132-2.

(73) Kwak, T. J.; Hossen, I.; Bashir, R.; Chang, W.-J.; Lee, C. H. Localized Dielectric Loss Heating in Dielectrophoresis Devices. *Scientific Reports* **2019**, *9*, 18977, DOI: 10.1038/s41598-019-55031-y.

(74) Green, N. G.; Ramos, A.; González, A.; Castellanos, A.; Morgan, H. Electric Field Induced Fluid Flow on Microelectrodes: The Effect of Illumination. *Journal of Physics D: Applied Physics* **2000**, *33*, L13–L17, DOI: 10.1088/0022-3727/33/2/102.

(75) Ramos, A.; Morgan, H.; Green, N. G.; Castellanos, A. Ac Electrokinetics: A Review of Forces in Microelectrode Structures. *Journal of Physics D: Applied Physics* **1998**, *31*, 2338–2353, DOI: 10.1088/0022-3727/31/18/021.

(76) Modarres, P.; Tabrizian, M. Frequency Hopping Dielectrophoresis as a New Approach for Microscale Particle and Cell Enrichment. *Sensors and Actuators B: Chemical* **2019**, *286*, 493–500, DOI: 10.1016/j.snb.2019.01.157.

(77) Manshadi, M. K. D.; Mohammadi, M.; Zarei, M.; Saadat, M.; Sanati-Nezhad, A. Induced-Charge Electrokinetics in Microfluidics: A Review on Recent Advancements. *Journal of Micromechanics and Microengineering* **2020**, *30*, 113001, DOI: 10.1088/1361-6439/abaf34.

(78) Dong, C. C.; Wang, Z. Y. On the Mechanism of AC Electroosmosis. *Advanced Materials Research* **2014**, *986–987*, 136–145, DOI: 10.4028/www.scientific.net/AMR.986-987.136.

(79) Modarres, P.; Tabrizian, M. Alternating Current Dielectrophoresis of Biomacromolecules: The Interplay of Electrokinetic Effects. *Sensors and Actuators B: Chemical* **2017**, *252*, 391–408, DOI: 10.1016/j.snb.2017.05.144.

(80) Green, N. G.; Ramos, A.; González, A.; Morgan, H.; Castellanos, A. Fluid Flow Induced by Nonuniform Ac Electric Fields in Electrolytes on Microelectrodes. I. Experimental Measurements. *Physical Review E* **2000**, *61*, 4011–4018, DOI: 10.1103/PhysRevE.61.4011.

(81) Lapizco-Encinas, B. H. On the Recent Developments of Insulator-Based Dielectrophoresis: A Review. *ELECTROPHORESIS* **2019**, *40*, 358–375, DOI: 10.1002/elps.201800285.

(82) Pesch, G. R.; Du, F. A Review of Dielectrophoretic Separation and Classification of Non-biological Particles. *ELECTROPHORESIS* **2021**, *42*, 134–152, DOI: 10.1002/elps.202000137.

(83) Sarno, B.; Heineck, D.; Heller, M. J.; Ibsen, S. D. Dielectrophoresis: Developments and Applications from 2010 to 2020. *ELECTROPHORESIS* **2021**, *42*, 539–564, DOI: 10.1002/elps.202000156.

(84) Stafford, H. H. (IMP TRUST FOR ENCOURAGEMEN). Means and Process of Separating Substances One from Another US Patent, 1498911A, 1924.

(85) Frederick, H. H. (US HOFFMAN MACHINERY CORP). Electrical Precipitation Method US Patent, 2573967A, 1951.

(86) Crissman, J. H.; Fritsche, G. R. (Gulf Research and Development Co). Filtering Process US Patent, 4009089A, 1977.

(87) Masuda, S.; Washizu, M.; Nanba, T. Novel Method of Cell Fusion in Field Constriction Area in Fluid Integration Circuit. *IEEE Transactions on Industry Applications* **1989**, *25*, 732–737, DOI: 10.1109/28.31255.

(88) Cummings, E. B.; Singh, A. K. In Micromachining and Microfabrication, ed. by Mastrangelo, C. H.; Becker, H., Santa Clara, CA, 2000, pp 151–160, DOI: 10.1117/12.395653.

(89) Cummings, E. B.; Singh, A. K. Dielectrophoresis in Microchips Containing Arrays of Insulating Posts: Theoretical and Experimental Results. *Analytical Chemistry* **2003**, *75*, 4724–4731, DOI: 10.1021/ac0340612.

(90) Cummings, E. Streaming Dielectrophoresis for Continuous-Flow Microfluidic Devices. *IEEE Engineering in Medicine and Biology Magazine* **2003**, *22*, 75–84, DOI: 10.1109/MEMB.2003.1266050.

(91) Cardenas-Benitez, B.; Jind, B.; Gallo-Villanueva, R. C.; Martinez-Chapa, S. O.; Lapizco-Encinas, B. H.; Perez-Gonzalez, V. H. Direct Current Electrokinetic Particle Trapping in Insulator-Based Microfluidics: Theory and Experiments. *Analytical Chemistry* **2020**, *92*, 12871–12879, DOI: 10.1021/acs.analchem.0c01303.

(92) Lapizco-Encinas, B. H.; Simmons, B. A.; Cummings, E. B.; Fintschenko, Y. Dielectrophoretic Concentration and Separation of Live and Dead Bacteria in an Array of Insulators. *Analytical Chemistry* **2004**, *76*, 1571–1579, DOI: 10.1021/ac034804j.

(93) Lapizco-Encinas, B. H.; Simmons, B. A.; Cummings, E. B.; Fintschenko, Y. Insulator-Based Dielectrophoresis for the Selective Concentration and Separation of Live Bacteria in Water. *ELECTROPHORESIS* **2004**, *25*, 1695–1704, DOI: 10.1002/elps.200405899.

(94) Lapizco-Encinas, B. H.; Davalos, R. V.; Simmons, B. A.; Cummings, E. B.; Fintschenko, Y. An Insulator-Based (Electrodeless) Dielectrophoretic Concentrator for Microbes in Water. *Journal of Microbiological Methods* **2005**, *62*, 317–326, DOI: 10.1016/j.mimet.2005.04.027.

(95) Lapizco-Encinas, B. H.; Ozuna-Chacón, S.; Rito-Palomares, M. Protein Manipulation with Insulator-Based Dielectrophoresis and Direct Current Electric Fields. *Journal of Chromatography A* **2008**, *1206*, 45–51, DOI: 10.1016/j.chroma.2008.05.077.

(96) P. Beech, J.; Jönsson, P.; O. Tegenfeldt, J. Tipping the Balance of Deterministic Lateral Displacement Devices Using Dielectrophoresis. *Lab on a Chip* **2009**, *9*, 2698–2706, DOI: 10.1039/B823275J.

(97) Calero, V.; Garcia-Sanchez, P.; Honrado, C.; Ramos, A.; Morgan, H. AC Electrokinetic Biased Deterministic Lateral Displacement for Tunable Particle Separation. *Lab on a Chip* **2019**, *19*, 1386–1396, DOI: 10.1039/C8LC01416G.

(98) Rabbani, M. T.; Sonker, M.; Ros, A. Carbon Nanotube Dielectrophoresis: Theory and Applications. *ELECTROPHORESIS* **2020**, *41*, 1893–1914, DOI: 10.1002/elps.202000049.

(99) Luo, J.; Abdallah, B. G.; Wolken, G. G.; Arriaga, E. A.; Ros, A. Insulator-Based Dielectrophoresis of Mitochondria. *Biomicrofluidics* **2014**, *8*, 021801, DOI: 10.1063/1.4866852.

(100) Pesch, G. R.; Du, F.; Baune, M.; Thöming, J. Influence of Geometry and Material of Insulating Posts on Particle Trapping Using Positive Dielectrophoresis. *Journal of Chromatography A* **2017**, *1483*, 127–137, DOI: 10.1016/j.chroma.2016.12.074.

(101) Weirauch, L.; Lorenz, M.; Hill, N.; Lapizco-Encinas, B. H.; Baune, M.; Pesch, G. R.; Thöming, J. Material-Selective Separation of Mixed Microparticles via Insulator-Based Dielectrophoresis. *Biomicrofluidics* **2019**, *13*, 064112, DOI: 10.1063/1.5124110.

(102) Weirauch, L.; Giesler, J.; Baune, M.; Pesch, G. R.; Thöming, J. *Shape-Selective Remobilization of Microparticles in a Mesh-Based DEP Filter at High Throughput*; preprint; In Review, 2022, DOI: 10.21203/rs.3.rs-1661826/v1.

(103) Hill, N.; Lapizco-Encinas, B. H. Continuous Flow Separation of Particles with Insulator-Based Dielectrophoresis Chromatography. *Analytical and Bioanalytical Chemistry* **2020**, *412*, 3891–3902, DOI: 10.1007/s00216-019-02308-w.

(104) Ozuna-Chacón, S.; Lapizco-Encinas, B. H.; Rito-Palomares, M.; Martínez-Chapa, S. O.; Reyes-Betanzo, C. Performance Characterization of an Insulator-Based Dielectrophoretic Microdevice. *ELECTROPHORESIS* **2008**, *29*, 3115–3122, DOI: 10.1002/elps.200700865.

(105) V. Crowther, C.; A. Hayes, M. Refinement of Insulator-Based Dielectrophoresis. *Analyst* **2017**, *142*, 1608–1618, DOI: 10.1039/C6AN02509A.

(106) Bhattacharya, S.; Chao, T.-C.; Ariyasinghe, N.; Ruiz, Y.; Lake, D.; Ros, R.; Ros, A. Selective Trapping of Single Mammalian Breast Cancer Cells by Insulator-Based Dielectrophoresis. *Analytical and Bioanalytical Chemistry* **2014**, *406*, 1855–1865, DOI: 10.1007/s00216-013-7598-2.

(107) Lorenz, M. Dielectrophoretic Filtration of Particles in Porous Media: Concept, Design, and Selectivity, Universität Bremen, 2021, DOI: 10.26092/ELIB/593.

(108) Deng, Y.-L.; Chang, J.-S.; Juang, Y.-J. Separation of Microalgae with Different Lipid Contents by Dielectrophoresis. *Bioresource Technology* **2013**, *135*, 137–141, DOI: 10.1016/j.biortech.2012.11.046.

(109) Chung, C.; Waterfall, M.; Pells, S.; Menachery, A.; Smith, S.; Pethig, R. Dielectrophoretic Characterisation of Mammalian Cells above 100 MHz. *Journal of Electrical Bioimpedance* **2011**, *2*, 64–71, DOI: 10.5617/jeb.196.

(110) Zhang, Z.-B.; Liu, X.-J.; Campbell, E. E. B.; Zhang, S.-L. Alternating Current Dielectrophoresis of Carbon Nanotubes. *Journal of Applied Physics* **2005**, *98*, 056103, DOI: 10.1063/1.2037866.

(111) Martinez-Duarte, R. A Critical Review on the Fabrication Techniques That Can Enable Higher Throughput in Dielectrophoresis Devices. *ELECTROPHORESIS* **2022**, *43*, 232–248, DOI: 10.1002/elps.202100179.

(112) Martinez-Duarte, R.; Camacho-Alanis, F.; Renaud, P.; Ros, A. Dielectrophoresis of Lambda-DNA Using 3D Carbon Electrodes: Microfluidics and Miniaturization. *ELECTROPHORESIS* **2013**, *34*, 1113–1122, DOI: 10.1002/elps.201200447.

(113) Faraghat, S. A.; Fatoyinbo, H. O.; Hoettges, K. F.; Hughes, M. P. Low-Cost, High-Throughput and Rapid-Prototyped 3D-integrated Dielectrophoretic Channels for Continuous Cell Enrichment and Separation. *ELECTROPHORESIS* **2023**, *44*, 947–955, DOI: 10.1002/elps.202200234.

(114) Williams, S. J.; Romero, N.; Parkes, L.; Jackson, D. J.; Naber, J. F. Inexpensive Three-Dimensional Dielectrophoretic Microfluidic Devices Using Milled Copperclad Substrates. *Journal of Electrostatics* **2015**, *75*, 49–53, DOI: 10.1016/j.elstat.2015.02.003.

(115) Shen, Y.; Elele, E.; Khusid, B. A Novel Concept of Dielectrophoretic Engine Oil Filter. *ELECTROPHORESIS* **2011**, *32*, 2559–2568, DOI: 10.1002/elps.201100072.

(116) Green, N.; Ramos, A.; Morgan, H. Numerical Solution of the Dielectrophoretic and Travelling Wave Forces for Interdigitated Electrode Arrays Using the Finite Element Method. *Journal of Electrostatics* **2002**, *56*, 235–254, DOI: 10.1016/S0304-3886(02)00069-4.

(117) Morgan, H.; Izquierdo, A. G.; Bakewell, D.; Green, N. G.; Ramos, A. The Dielectrophoretic and Travelling Wave Forces Generated by Interdigitated Electrode Arrays: Analytical Solution Using Fourier Series. 10.

(118) Sun, T.; Morgan, H.; Green, N. G. Analytical Solutions of Ac Electrokinetics in Interdigitated Electrode Arrays: Electric Field, Dielectrophoretic and Traveling-Wave Dielectrophoretic Forces. *Physical Review E* **2007**, *76*, 046610, DOI: 10.1103/PhysRevE.76.046610.

(119) Arnold, W. M.; Schwan, H. P.; Zimmermann, U. Surface Conductance and Other Properties of Latex Particles Measured by Electrorotation. *The Journal of Physical Chemistry* **1987**, *91*, 5093–5098, DOI: 10.1021/j100303a043.

(120) Cottet, J.; Fabregue, O.; Berger, C.; Buret, F.; Renaud, P.; Frénéa-Robin, M. MyDEP: A New Computational Tool for Dielectric Modeling of Particles and Cells. *Biophysical Journal* **2019**, *116*, 12–18, DOI: 10.1016/j.bpj.2018.11.021.

(121) Vykoukal, J.; M. Vykoukal, D.; Freyberg, S.; U. Alt, E.; C. Gascoyne, P. R. Enrichment of Putative Stem Cells from Adipose Tissue Using Dielectrophoretic Field-Flow Fractionation. *Lab on a Chip* **2008**, *8*, 1386–1393, DOI: 10.1039/B717043B.

(122) Shim, S.; Stemke-Hale, K.; Noshari, J.; Becker, F. F.; Gascoyne, P. R. C. Dielectrophoresis Has Broad Applicability to Marker-Free Isolation of Tumor Cells from Blood by Microfluidic Systems. *Biomicrofluidics* **2013**, *7*, 011808, DOI: 10.1063/1.4774307.

(123) Moschou, D.; Tserepi, A. The Lab-on-PCB Approach: Tackling the µTAS Commercial Upscaling Bottleneck. *Lab on a Chip* **2017**, *17*, 1388–1405, DOI: 10.1039/C7LC00121E.

(124) Huang, Y.; Yang, J.; Wang, X.-B.; Becker, F. F.; Gascoyne, P. R. The Removal of Human Breast Cancer Cells from Hematopoietic CD34 $^{+}$ Stem Cells by Dielectrophoretic Field-Flow-Fractionation. *Journal of Hematotherapy & Stem Cell Research* **1999**, *8*, 481–490, DOI: 10.1089/152581699319939.

(125) Wang, X.-B.; Yang, J.; Huang, Y.; Vykoukal, J.; Becker, F. F.; Gascoyne, P. R. C. Cell Separation by Dielectrophoretic Field-flow-fractionation. *Analytical Chemistry* **2000**, *72*, 832–839, DOI: 10.1021/ac990922o.

(126) Yang, J.; Huang, Y.; Wang, X.-B.; Becker, F. F.; Gascoyne, P. R. Differential Analysis of Human Leukocytes by Dielectrophoretic Field-Flow-Fractionation. *Biophysical Journal* **2000**, *78*, 2680–2689, DOI: 10.1016/S0006-3495(00)76812-3.

(127) Balasubramanian, P.; Kinders, R. J.; Kummar, S.; Gupta, V.; Hasegawa, D.; Menachery, A.; Lawrence, S. M.; Wang, L.; Ferry-Galow, K.; Davis, D.; Parchment, R. E.; Tomaszewski, J. E.; Doroshow, J. H. Antibody-Independent Capture of Circulating Tumor Cells of Non-Epithelial Origin with the ApoStream® System. *PLOS ONE* **2017**, *12*, ed. by Najbauer, J., e0175414, DOI: 10.1371/journal.pone.0175414.

(128) Burt, J. P. H.; Al-Ameen, T. A. K.; Pethig, R. An Optical Dielectrophoresis Spectrometer for Low-Frequency Measurements on Colloidal Suspensions. *Journal of Physics E: Scientific Instruments* **1989**, *22*, 952–957, DOI: 10.1088/0022-3735/22/11/011.

(129) Price, J. A.; Burt, J. P.; Pethig, R. Applications of a New Optical Technique for Measuring the Dielectrophoretic Behaviour of Micro-Organisms. *Biochimica et Biophysica Acta (BBA) - General Subjects* **1988**, *964*, 221–230, DOI: 10.1016/0304-4165(88)90170-5.

(130) Du, F.; Ciaciuch, P.; Bohlen, S.; Wang, Y.; Baune, M.; Thöming, J. Intensification of Cross-Flow Membrane Filtration Using Dielectrophoresis with a Novel Electrode Configuration. *Journal of Membrane Science* **2013**, *448*, 256–261, DOI: 10.1016/j.memsci.2013.08.016.

(131) Du, F.; Hawari, A. H.; Larbi, B.; Ltaief, A.; Pesch, G. R.; Baune, M.; Thöming, J. Fouling Suppression in Submerged Membrane Bioreactors by Obstacle Dielectrophoresis. *Journal of Membrane Science* **2018**, *549*, 466–473, DOI: 10.1016/j.memsci.2017.12.049.

(132) Hakoda, M.; Otaki, T. Analytical Characteristic of Chromatography Device Using Dielectrophoresis Phenomenon. *Key Engineering Materials* **2011**, *497*, 87–92, DOI: 10.4028/www.scientific.net/KEM.497.87.

(133) Giesler, J. Online Repository for "High Throughput Dielectrophoretic Separator Based on Printed Circuit Boards" Zenodo, https://doi.org/10.5281/zenodo.6806667.

(134) Marsono, B. D.; Yuniarto, A.; Purnomo, A.; Soedjono, E. Comparison Performances of Microfiltration and Rapid Sand Filter Operated in Water Treatment Plant. *IOP Conference Series: Earth and Environmental Science* **2022**, *1111*, 012048, DOI: 10.1088/1755-1315/1111/1/012048.

(135) Liu, R.; Wang, L.; Yang, L.; Liu, Q.; Gao, Y.; Ye, J.; Xiao, J.; Hu, Q.; Zhang, X. Ultrafiltration and Microfiltration Membrane Performance, Cleaning, and Flux Recovery for Microalgal Harvesting. *Journal of Applied Phycology* **2020**, *32*, 3101–3112, DOI: 10.1007/s10811-020-02204-2.

(136) Giesler, J. Online Repository for "Sorting Lithium-Ion Battery Electrode Materials Using Dielectrophoresis" Zenodo, https://doi.org/10.5281/zenodo.7593873.

<

List of student works supervised

This thesis does not contain any data produced from students within their bachelor's or master's thesis. However, I highly acknowledge their input and insights I gained from their work. The following works were supervised by me during my time as doctoral candidate:

- *Erstellung einer Designrichtlinie für die Frequenzauswahl in der dielektrophoretischen Partikelchromatographie* by Friederike Baumgart in 2020.
- *Toward Developing an Insulator-based Dielectrophoretic Device for Continuous Sorting of Mitochondria* by Yara Ehlert in 2022.
- *Development of design criteria for a microchannel for sorting particles by dielectrophoresis* by Simon Alves Martins in 2022.

Contribution to Publications

Aricle	[1]	[2]	[3]	[4]
Concept	JG, GRP, MB, JT	JG, MB, JT, GRP	JG, MB, JT, GRP	JG, MB, JT, GRP
Experiments and/or Simulation	JG	JG	JG	JG
Visualization & Writing	JG	JG	JG	JG
Review & Editing	JG, GRP, MB, JT, LW, MPS	JG, MB, JT, LW, GRP	JG, MB, JT, LW, GRP	JG, MB, JT, LW, AR, GRP
Supervision	MB, GRP	MB, GRP	MB, GRP	MB, GRP
Other	[1]	-	-	[2]

[1] MPS fabricated the electrodes and SU8 master and contributed their layout.
[2] Alica Rother performed the chemical analysis of the samples.

Abbreviations	Name
JG	Jasper Giesler
JT	Prof. Dr.-Ing. Jorg Thöming
MB	Dr. Michael Baune
GRP	Prof. Dr.-Ing. Georg R. Pesch
LW	Laura Weirauch
MPS	Prof. Dr.-Ing. Marc-Peter Schmidt
AR	Alica Rother